Turun yliopisto
University of Turku

TARGETED PROTEOMICS IN CHARACTERIZING IRON-DEPRIVED CYANOBACTERIA: INSIGHTS INTO THE REGULATION OF IRON-SULFUR CLUSTER BIOGENESIS

Linda Vuorijoki

TURUN YLIOPISTON JULKAISUJA - ANNALES UNIVERSITATIS TURKUENSIS
Sarja - ser. AI osa - tom. 566 | Astronomica - Chemica - Physica - Mathematica | Turku 2017

Turun yliopisto
University of Turku

TARGETED PROTEOMICS IN CHARACTERIZING IRON-DEPRIVED CYANOBACTERIA: INSIGHTS INTO THE REGULATION OF IRON-SULFUR CLUSTER BIOGENESIS

Linda Vuorijoki

TURUN YLIOPISTON JULKAISUJA – ANNALES UNIVERSITATIS TURKUENSIS
Sarja - ser. A I osa - tom. 566 | Astronomica - Chemica - Physica - Mathematica | Turku 2017

University of Turku

Faculty of Mathematics and Natural Sciences
Department of Biochemistry
Laboratory of Molecular Plant Biology

Supervised by

Prof. Eva-Mari Aro
Molecular Plant Biology
Department of Biochemistry
University of Turku
FI-20014 Turku, Finland

Dr. Pauli Kallio
Molecular Plant Biology
Department of Biochemistry
University of Turku
FI-20014 Turku, Finland

Reviewed by

Prof. Karin Stensjö
Ångström Laboratory
Department of Chemistry
Uppsala University
Box 523, 75120 Uppsala, Sweden

Prof. Toivo Kallas
Microbial Genetics and Biotechnology
Department of Biology
University of Wisconsin Oshkosh
Oshkosh, WI 54901, USA

Opponent

Dr. Janneke Balk
Department of Biological Chemistry
John Innes Centre
Colney Lane
Norwich
NR4 7UH, UK

The originality of this thesis has been checked in accordance with the University of Turku quality assurance system using the Turnitin OriginalityCheck service.

ISBN 978-951-29-6966-1 (PRINT)
ISBN 978-951-29-6967-8 (PDF)
ISSN 0082-7002 (PRINT)
ISSN 2343-3175 (PDF)
Painosalama Oy - Turku, Finland 2017

To persistence

LIST OF ORIGINAL PUBLICATIONS

This thesis is based on following publications, which are referred in the text by the Roman numerals.

I. Vuorijoki L, Isojärvi J, Kallio P, Kouvonen P, Aro EM, Corthals GL, Jones PR, Muth-Pawlak D (2016) Development of a Quantitative SRM-Based Proteomics Method to Study Iron Metabolism of *Synechocystis* sp. PCC 6803. *J Proteome Res* **15**: 266-279

II. Vuorijoki L, Tiwari A, Kallio P, Aro E-M (2017) Inactivation of iron-sulfur cluster biogenesis regulator SufR in Synechocystis sp. PCC 6803 induces unique iron-dependent protein-level responses. *Biochimica et Biophysica Acta (BBA) - General Subjects* **1861**: 1085-1098

III. Vuorijoki L, Kallio P, Aro E-M (2017) SRM dataset of the proteome of inactivated iron-sulfur cluster biogenesis regulator SufR in Synechocystis sp. PCC 6803. *Data in Brief* **11**: 572-575

IV. Georg J, Kostova G, Vuorijoki L, Schön V, Kadowaki T, Huokko T, Baumgartner D, Müller M, Klähn S, Allahverdiyeva Y, Hihara Y, Futschik ME, Aro EM, Hess WR (2017) Acclimation of oxygenic photosynthesis to iron starvation is controlled by the sRNA IsaR1. *Curr Biol* 27: 1425-1436.e1427

TABLE OF CONTENTS

ABBREVIATIONS

ARTO	Alternative respiratory terminal oxidase
ATP	Adenosine triphosphate
BG-11	Blue-Green growth medium for cyanobacteria
cDNA	Complementary DNA
Chl *a*	Chlorophyll a
CIA	Cytosolic iron-sulfur cluster assembly
Cm^R	Chloramphenicol resistance cassette
CO_2	Carbon dioxide
CopraRNA	Comparative prediction algorithm for small RNA targets
CS	Control strain
Cyt	Cytochrome
DCMU	3-(3,4-dichlorophenyl)-1,1-dimethylurea
DDA	Data dependent acquisition
DFB	Desferrioxamine B
DIA	Data independent acquisition
DNA	Deoxyribonucleic acid
DTT	Dithiotreitol
EMP	Embden–Meyerhof–Parnas
EMSA	Electrophoretic mobility shift assay
Fdx	Ferredoxin
Fe	Iron atom
Fe^{2+}	Ferrous iron
Fe^{3+}	Ferric iron
FMN	Flavin mononucleotide
FUR	Ferric uptake regulator
Fut	Ferric uptake transporter
GOE	Great Oxidation Event
HiPIP	High potential iron-sulfur protein
HPLC	High-performance liquid chromatogram
IAA	Iodoacetamide
IdiA	Iron deficiency inducible protein A
IMAC	Immobilized metal affinity-chromatography
IntaRNA	Interacting RNA –tool
iRT	indexed retention time
IsaR1	Iron-stress activated RNA 1
ISC	Iron-sulfur cluster
IsiA/B	Iron starvation inducible protein A/B

Km^R	Kanamycin resistance cassette
mRNA	Messenger ribonucleic acid
MS/MS	Tandem mass spectrometry
MudPIT	Multidimensional protein identification technology
mV	Millivolt, unit for electrical potential
m/z	Mass-to-charge -ratio
N_2	Molecular nitrogen
$NADP^+$	Nicotinamide adenine dinucleotide phosphate (oxidized)
NADPH	Nicotinamide adenine dinucleotide phosphate (reduced)
ncRNA	Non-coding RNA
NDH	NADH dehydrogenase
NIF	Nitrogen fixation
OCP	Orange carotenoid protein
OD_{750nm}	Optical density at absorbtion wavelength 750 nanometers
OEC	Oxygen evolving complex
P680	Reaction center chlorophyll a, primary electron donor of PS II
P700	Reaction center chlorophyll a, primary electron donor of PS I
PBS	Phosphate-buffered saline -solution
PCC	Pasteur culture collection
PCR	Polymerase chain reaction
PETC	Photosynthetic electron transfer chain
pH	Negative logarithm of the proton concentration
PQ	Plastoquinone
PQH_2	Plastoquinol
PRM	Parallel reaction monitoring
PS	Photosystem
pSRM	Pseudo selected reaction monitoring
PTP	Proteotypic peptides
QQQ-MS	Triple quadruple mass spectrometer
RNA	Ribonucleic acid
ROS	Reactive oxygen species
RT-qPCR	Reverse transcriptase quantitative reverse transcription PCR
RuBisCo	Ribulose bisphosphate carboxylase/oxygenase
S	Inorganic sulfur
SAM	*S*-Adenosyl methionine
SDH	Succinate dehydrogenase
SDS	Sodium dodecyl sulfate
sGFP	Superfolder green fluorescent protein

sp.	Species
SRM	Selected reaction monitoring
sRNA	Small ribonucleic acid
SUF	Sulfur utilization factor
SWATH	Sequential windowed acquisition of all theoretical fragment ion mass spectra
TCA	Tricarboxylic acid cycle
TES	2-[[1,3-dihydroxy-2-(hydroxymethyl)propan-2-yl]amino] ethanesulfonic acid
TSS	Transcriptional start site
TU	Transcriptional unit
5’ UTR	Five prime untranslated region, leader RNA
WT	Wild type

ABSTRACT

Cyanobacteria comprise a diverse group of widely distributed gram-negative bacteria, which have the unique capacity amongst prokaryotes to perform oxygenic photosynthesis. Acclimation to iron deprivation, a key theme in this Thesis, involves several metabolic changes, which are closely interlinked with the high demand for iron cofactors in the photosynthetic electron transfer chains of these organisms. In order to gain in-depth information on the protein-level changes occurring under iron deprivation, a targeted MS-based proteomics method, *selected reaction monitoring* (SRM), was developed for the cyanobacterial model species *Synechocystis* sp. PCC 6803. Altogether 106 proteins were selected as SRM-target proteins, representing various key metabolic pathways and possible metabolic nodes linked with iron-dependent enzymatic reactions. The SRM analysis resulted in a high-quality dataset, which verified several responses to iron deprivation, such as those related to remodeling of photosynthetic apparatus and induction of several iron acquisition proteins. New information was obtained, for example, on the elevated levels of proteins acting as electron sinks to alleviate the overreduction of the photosynthetic electron transfer chain caused by the increase in Photosystem II to Photosystem I ratio under iron deprivation. As a demonstration of the sensitivity of the system, 64 of the quantified target proteins had not been detected in earlier discovery-based proteomics assays.

The validated SRM method was subsequently applied to study the regulation of iron-sulfur biogenesis in *Synechocystis sufR* and *isaR1* mutant strains. SufR has been characterized as a transcriptional repressor of the *sufBCDS* operon, which is responsible of the Fe-S cluster biogenesis in cyanobacteria. Deletion of *sufR* caused drastic induction of the *sufBCDS* operon proteins under Fe-sufficiency, while the proteins carrying Fe-S cofactors were downregulated. Under extended Fe-depletion, increased expression of the apo-form Fe-S proteins was observed in comparison to the wild type strain under the same conditions. IsaR1, a small regulatory RNA, was found to be responsible for the repression of several genes for Fe and Fe-S proteins as well as tetrapyrrole biosynthesis genes under Fe-deprivation. Hence, IsaR1 affects the photosynthetic apparatus both directly and indirectly upon acclimation to iron deprivation. Importantly, both SufR (transcriptional repressor protein) and IsaR1 (small regulatory RNA) were identified to repress the *sufBCDS* operon; SufR under Fe-sufficiency and IsaR1 under Fe-deprivation. Such complex mixed regulatory circuit highlights the importance of tight control over the biogenesis of Fe-S clusters as part of the metabolic acclimation to varying iron conditions.

TIIVISTELMÄ

Syanobakteerit muodostavat monimuotoisen ryhmän gram-negatiivisiä bakteereita, joille tunnusomaista on fotosynteesi – luonnollinen kyky muodostaa hiilipohjaisia yhdisteitä ilman hiilidioksidista ja vedestä käyttäen energiana auringon valoa. Tämän väitöskirjan keskeisenä teemana on syanobakteerien rauta-aineenvaihdunta ja sen säätely, osana fotosynteesille välttämättömien raudasta riippuvaisten elektoninsiirtoketjujen toimintaa. Tavoitteena oli kehittää *Synechocystis* sp. PCC 6803 -syanobakteerille räätälöity massaspektrometriaan perustuva kohdennettu proteomiikkamenetelmä SRM (*selected reaction monitoring*) ja soveltaa sitä raudan puutokseen liittyvien solunsisäisten muutosten havaitsemiseen proteiinitasolla. Kohdeproteiineiksi SRM-analyysiin valittiin 106 entsyymiä, jotka edustivat solun toiminnalle keskeisiä aineenvaihduntareittejä, sekä erilaisia rautametaboliaan liittyviä reaktioita. Menetelmällä saadut tulokset antoivat yksityiskohtaista tietoa solun sopeutumisesta raudan puutokseen, kuten muutoksista fotosynteesikoneistossa, sekä elektroninsiirtoketjua suojaavissa mekanismeissa. Osoituksena kehitetyn SRM-menetelmän herkkyydestä, analyysi antoi kvantitatiivista tietoa 64:stä proteiinista, joita ei aikaisemmin pystytty havaitsemaan vaihtoehtoisella shotgun-proteomiikkamenetelmällä.

Kehitettyä SRM-menetelmää sovellettiin edelleen elektroninsiirtoreaktioille välttämättömien rautarikki (Fe-S) -klusterien metabolian tutkimiseen. Kohteena olivat SufR, joka säätelee näiden kofaktorien biogeneesistä vastaavan *suf* operonin toimintaa, sekä sRNA IsaR1, jolla on tärkeä rooli solun sopeutumisessa raudan puutokseen. SufR-proteiinin inaktivaatio johti *suf* operonin yliekspressioon, samalla kun Fe-S –kofaktoreita sitovien proteiinien määrä solussa väheni. IsaR1:n havaittiin repressoivan tiettyjen Fe-S –proteiinien ekspressiota ja tetrapyrroli-pigmenttien biogeneesiä, ja siten vaikuttavan sekä suoraan että välillisesti fotosynteesikoneiston toimintaan silloin kun rautaa on rajoittava määrä. Yhtenä väitöskirjan merkittävämpänä löytönä, SufR:n ja IsaR1:n osoitettiin molempien vaikuttavan *suf* operonin toimintaan ja muodostavan koordinoidun säätelysysteemin, joka reagoi hyvin herkästi solunsisäiseen raudan määrään. Monimutkainen mekanismi korostaa Fe-S –kofaktorien merkitystä fotosynteettisten organismien rauta-aineenvaihdunnan säätelyssä, osana solun resurssien jakamista ja raudan puutteen aiheuttamien vaurioiden rajoittamista.

1. INTRODUCTION

1.1. Cyanobacteria –the fittest of the survivors

1.1.1. Diversity and adaptability of cyanobacteria

Cyanobacteria constitute a diverse and widely distributed group of gram-negative bacteria, which can perform oxygenic photosynthesis. They reduce atmospheric CO_2 into carbohydrates with the electrons obtained from the solar-powered water-splitting reaction, with concomitant release of O_2. During evolution, cyanobacteria have adapted to both aquatic and terrestrial habitats, including harsh environments (Rippka et al., 1981). The successful colonization of cyanobacteria to a variety of ecological niches can be explained not only by their long evolutionary history, but by their unique cell structure, physiology and metabolism.

The early origin of cyanobacteria dates back about 3,5 billion years, as suggested by the discovery of the earliest fossil traces (Schopf, 1993). The evolution of cyanobacteria and the beginning of oxygenic photosynthesis on Earth had a significant impact on the overall atmospheric composition as carbon dioxide (CO_2) was assimilated into diverse carbon-based organic molecules. This was accompanied by the oxidation of abundant compounds such as gaseous hydrogen sulfide (H_2S) and ferrous iron (Fe^{2+}) in the Earth's crust (Canfield et al., 2006; Sleep and Bird, 2008). Eventually, upon the Great Oxidation Event (GOE) approximately 2,3 billion years ago (Holland, 2002; Bekker et al., 2004), the photosynthetic activity of the early cyanobacteria resulted in gradual accumulation of oxygen to the atmosphere at the same time as the oxygen sinks became saturated (Rantamaki et al., 2016). This, together with the following endosymbiotic events, set off the evolution of aerobic metabolism and multicellular life. While proteobacteria evolved into mitochondria, which could produce energy for the organism via aerobic respiration, the photosynthetic cyanobacteria evolved into oxygen producing chloroplasts of plants and algae (Hedges et al., 2004).

Although classified as gram-negative bacteria, cyanobacteria have a unique cell wall structure distinguishable from other prokaryotes (Hoiczyk and Hansel, 2000). The characteristic features include considerably thicker peptidoglycan layer than in other gram-negative bacteria (Golecki, 1988), and a distinctive outer membrane (Jürgens and Weckesser, 1985). The cyanobacterial outer membrane includes an unusual lipopolysaccharide composition, but also photoprotective carotenoid pigments, providing protection against UV radiation, which was especially important at the time when the ozone layer did not yet exist (Resch and Gibson, 1983; Jürgens and Weckesser, 1985). The periplasmic space of the cell wall, is separated from the

cytoplasm by the cytoplasmic membrane, where oxygenic respiration takes place (Peschek et al., 1988). The cytoplasmic membranes as well as the intracellular thylakoid membranes, contain medium chain-length hydrocarbons (mainly C15 and C17) in their structure (Schirmer et al., 2010). This unique feature among prokaryotes has been suggested to contribute to membrane fluidity, growth and photosynthetic activity, especially at low temperatures (Berla et al., 2015). Although the exact biological role of hydrocarbons (alkanes and alkenes) is still not comprehensively understood, they are expected to be particularly important components of the thylakoid membrane, which is the site for photosynthesis as well as respiratory electron transfer chains (Mullineaux, 2014).

All cyanobacteria are able to perform oxygenic photosynthesis by two interlinked photosystems (II and I), which span over the thylakoid membrane. The two photosystems are connected by the cytochrome b_6f (Cyt b_6f) complex, which mediates electron flow from PSII to PSI in the photosynthetic electron transfer chain (PETC). Photosynthetic electron transfer is initiated by the excited photosystem reaction center chlorophylls, P680* in PSII and P700* in PSI, which capture light energy from the surrounding light harvesting pigments; chlorophyll *a* (Chl *a*), phycobilins and carotenoids. The oxidized $P680^+$ of PSII extracts electrons from H_2O at the oxygen-evolving complex that includes a manganese cluster on the lumenal side of the thylakoid membrane (Yachandra et al., 1996), resulting in a release of molecular oxygen and protons. This generates a proton gradient across the thylakoid membrane, which is further augmented by the plastoquinone (PQ) -mediated proton translocation from the cytoplasmic side of the thylakoid membrane to the lumen. In the process, two protons are released to the thylakoid lumen upon plastoquinol (PQH_2) oxidation in a Q-cycle mechanism within the Cyt b_6f complex, where one electron returns back to PQ pool and the other electron is forwarded to plastocyanin (PC) or cytochrome *c*-553 in the PETC (Cramer et al., 1996). Reduced PC of Cyt *c*-553 then donates an electron to oxidized P700 ($P700^+$), filling an electron hole in the PSI reaction center that was formed by charge separation at P700* (Brettel, 1997; Webber and Lubitz, 2001). Electrons excited in PSI reduce ferredoxin (Fdx) and finally $NADP^+$ to NADPH (nicotinamide adenine dinucleotide phosphate) that is the main reductant in photosynthesis-powered metabolism. The proton gradient generated in the PETC is used by the membrane-embedded ATP synthase to produce ATP (adenosine triphosphate). The two products of the photosynthetic reactions, NADPH and ATP, are the primary forms of chemical energy indispensable for essentially all biochemical processes.

Cyanobacteria can deploy different metabolic modes depending on the environmental conditions, ranging from photoautotrophy to strictly heterotrophic growth (Rippka,

1972). As most cyanobacteria grow in habitats where light and CO_2 are sufficient, their primary mode of metabolism is photoautotrophy, *i. e.* the ability to use sunlight to convert CO_2 and water into carbohydrates. Carbon fixation occurs in specialized compartments called carboxysomes, and the primary reaction is catalyzed by the enzyme ribulose-1,5-bisphosphate carboxylase/oxygenase (RuBisCo) in the Calvin-Benson-Bassham cycle (Bassham et al., 1950). This reaction is powered by the energy obtained from photosynthetic light reactions in the form of ATP and NADPH. As an auxiliary mode of metabolism, cyanobacterial species can use reduced sugars, either extracellular or derived from intracellular glycogen reserves for heterotrophic as well as photoheterotrophic growth upon transition to darkness or to low light conditions (mixotrophy) (Fay, 1965; Marquez et al., 1993; Vonshak et al., 2000; Kämäräinen et al., 2016).

Based on the type of carboxysome and RuBisCo, cyanobacteria can be divided into two ecologically distinct groups; α- and β-cyanobacteria (Badger and Price, 2003). The α-cyanobacteria are typically marine species, and together with diatoms are responsible for most of the net primary production in the oceans (Field et al., 1998; Falkowski, 2002), whilst β-cyanobacteria can be found in both freshwater and marine environments (Badger et al., 2006). The CO_2 fixed by the cyanobacteria and other marine algae eventually sinks to the depths of the oceans and during millions of years becomes fossilized into natural gas, oil and coal (Falkowski, 2002). By burning these fossil fuel reserves for energy production, carbon is currently released back to the atmosphere at a much faster rate than the primary producers can assimilate. As an attempt to balance the global carbon cycle, cyanobacteria have become a promising target for engineering efficient direct biofuel factories for renewable energy production.

1.1.2. Iron as a limiting factor of primary production

Besides the importance of an appropriate amount of light, suitable temperature and pH, chemical elements play an important role, both as primary nutrients and trace elements, in supporting optimal cyanobacterial growth and photosynthetic activity. The primary limiting nutrients in aquatic environments are phosphorous (P) and nitrogen (N) (Redfield, 1958; Dugdale, 1967; Sommer, 1989), followed by inorganic carbon (C) (Klemer et al., 1995; Ibelings and Maberly, 1998). While both phosphorous and nitrogen are crucial components of nucleotides, nitrogen is essential also in amino acids among other cellular biomolecules. As nitrogen fixation is a slow and energetically expensive process (Dixon and Kahn, 2004), the availability of nitrogen in the form of readily available ammonium is often considered to be the major limiting factor in many aquatic environments (Dugdale, 1967; Ryther and Dunstan, 1971; Falkowski, 1997).

Biological nitrogen fixation itself is known to be dependent on the availability of one particular trace element: Iron (Martin and Fitzwater, 1988; de Baar et al., 1995; Falkowski, 1997). Besides being an indispensable cofactor in the active centers of the nitrogenase reductase and nitrogenase enzyme (Raven, 1988), iron is required in high stoichiometric quantities in the PETC, which is essential for all organisms performing oxygenic photosynthesis. Consequently, the iron requirement of cyanobacteria exceeds the iron quota of other non-photosynthetic bacteria by at least one order of magnitude (Finney and O'Halloran, 2003; Keren et al., 2004; Shcolnick et al., 2009).

The extensive use of iron as a cofactor in several proteins can be explained by the vast amounts of bioavailable iron under the anaerobic and reducing conditions of the early Earth at the time that cyanobacteria originated. The accumulation of oxygen upon the Great Oxygenation Event led to oxidation of the iron from the ferrous (Fe^{2+}) to the ferric (Fe^{3+}) form, which subsequently resulted in precipitation of iron as ferric hydroxides at neutral pH (Byrne and Kester, 1976). Ironically, although iron is the fourth most abundant element in the Earth's crust, the poor solubility of the ferric iron complexes limits cyanobacterial photosynthesis in one third of the oceanic and fresh water regions (Martin et al., 1991; Boyd et al., 2007; Schoffman et al., 2016), where the macronutrients N, P and C are plentiful. In fact, iron concentrations rarely exceed nanomolar levels (Wurtsbaugh and Horne, 1983; Johnson et al., 1997; Twiss et al., 2000; Morel and Price, 2003; North et al., 2007) – even in shallow coastal waters and lakes which are replenished by iron from fluvial inputs, and undergo reductive dissolution of iron oxides as organic matter is being degraded (Schoemann et al., 1998).

1.1.3. Acclimation of cyanobacteria to iron deprivation

Enzyme-bound iron can either be part of the porphyrin ring of haem, can form a complex with other iron molecules in (non-haem) mono- or di-iron reaction centers, or can combine with sulfide to form iron-sulfur (Fe-S) clusters. All these forms can be found in the complete PETC, which contains as many as 21-24 iron atoms (Fig. 1). When the PSI complexes are in trimeric form, the number of iron atoms in PETC can be as high as 48. PSII has haem-binding Cyt *b*-559 and Cyt *c*-550 proteins, and one non-haem iron located between the PQ binding pockets Q_A and Q_B of the D2 and D1 proteins (Zouni et al., 2001; Kamiya and Shen, 2003). The Cyt b_6f complex has four haems; three in Cyt b_6 and one in Cyt *f*, in addition to one [2Fe-2S] cluster, which is bound by a Rieske Fe-S protein (Kurisu et al., 2003; Stroebel et al., 2003). After the Cyt b_6f complex, electrons are transferred to the P700 reaction center of PSI either via haem-containing Cyt *c*-553 or copper-containing plastocyanin, depending on the availability of copper (Wood, 1978; Sandmann and Boger, 1980; Laudenbach et al., 1990; Zhang et al., 1992). In PSI, electron flow continues from the excited reaction center chlorophyll P700, to the

modified chlorophyll (A_0) and phylloquinone (A_1), and further to the three [4Fe-4S] clusters, named F_X, F_A and F_B. The first iron-sulfur cluster, F_X (-710 mV), is coordinated to cysteine residues in PsaA and PsaB subunits (McDermott et al., 1989), while the two other [4Fe-4S] clusters of PSI, F_A and F_B, are bound to the PsaC subunit. Electrons are passed on from F_B to the [2Fe-2S] cluster containing Fdx protein, or the flavodoxin (IsiB) protein if iron is scarce (Hutber et al., 1977; Golbeck, 1999).

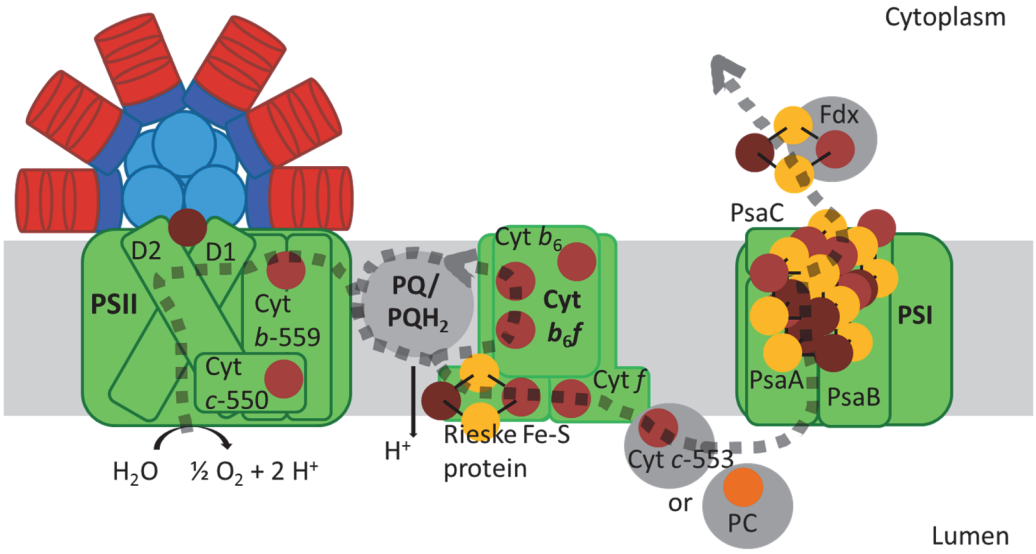

Figure 1. Simplified scheme of the photosynthetic electron transfer chain showing iron-containing sites. The dots represent the ferrous (red) and ferric (dark red) iron, sulfur (yellow) and copper (orange) centers. The dashed line represents electron flow. Expression of the copper binding plastocyanin (PC) protein depends on the availability of copper, and participates more often in the electron transfer between Cyt b_6f and PSI than Cyt *c*-553 (Zhang et al., 1992). Under iron depletion the [2Fe-2S] binding Fdx protein on the acceptor side of PSI is replaced by flavodoxin (IsiB). These alterations in the PETC composition cause the iron quota of single PS unit with monomeric PSI to range from 21 to 24 atoms, depending on the environmental conditions.

The oxygenation of the Earth's atmosphere forced cyanobacteria to develop strategies to cope with scarce amounts of bioavailable iron, but also to avoid the deleterious effects of the Fenton reactions, in which the reaction between hydrogen peroxide (H_2O_2) and free ferrous iron leads to the formation of hydroxide and hydroxyl radicals, and thereby to more pronounced oxidative stress (Latifi et al., 2005). Strict control over the intracellular iron pool is therefore required and largely achieved by a global transcriptional regulator called Fur; *ferric uptake regulator* (Hantke, 1981). In addition to controlling the expression of iron acquisition and storage genes, a wide variety of genes involved in *e. g.* photosynthesis, oxidative stress responses, and cellular morphology are regulated by Fur (Gonzalez et al., 2014). This regulation is affected by the intracellular iron concentration. Binding of the iron-bound Fur to so-called Fur-

boxes in promoter regions represses the target genes, while in the absence of iron the repression is alleviated (de Lorenzo et al., 1987; Escolar et al., 1999; Pecqueur et al., 2006). The role of Fur in different organisms may vary, as for example in the cyanobacterium *Synechocystis* sp. PCC 6803 the iron-free FurA (homolog for Fur) is degraded by the proteolytic FtsH1/ FtsH3 complex (Krynická et al., 2014), while in other cyanobacteria FurA is expressed at a constant level even under iron deprivation (Hernandez et al., 2002; Gonzalez et al., 2014). Although Fur is an important modulator of iron-responsive genes under varying iron concentrations, the expression of several genes can also be indirectly controlled by Fur. In *Escherichia coli*, Fur controls the transcription of a small regulatory RNA (sRNA) called RyhB, which complements the Fur-mediated regulation under iron-limiting conditions (Massé and Gottesman, 2002). A similar regulatory mechanism could also exist in cyanobacteria, as the genes encoding the iron-rich PSI and Cyt b_6f complexes are not identified as targets of FurA, but are still affected upon iron deprivation (Shi et al., 2007; Shcolnick et al., 2009; Gonzalez et al., 2014).

The strategies that cyanobacteria deploy in acclimation to low iron concentrations include decrease and/or replacement of the Fe or Fe-S containing proteins, such as those taking part in photosynthesis. As a consequence of the decreased amounts of PSII and especially of the iron-rich PSI complexes, the light absorption of associated Chl *a* and phycobilin pigments is decreased. Further, the amount of NAD(P)H dehydrogenase (NDH-1) complexes decreases on the thylakoid membrane, due to several bound Fe-S clusters in these complexes. This diminishes the respiratory electron flow towards the PQ pool, which has been implied to remain mostly oxidized under iron deprivation (Ivanov et al., 2006). The observed decrease in the amounts of flavodiiron proteins Flv2 and Flv4 under iron deprivation (Hernández-Prieto et al., 2012) can further lead to increased damage in PSII (Bersanini et al., 2014; Chukhutsina et al., 2015). This, in turn, can diminish electron flow from PSII toward carbon fixation (Zhang et al., 2012), which have been shown to be repressed in transcriptome (Singh et al., 2003; Shcolnick et al., 2009; Hernández-Prieto et al., 2012), but not in proteome analyses (Wegener et al., 2010). Several transcriptomics studies have additionally shown a coordinated acclimation of carbon and nitrogen metabolism to iron deprivation, with increased expression of nitrogen assimilation genes and decreased expression of genes associated with carbon uptake in *Synechocystis* (Shcolnick et al., 2009; Hernández-Prieto et al., 2012).

The downregulation of iron-containing proteins under iron-limited conditions is compensated by the upregulation of proteins that do not rely on iron as a cofactor. A well-known example is the replacement of [2Fe-2S] binding ferredoxin with flavodoxin

IsiB, which uses flavin mononucleotide (FMN) as a cofactor (Laudenbach et al., 1988; Bottin and Lagoutte, 1992). The coexpression of IsiB and the chlorophyll-binding antenna protein CP43' (IsiA), encoded by the same bicistronic operon, is one of the clearest indicators of iron deficiency in most cyanobacteria (Laudenbach and Straus, 1988; Geiß et al., 2001). Under iron deficiency, IsiA proteins accumulate and aggregate as a single antenna ring around trimeric PSI complex, and provide protection against photo-oxidative stress (Bibby et al., 2001; Boekema et al., 2001; Yeremenko et al., 2004; Ihalainen et al., 2005). Under prolonged iron deficiency, the trimeric PSI complexes begin to decompose to monomeric forms surrounded by single or double rings of IsiA, which further continue to self-assemble even without PSI (Yeremenko et al., 2004). The iron-deficiency-induced protein A (IdiA) has a role similar to IsiA in the protection of PSII acceptor side by interacting with the non-haem iron between Q_A and Q_B, when phycobilisomes become degraded (Exss-Sonne et al., 2000; Michel and Pistorius, 2004; Lax et al., 2007). Interestingly, IdiA has also been shown to be involved in ferric iron transport, and has been named FutA1 in that context (see below) (Tolle et al., 2002).

Although several marine and freshwater cyanobacteria can excrete ferric-iron-binding siderophores to increase the amount of bioavailable iron (Murphy et al., 1976; Mawji et al., 2008; Hopkinson and Morel, 2009), many cyanobacteria do not produce siderophores, but can still take up Fe-siderophore complexes as well as free inorganic iron (Kranzler et al., 2011; Jiang et al., 2015). The transport of iron across the outer membrane occurs mainly via the TonB-ExbB-ExbD system (Jiang et al., 2015), although passive diffusion of inorganic iron through unspecific porins has also been shown to occur (Fujii et al., 2011). Once delivered to the periplasmic space, the free ferric iron is either transported through the plasma membrane via the cation diffusion facilitator (CDF) system (Jiang et al., 2012) or captured by the FutA2 protein, which delivers the ferric iron either to FeoB or FutABC transport systems. In the so-called reductive iron uptake, the FutA2-bound ferric iron is reduced to the ferrous form by the Alternative Respiratory Terminal Oxidase (ARTO)(Kranzler et al., 2014), followed by transport though the plasma membrane via FeoB (Kranzler et al., 2011). This reductive iron uptake has shown to be the most efficient transport mechanism in cyanobacteria (Katoh et al., 2001; Kranzler et al., 2014), while the FutABC system appears to provide an additional, ferric iron transport mechanism, which also has a regulatory function in reductive iron uptake (Kranzler et al., 2014). The FutABC-transporter is an ATP-binding-cassette-type transporter system (Katoh et al., 2001), which consists of i) membrane associated FutB and FutC subunits, ii) the abovementioned periplasmic FutA2, and iii) the thylakoid associated FutA1 (IdiA) protein.

To avoid the toxic effects of free intracellular iron, the available ferrous iron can be efficiently sequestered by the ferritin family proteins and stored as ferric oxides, thus minimizing the chance of oxidative stress through generation of hydroxyl radicals (Shcolnick et al., 2009). Under iron starved conditions the stored iron can be released by the DPS (DNA Protection during Starvation) family protein MrgA, which also belongs to the ferritin family (Shcolnick et al., 2007).

1.1.4. *Synechocystis* sp. PCC 6803 as a model species

Synechocystis sp. PCC 6803 (hereafter *Synechocystis*) is a non-toxic, non-nitrogen fixing, non-siderophore-producing, unicellular, freshwater β-cyanobacterium, which was the first photosynthetic organism to be completely sequenced (Kaneko et al., 1996). The easy access to this genetic information via sequence databases, together with the ability of *Synechocystis* to easily take in exogenous DNA (Barten and Lill, 1995), has promoted this strain to be extensively used in fundamental research of cyanobacteria. Consequently, *Synechocystis* has become the most explored cyanobacterial species in research focusing on oxygenic photosynthesis and associated processes. A widely used, glucose-tolerant, laboratory sub-strain of *Synechocystis* has also allowed the study of a heterotrophic metabolism in complete darkness in the presence of glucose, with the growth activated by only five minutes of daily pulse of white light (Anderson and McIntosh, 1991). The information gained from fundamental research of *Synechocystis* has been invaluable in understanding the physiology of cyanobacteria as well as that of other photosynthetic organisms. In addition, the knowledge obtained from applied techniques has enabled efficient and rational engineering of photosynthetic organisms toward biotechnological applications (Angermayr et al., 2015; Gudmundsson and Nogales, 2015).

1.2. Iron-sulfur clusters in biological processes

1.2.1. Structure and function of iron-sulfur clusters

Iron–sulfur (Fe–S) clusters are essential cofactors in numerous important processes that enable life on Earth, such as photosynthesis, respiration and nitrogen fixation (Rouault and Tong, 2005). Fe-S clusters are composed of iron and sulfur, which can be organized in several complex forms. In the simplest form, as represented by rubredoxin, one iron atom is coordinated by four cysteine residues of the protein (Lovenberg and Sobel, 1965). Actual Fe-S clusters have two ([2Fe-2S]), three ([3Fe-4S]), four ([4Fe-4S] and [4Fe-3S]) or eight ([8Fe-7S]) iron atoms linked to inorganic sulfur. The iron atoms of these clusters are most commonly coordinated to cysteine residues, but they can also be bound via two histidine residues to one of the two iron atoms of

[2Fe-2S] cluster as in the case of Rieske Fe-S clusters (Gurbiel et al., 1989), or via aspartate (Gruner et al., 2011), glutamate (Volbeda et al., 2012) or arginine (Berkovitch et al., 2004) residues to one iron of the [4Fe-4S] cluster. Besides coordinating the clusters in the correct orientation in the enzyme, the ligation to these residues provides stability to the cluster by allowing electron delocalization across the cluster (Beinert and Kiley, 1999).

Fe-S clusters have diverse biological functions as part of gene regulation, electron transfer, and catalytic reactions that relate to their specific electrochemical properties. These clusters span over an exceptionally wide range of redox potentials [from -710 to +321 mV; (Holton et al., 1996; Fromme and Grotjohann, 2006)], which allows them to accept or donate electrons under physiological conditions where other cofactors, *e. g.* NAD(P), flavins, haems, quinones etc., cannot function (Imlay, 2006). Upon electron transfer, the cluster redox states change between +1 and +2 in ferredoxin-type low potential Fe-S cluster proteins, while in high-potential iron-sulfur proteins (HiPIP) the cluster redox states typically shuffles between +2 and +3 (Imlay, 2006). An unusual range of redox states from +3 to +5, resulting from two-electron donation, has been characterized for the high-potential, oxygen tolerant, [4Fe-3S] cluster of the membrane-bound NiFe-hydrogenase of *Hydrogenovibrio marinus* (Shomura et al., 2011). The oxidation state of each iron in the Fe-S cluster is typically +2 or +3.

The ability of protein-bound Fe-S clusters to sense changes in the redox environment and pass on this information via the changed redox state, can induce alterations in the protein frame. The ferrous and ferric forms of iron have different ligand preferences. Ferrous iron prefers interactions with sulfur in cysteine and nitrogen in histidine, while ferric iron prefers to make bonds with oxygen in aspartate (Outten and Theil, 2009). Hence, the oxidation state of the Fe atoms in the Fe-S cluster can alter the coordination to the protein, and transduce signals of the changing redox state of the cell. For example, the oxidation state change of the Fe-S cluster can affect the DNA binding affinity of the associated transcription factor and lead to changes in the expression of redox responsive genes (Ding et al., 1996; Shen et al., 2007). Besides the electrostatic interactions between Fe-S cluster and amino acid residues of the protein, the overall protein structure with hydrogen bonding to the inorganic sulfur and terminal cysteine ligands have been shown to increase the redox potential of the cluster (Yang et al., 2004; Kolling et al., 2007; Birrell et al., 2016). Consequently, the effect of cluster solvation or solvent exposure, *i. e.* hydrogen bonding between H_2O and the cluster has also an impact on the cluster redox potential.

In addition to being flexible redox sensors, the functional versatility of iron-sulfur clusters enables their participation in catalytic reactions by substrate binding or radical mechanisms. Non-redox, substrate-binding reactions occur in dehydratase enzymes such as in aconitase, where a solvent-exposed iron of the [4Fe-4S] cluster is available for the citrate-isocitrate isomerization reaction (Emptage et al., 1983). Radical mechanisms, on the other hand, are used mainly in reactions involving enzymes of the radical-SAM superfamily (Imlay, 2006), where the cluster functions both as a coordinating ligand as well as a redox catalyst for activating aliphatic substrates.

1.2.2. Oxygen sensitivity of iron-sulfur clusters

The redox properties that allow Fe-S clusters to participate in diverse and challenging reactions make many of them highly sensitive towards oxidation. The ability to transfer one electron at a time between redox partners can lead to deleterious effects as the Fe-S clusters can overcome the spin restriction of molecular oxygen (O_2), resulting in formation of reactive oxygen species (ROS) such as superoxide and hydrogen peroxide. These univalent oxidants can further convert the catalytically active $[4Fe\text{-}4S]^{2+}$ clusters of dehydratases to an unstable $[4Fe\text{-}4S]^{3+}$ state, which then degrade to an inactive $[3Fe\text{-}4S]^{1+}$ form upon the release of the solvent-exposed iron (Flint et al., 1993; Varghese et al., 2003). The released Fe^{2+} iron can further react with hydrogen peroxide in a Fenton reaction and result in escalated oxidative stress due to formation of highly reactive hydroxyl radicals and hydroxide ions.

The impact of the electrostatic environment on cluster stability becomes evident in the case of spinach dihydroxy-acid dehydratase, which has been shown to be resistant to oxidation since the $[2Fe\text{-}2S]^{2+}$ cluster is buried within the hydrophobic core of the protein, and is thus less accessible to oxidants (Flint et al., 1993). Furthermore, the degradation of the sheltered cluster differs from the solvent exposed hydratases, as the two cluster-bound irons are in the ferric (Fe^{3+}) form and the electrons come from the sulfide rather than from iron upon cluster oxidation (Flint et al., 1993). This is in line with the proposed mechanism of Fe-S cluster degradation via oxidation of the inorganic sulfide ligand (S^{2-}) in the Fe-S cluster of spinach ferredoxin (Petering et al., 1971). The sulfide is oxidized to sulfane (S^0), which binds covalently to the cysteine residues of the protein which used to coordinate the iron atoms of the Fe-S cluster. This cysteine-bound sulfane sulfur (cysteine persulfide) can be reduced back to sulfide, possibly by a rhodanese enzyme (Agrò et al., 1971; Cerletti, 1986; Laudenbach et al., 1991) or a cysteine desulfurase (Zheng et al., 1993), and used in restoration of the [4Fe-4S] cluster if iron and reducing power are available (Zhang et al., 2012; Crack et al., 2014).

While oxygen sensitivity can be a problem for enzymes relying on intact Fe-S clusters, many transcription factors have evolved specifically to exploit the oxidation and degradation of a cluster, and the associated conformational change of the protein as a means to relay information about the oxidative state of the cell via gene regulation (see section 1.2.1). This type of regulatory mechanism is employed by the transcriptional regulators of the iron-sulfur cluster biogenesis; SufR and IscR (see section 1.2.4.)

1.2.3. Iron-sulfur cluster biogenesis

Due to the destructive natures of free inorganic iron and sulfur, Fe-S cluster assembly needs to be tightly controlled to avoid the release of cluster components. In prokaryotes, Fe-S clusters are known to be assembled by three distinct proteinaceous machineries called NIF (nitrogen fixation), ISC (iron-sulfur cluster) and SUF (sulfur utilization factor), which all deliver iron and sulfur to a scaffold protein for assembly, followed by transfer of Fe-S clusters to the apoproteins. In eukaryotes, there is an additional CIA (cytosolic iron-sulfur cluster assembly) system for cytosolic iron-sulfur proteins. It is, however, strictly dependent on the ISC proteins, which are exported from mitochondria for use by the CIA machinery (Lill and Mühlenhoff, 2005).

Although genes associated with Fe-S cluster assembly have been identified in cyanobacteria, little is known about their actual function. All of the three major Fe-S cluster assembly pathways are represented in the *Synechocystis* genome, but their coverage and relative importance is different in comparison to other bacteria. The ISC pathway, for example, is considered to have a housekeeping role in Fe-S cluster assembly in non-photosynthetic bacteria (Zheng et al., 1998), but the system components are only partially represented in cyanobacteria (Balasubramanian et al., 2006). The NIF system, on the other hand, is utilized specifically in the formation and insertion of Fe-S cluster complexes of nitrogenase enzymes in nitrogen fixing species (Hu and Ribbe, 2011), such as cyanobacteria, azotobacteria and green sulfur bacteria. The SUF system is conserved among photosynthetic microorganisms and in plants, but is also found in archaea and in facultatively anaerobic bacteria as well as in non-photosynthetic apicoplasts of malaria parasites (Fig. 2). As the SUF system is typically recruited for the assembly of Fe-S clusters under conditions of oxidative stress or iron limitation (Takahashi and Tokumoto, 2002; Nachin et al., 2003; Outten et al., 2004), it is understandable that it is the dominant Fe-S cluster assembly system in the oxygenic photosynthetic cyanobacteria that are arguably under continual oxidative stress.

The assembly of Fe-S clusters requires two relevant initial events: Sulfur mobilization and iron acquisition. In the NIF system, initial phases of cluster formation occur via NifS which functions as a cysteine desulfurase by utilizing a pyridoxal 5'-phosphate -

dependent mechanism, where cysteine persulfide is formed on NifS. This persulfide is transferred to iron-bound NifU protein, which functions as a scaffold protein to assemble a nascent cluster. The cluster is further assembled on NifB and rearranged by NifE and NifN to ultimately form the most complex Fe-S cluster in nature; the [Mo–7Fe–9S] cluster of the dinitrogenase enzyme (Hu and Ribbe, 2011). The corresponding cluster assembly in the ISC system is carried out by IscS and IscU, but the biosynthesis is less complex due to the more simple structure of the Fe-S clusters; [2Fe-2S] and [4Fe-4S]. Besides IscS and IscU, the ISC-assembly system requires the HscAB chaperone system to transfer [2Fe-2S] clusters to the apoproteins, and ferredoxin to form reduced [4Fe-4S] clusters from two [2Fe-2S] clusters (Chandramouli et al., 2007). In *Synechocystis*, there are two IscS homologues, IscS1 and IscS2, but unlike in non-photosynthetic bacteria, they are not essential (Tirupati et al., 2004). Further, there are no genes homologous to IscU (Balasubramanian et al., 2006), suggesting that the ISC system has a less significant role in cyanobacteria.

The assembly of the Fe-S clusters by the SUF system differs from that of NIF and ISC systems. First, the SufS protein (encoded by the *sll0077* gene in *Synechocystis*), which is responsible of providing sulfur to the nascent Fe-S clusters in cyanobacteria, has a cystine lyase activity in addition to the NifS/IscS-like cysteine desulfurase activity (Kessler, 2004). In addition, the desulfurase activity of SufS is very poor, and requires an interaction with SufE to effectively mobilize the sulfur (Loiseau et al., 2003; Ollagnier-de-Choudens et al., 2003). Besides enhancing the desulfurase activity, the careful sulfane sulfur transfer from SufS to SufE via specific cysteinyl residues minimizes the release of sulfide and risk of oxidative damage. Further stimulation for SufS activity stems from the presence of the SufBCD complex (Outten et al., 2003), which might provide additional shelter for the assembly of the cluster. The exact function of each component of the SufBCD complex is not yet known, but it have been shown that in *E. coli* the complex serves as a scaffold for Fe-S cluster assembly, while SufA delivers the cluster to apoproteins (Chahal et al., 2009). The *E. coli* SufB contains cysteine residues that function as ligands for [4Fe-4S] cluster binding (*i. e.* a C-X_2-C-X_3-C motif), whereas SufD has multiple histidine residues, which could be used in binding of iron. SufC is an ATPase with an unusual ATP-binding-cassette-like component (Nachin et al., 2003) and could provide the energy for iron acquisition. Interestingly, despite the relatively high similarity among *E. coli* and cyanobacterial SufB and SufD amino acid sequences, the very features that implicate SufB in binding the Fe-S cluster and SufD in coordinating the iron, are either lacking (Fig. 2 a) or less well represented in cyanobacteria (namely, 13 histidine residues in *Synechocystis* SufD vs. 23 in *E. coli*). *Synechocystis* SufC on the other hand has an ATPase activity as well as high sequence similarity to the *E. coli* counterpart (Kitaoka et al., 2006). In *Arabidopsis thaliana*, the SufB homolog AtNAP1

(At4g04770) has been shown to also possess ATPase activity, which is not observed in *E. coli* (Xu et al., 2005). Thus, it is possible that both SufB and SufC are required for providing energy for the iron acquisition in *A. thaliana*, and perhaps also in other photosynthetic organisms.

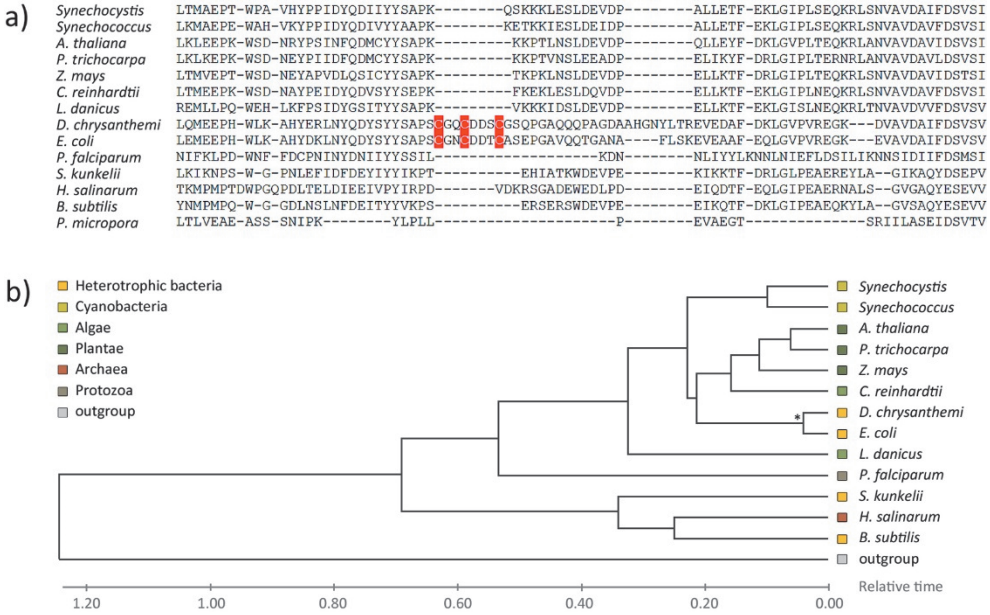

Figure 2. Sequence comparison of 13 SufB homologs from photosynthetic and non-photosynthetic organisms. (**a**) Partial amino acid sequence alignment with the [4Fe-4S] cluster binding cysteine residues, identified in two species, highlighted in red. (**b**) The phylogenetic tree of the complete SufB sequences was based on the alignment constructed by a neighbor-joining method. The sequences were aligned with MUSCLE, multiple sequence alignment tool (v. 3.8.31) (Edgar, 2004), and the tree was constructed by the Maximum Parsimony method with Subtree-Pruning-Regrafting (SPR) algorithm. The relative divergence times for all homologs were estimated with the Reltime method (Tamura et al., 2012) and the JTT matrix-based model (Jones et al., 1992) implemented in MEGA7 software (Kumar et al., 2016). Full species names and UniprotKB accession numbers for SufB homologs: *Synechocystis*; *Synechocystis* sp. PCC 6803; Q55790, *Synechococcus*: *Synechococcus* sp. PCC 7002; Q6UAC0, *A. thaliana*: *Arabidopsis thaliana*; Q9ZS97, *P. trichocarpa*: *Populus trichocarpa*; B9H1C6, *Z. mays*: *Zea mays*, B6SVH9, *C. reinhardtii*: *Chlamydomonas reinhardtii*; A8JE40, *D. chrysanthemi*: *Dickeya chrysanthemi*; Q9EXP5, *E. coli*: *Escherichia coli*; P77522, *L. danicus*: *Leptocylindrus danicus*; A0A023HCD2, *P. falciparum*: *Plasmodium falciparum* (isolate 3D7); Q25799, *S. kunkelii*: *Spiroplasma kunkelii*; A0A0K2JEM7, *H. salinarum: Halobacterium salinarum*; B0R3K1, *B. subtilis*: *Bacillus subtilis* (strain 168); O32162, and *P. micropora*: *Paulinella micropora;* A0A1L5YCI2 (outgroup).

The Fe-S cluster assembly scaffolds have been classified into two categories, the U-type and the A-type, based on their ability to assemble and mobilize clusters. The U-type scaffold proteins usually require chaperones to transfer the clusters to apoproteins. The A-type scaffold/carrier proteins either deliver the cluster from the U-type scaffold to apoproteins or act as alternative scaffolds for the cluster assembly, and possibly participate in iron acquisition (Ayala-Castro et al., 2008). The cyanobacterial Nfu

protein, which is similar to the C-terminal domain of *Azotobacter vinelandii* NifU protein, has the ability to transfer clusters to ferredoxin (Nishio and Nakai, 2000), indicating that it is not a typical U-type scaffold protein. As both Nfu protein and the proteins encoded by the *sufBCDS* operon (hereafter *suf* operon) are essential in cyanobacteria (Balasubramanian et al., 2006), there is a possibility they could complement each other in cluster assembly and delivery. The SufBCD-SE complex could act as U-type scaffold, while Nfu could transfer the Fe-S cluster to the target proteins, thus acting as an A-type protein. However, the Suf complex could also assemble the clusters within the apoproteins, as suggested by Outten et al. (Outten et al., 2003). The A-type scaffold proteins in cyanobacteria are IscA (encoded by *slr1565* in *Synechocystis*) (Balasubramanian et al., 2006) and SufA (encoded by *slr1417* in *Synechocystis*) (Wollenberg et al., 2003). Despite the nonessential roles of IscA and SufA in the cyanobacterium *Synechococcus* sp. PCC 7002 (hereafter *Synechococcus*), their deletion led to clear phenotypes under iron deprivation and redox stress, respectively (Balasubramanian et al., 2006). It was suggested that IscA would be involved in the regulation of iron homeostasis, due to its repressive effect on iron stress inducible genes (*isiA*, *sidA* and *sidC*) as well as on the *suf* operon and *iscS1* and *iscS2* genes under iron sufficiency. SufA, on the other hand, was suggested to be involved in sensing redox stress, as it was shown to repress the *suf* operon under oxidative and iron-deprived conditions (Balasubramanian et al., 2006).

1.2.4. Regulation of iron-sulfur cluster biogenesis

In order to maintain the physiological levels of the Fe-S clusters, Fe-S cluster biogenesis needs to correspond to the synthesis of the target apoproteins in which they are to be incorporated. If this balance is not achieved, it either results in accumulation of non-functional apoproteins or formation of soluble iron and sulfur or insoluble iron sulfides (Frazzon and Dean, 2001). To synchronize the demand and supply of Fe-S clusters, the cell typically relies on a feedback regulation model where the apo- or holo-form Fe-S cluster proteins control the genes responsible for Fe-S cluster biosynthesis (Schwartz et al., 2001).

The regulation of Fe-S cluster biosynthesis pathways has been best characterized in *E. coli,* and the regulatory features are commonly considered to be valid also for other bacteria due to the high level of amino acid sequence similarity of the associated proteins. However, the specific requirements for Fe-S clusters in different organisms vary due to diverse growth habitats and metabolic modes, and therefore one should be cautious in making generalizations between different bacterial species. An example of the sequence differences is presented in Fig. 2, where SufB homologs from 13 species were compared in a phylogenetic analysis.

The central regulator for Fe-S biogenesis in *E. coli* is IscR, a negative as well as positive transcriptional regulator for more than 40 genes (Giel et al., 2006). Many of these genes are involved in Fe-S cluster assembly, including *erpA* and *nfuA* genes in addition to the operons *iscRSUA-hscBA-fdx* and *sufABCDSE*. Both ErpA and NfuA are A-type carrier/scaffold proteins in *E. coli*, which are expressed under oxidative stress and iron starvation (Loiseau et al., 2007; Angelini et al., 2008; Py et al., 2012). The *isc* operon encode proteins that constitute the "housekeeping" Fe-S cluster biogenesis machinery (Zheng et al., 1998; Schwartz et al., 2001), while the *suf* operon encoding proteins comprise the Fe-S cluster biogenesis system under oxidative stress and iron-deprived conditions in *E. coli* (Lee et al., 2004; Outten et al., 2004). Homodimeric IscR binds a labile [2Fe-2S] cluster, which is used for sensing changes in intracellular redox state and iron availability (Schwartz et al., 2001; Nesbit et al., 2009). The sensory function of the Fe-S cluster in IscR is associated with the coordination of the cluster with three cysteines and one histidine (Fleischhacker et al., 2012). This structural conformation results in less efficient insertion of the Fe-S cluster in IscR, which ensures that the need for Fe-S cluster biogenesis for other proteins is fulfilled before holo-IscR can be formed. The cluster-bound IscR acts as a repressor for *iscRSUA* along with a range of several genes encoding Fe-S cluster binding and biogenesis proteins (Giel et al., 2006). As the cluster degrades, the binding affinity of apo-IscR to the promoter decreases resulting in the derepression of the target genes (Fleischhacker et al., 2012). As an alternative functional mode, under oxidative stress or iron deprivation, the cluster-free IscR binds to the promoter region of *sufABCDSE* and activates gene expression (Yeo et al., 2006). In addition to the role of IscR, the transition for using the SUF system as the predominant pathway for Fe-S cluster assembly under iron starvation is further enhanced by the effect of sRNA RyhB and the iron-sensor regulator Fur. RyhB binds upstream of *iscS* causing the 3' end of the *iscRSUA* transcript to be degraded, while *iscR* gets translated to apo-IscR, and leads to the induction of the *suf* operon (Desnoyers et al., 2009). In addition, both RyhB and *suf* operon are repressed by Fur under iron sufficient conditions, while in the absence of iron the abolished repression by Fur results in further *suf* operon induction (Patzer and Hantke, 1999). The regulatory circuit comprised of IscR and RyhB also controls the expression of ErpA (Mandin et al., 2016). Under iron sufficient conditions the transcription of *erpA* is repressed by IscR, whilst under iron deprived conditions the repression occurs via RyhB. It thus appears that the role of regulatory sRNAs (here specifically RyhB) is highly important in reallocating the available iron to the essential proteins under iron limitation, when the global iron-dependent regulator Fur cannot repress the genes involved in iron metabolism, such as the ISC system in Fe-S cluster biogenesis. The fine-tuned control of the regulatory circuit composed of a transcription factor and an sRNA also allows the induction of *isc*

operon and *erpA* gene within a narrow iron concentration range, where their expression is absolutely needed (Mandin et al., 2016).

In cyanobacterial model species *Synechocystis* and *Synechococcus*, the ISC system components are non-essential and only partially represented, as opposed to the SUF system which is both vital and fully represented, and thus considered to be the dominant Fe-S cluster assembly system (Seidler et al., 2001; Balasubramanian et al., 2006). In this system the Suf proteins are encoded by the *suf* operon, which is under regulation by SufR (Wang et al., 2004). Like IscR, SufR is a homodimeric transcriptional repressor with three cysteines and one non-cysteine residue for Fe-S cluster binding (Shen et al., 2007; Fleischhacker et al., 2012). There is also apparent functional analogy between the proteins, as both are known to regulate their own expression*; iscR* is regulated as a part of *iscRSUA* operon (Schwartz et al., 2001), whilst *sufR* is regulated independently from its own promoter, which has lower affinity to SufR than the *suf* operon promoter (Shen et al., 2007). In other aspects, SufR differs from IscR at least in terms of three distinctive features. First, IscR has a winged helix-turn-helix (wHTH) DNA binding domain characteristic of the Rrf2 family of transcriptional regulators (Finn et al., 2010), whereas SufR uses its N-terminal basic helix-loop-helix (bHLH) domain to bind DNA (Wang et al., 2004). Second, the homodimeric IscR binds one [2Fe-2S] cluster (Nesbit et al., 2009), while the homodimeric SufR binds two [4Fe-4S] clusters (Shen et al., 2007). Third, the oxidation state of the [4Fe-4S] cluster in SufR determines its binding to the *suf* operon and *sufR* promoter regions in *Synechocystis* (Shen et al., 2007), unlike in IscR where DNA binding is affected only by the presence or absence of the cluster (Fleischhacker et al., 2012). In the SUF system, the holo-SufR with a reduced $[4Fe\text{-}4S]^{1+}$ cluster has a similar binding affinity to the DNA as the apo-SufR, whereas the oxidized holo-SufR with a $[4Fe\text{-}4S]^{2+}$ cluster has the highest affinity to DNA (Shen et al., 2007).

The SufR-directed regulation applies the same principles as described for IscR; once the cellular demand for Fe-S cluster biogenesis is fulfilled, the [4Fe-4S] clusters are formed on SufR and *suf* operon becomes repressed. This repression is alleviated when the need for Fe-S cluster proteins increase; the resulting apo-SufR becomes less tightly bound to the *suf* promoter and transcription can be initiated. The induction of *sufR* and the *suf* operon would be expected to occur also under darkness, when the conditions are more reducing in cyanobacteria, and the DNA binding affinity of SufR decreases due to cluster reduction. However, differential RNA sequencing carried out in *Synechocystis* has shown that the induction of *sufR* transcripts in darkness is, surprisingly, not accompanied by the induction of the *suf* operon (Mitschke et al., 2011). In addition to *suf* operon regulation, SufR could also modulate transcription of a Fe-S cluster binding

protein, pyruvate:flavodoxin oxidoreductase (NifJ), as suggested by comparative genomics analysis (Novichkov et al., 2013).

Initially, SufR has been suggested to control PSI biogenesis in *Synechocystis*, as suppressor mutations found in the *sufR* gene compensated primary mutations in the PSI subunit *psaC* and restored the mutated PsaC to WT levels (Yu et al., 2003). The accumulation Fe-S cluster biogenesis proteins via the induced *suf* operon facilitated the maintenance of the F_B-[4Fe-4S] cluster in PsaC, thus allowing the photoautotrophic growth of the mutated strain. The deletion of *sufR* has been further studied in *Synechococcus*, where constitutive induction of the *suf* operon under standard, oxidative and iron-deprived conditions has been reported (Wang et al., 2004). The induction of the *suf* operon was shown to inhibit growth under standard conditions, but conferred a growth advantage under iron limiting conditions. The advantage was proposed to be based on efficient scavenging of iron by the SufBCD complex and its subsequent insertion into Fe-S cluster proteins.

1.3. Quantitative proteomics

1.3.1. Mass spectrometry-based proteomics

Mass spectrometry (MS)-based proteomics is an indispensable tool in global analysis of proteins in the cell as a part of systems biology research that aims to integrate data from different omics levels into a model that simulates organismal physiology as accurately as possible (Ideker et al., 2001). This kind of data integration can result in a more accurate description of biological events than could be obtained from any one method alone. The results can either verify (positive correlation) or contradict (negative correlation) existing data, and either way lead to more complete interpretation of complex data and underlying biology. In iron deprived *Synechocystis* cells, for example, 90 out of 1182 quantified proteins appear to have expression trends (fold change > ±1.5) different from those of transcript levels, as calculated from the available published data (Wegener et al., 2010). This kind of negative correlation can be explained by underlying post-transcriptional regulation (Georg et al., 2009; Huang et al., 2013), altered mRNA or protein stability (Eisenhut et al., 2007), or the timepoints of respective analyses. Thus, the complementary methods are crucial for revealing additional regulatory steps and underlying biological processes occurring at different omics levels.

The main technological challenges in proteomics stem from the fact that peptides, which are measured in a mass spectrometer, cannot be amplified as are oligonucleotides in DNA. Therefore the identification and quantification of proteins

relies on sensitive instruments in the challenging effort to detect even the least abundant peptides. Most MS-based proteomics workflows use a “bottom-up” strategy, where proteins are digested into peptides prior their analysis on a mass spectrometer. The proteins are usually digested with a trypsin protease (EC 3.4.21.4), which specifically cleaves the protein on the C-terminal side of arginine and lysine, generating peptides with basic C-termini. Concurrently, the peptides are usually treated with reducing and alkylating agents to avoid disulfide bond formation. Prior entering the mass spectrometer, the peptides are volatilized and ionized into the gas phase. This is most commonly accomplished by either of the following soft ionization techniques; matrix-assisted laser desorption ionization (MALDI) (Karas and Hillenkamp, 1988) or electrospray ionization (ESI) (Fenn et al., 1989). In MALDI, the ultraviolet-absorbing matrix, mixed and embedded with peptide analytes, sublimates as pulses of laser light hit the matrix, and the charged peptides vaporize into the gas phase. As the peptides collide with one another, they become fragmented and are accelerated to a mass analyzer. While MALDI is mostly used to analyze low-complexity samples, ESI is preferred for analysis of complex and unfractionated samples (Aebersold and Mann, 2003) due to the interface with a high-performance liquid chromatography (HPLC) system. Such systems are referred to as LC-ESI-MS systems. The HPLC can perform one or two dimensional peptide separation based on hydrophobicity and/or charge of the peptides (Washburn et al., 2001). The peptide ionization takes place at the end of the HPLC column and is generated by a strong electric field.

The positively charged (usually doubly protonated in ESI) peptide ions are guided by sophisticated and precise ion optics devices in the vacuum system of the mass spectrometer to the mass analyzer, which can be either an ion trap, quadrupole, time-of-flight (TOF) or Fourier transform ion cyclotron resonance (FTICR)-based Orbitrap analyzer. Many mass spectrometers take advantage of hybrid configurations of different analyzers in tandem mass spectrometry (MS/MS), where both precursor and fragment ions of the peptide are measured. The mass analyzers determine the mass-to-charge (*m/z*) ratio for the ions, which are measured and separated on the basis of the resolution, sensitivity and mass accuracy of the mass analyzer (Olsen et al., 2005). In LC-ESI systems, the mass spectrometer analyzes the peptides as they arrive at the analyzer according to their elution times from the HPLC. This results in acquisition of MS1 spectra, where the intensity of the *m/z* peak relates to the abundance of respective peptide. However, the abundance of different peptides cannot be compared directly because of different ionization efficiencies. In data-dependent acquisition (DDA) analysis, only the most abundant precursor ions in the MS1 spectrum are selected for fragmentation (Liu et al., 2004), giving rise to fragment ions. A collision induced dissociation (CID) and higher energy collisional dissociation (HCD) are the most

common fragmentation methods, which mainly result in peptide bond breakages, generating b- and y-ions (Roepstorff and Fohlman, 1984). Due to the breakage between amino acids, the *m/z* series (*i. e.* the MS2 spectra) of either b- or y-ions give rise to an amino acid sequence of the peptide they are derived from and thus can be used for peptide identification. The acquired MS2 spectra is typically compared against an existing sequence databases with a search engine, such as Mascot (Perkins et al., 1999) or Sequest (MacCoss et al., 2002), which calculates a probability score for peptide-identification based on peptide spectral match (PSM). The PSMs are usually validated by searching the MS2 data also against a decoy database (Moore et al., 2002), from which a false positive discovery rate (FDR) is obtained. Further improvement of peptide identification is provided by rescoring the target and decoy search results with validation algorithms such as Percolator (Käll et al., 2007; Brosch et al., 2009). Importantly, in addition to their use in identification, the number of MS2 spectra acquired for each peptide can also be used in spectral counting -based quantification.

1.3.2. Quantitative proteomics strategies

The MS-based protein quantification methods include a vast array of different strategies, which all have their advantages and limitations, and need to be considered to properly address the specific research questions in each case [see review (Domon and Aebersold, 2010)]. These strategies range from discovery to targeted approaches relying either on label-based or label-free, absolute or relative quantification, either at the MS1 or MS2 level. The general principles and workflows of existing proteomics strategies are described below.

The most widely used MS-based strategy is based on the DDA approach, which is commonly referred to as *shotgun* or *discovery proteomics*. The approach is suitable for identification of thousands of proteins from complex mixtures, but the analysis commonly results in poor reproducibility and a low dynamic range of peptide detection (Domon and Aebersold, 2010). The limited analytical capacity of the shotgun strategy results from the stochastic MS1-phase selection of only the most abundant precursor peptides for fragmentation (Michalski et al., 2011). This poses a problem for the detection of proteins present at low concentrations, which are masked by the large amounts of peptides derived from the most abundant proteins at any given time. Extensive sample fractionation is a way to increase the proteome coverage, but this can be costly and time consuming. Quantification by the shotgun method often relies on sample labeling, as it provides an internal reference and thus improves the precision of quantification (Käll and Vitek, 2011), but this requires extra sample processing steps, increases sample complexity and decreases the number of identifications. The shotgun measurements are either based on the MS1 precursor peak area or intensity (used for

metabolic labeling methods such as SILAC; Stable Isotope Labeling with Amino acids in Cell culture, and ^{15}N labeling), or on the number of identified MS2 spectra, referred to as spectral counting (used for chemical labeling methods such as iTRAQ; isobaric Tags for Relative and Absolute Quantification, TMT; Tandem Mass Tag, ICAT; Isotope-Coded Affinity Tag, and dimethyl labeling of amine groups). Of the available shotgun -based MS methods, the label free spectral counting, TMT, iTRAQ, ^{15}N metabolic labeling, and dimethyl labeling have been established and applied in cyanobacteria (Gan et al., 2005; Chong et al., 2006; Pandhal et al., 2008; Wegener et al., 2010; Guo et al., 2014; Spät et al., 2015).

A *directed* MS-approach alleviates the limitations of shotgun proteomics by separating the MS-analysis into two phases; i) MS1 level analysis (typically with an ion-trap-Orbitrap hybrid mass analyzer), including quantification of all detected precursor ions, followed by another run focusing on ii) MS2 level sequencing of the selected precursor ions from the first phase (Schmidt et al., 2008). The information acquired from the first phase (such as precursor ion charge state, *m/z* -ratio and chromatographic retention time) is used to design the second phase, with focus on the selected targets. With this approach, also known as *accurate inclusion mass screening* (AIMS) (Jaffe et al., 2008), an increased proteome coverage can be achieved compared to DDA analysis, and also low intensity precursor ions can be identified and quantified.

Both discovery and directed MS strategies can expedite the development of *targeted* MS experiments by providing information about precursor and fragment ions (Jaffe et al., 2008). This is a prerequisite for the design of *selected reaction monitoring* (SRM) assays, constituting one of the central focal themes in this Thesis. Targeted proteomics relies on the selective power of a quadruple (Q) mass analyzer, which permits only precursor ions with a certain *m/z* ratio to be selected for fragmentation. Although this also enables the detection of low abundant peptides from complex samples, the characteristic low resolution of the analyzer can also lead to incorporation of interfering ions. To enhance the specificity of measuring the precursor-derived fragment ions (*i. e.* transitions), a quadruple mass analyzer can be used in combination with i) another quadrupole (QQQ), which increases the sensitivity and selective power (SRM)(Anderson and Hunter, 2006), or with ii) an Orbitrap analyzer (Q-Orbitrap), which increases the selectivity even further due to the high resolution and mass accuracy (parallel reaction monitoring; PRM) (Peterson et al., 2012). In QQQ, the middle quadruple acts as a collision cell where fragmentation is achieved by CID, while in Q-Orbitrap the fragmentation occurs in an HCD collision cell. In SRM the two quadrupoles act as mass filters and only specific precursor and fragment ion *m/z* -ratios are targeted, whereas in PRM all the fragment ions are detected in Orbitrap after the specific

precursor ion selection. As an outcome, the few (typically 3-5) selected fragment ions are detected with greater precision in SRM, due to more data points for every fragment ion and increased time to measure them (*i. e.* shorter cycle times and longer dwell times, respectively). However, due to the high resolution of Orbitrap, the full fragment ion spectra with fewer interfering signals is recorded in PRM, hence improving the selectivity over SRM. Furthermore, the tedious effort required to develop optimized assays is avoided, as all fragment ions are monitored.

For several years SRM has been considered as the gold-standard method in MS-based protein quantification (Gillet et al., 2012; Marx, 2013). In recent years, however, several variations of SRM have been developed in an attempt to further improve the quantification. *Selected ion monitoring* (SIM) exploits the same instrument configuration as PRM, and despite being a sensitive quantitation method, an additional level of selectivity is missing, since the workflow includes only the precursor ion selection in the first quadrupole. Pseudo-SRM (pSRM) (Scherl et al., 2008), on the other hand, uses the combination of *linear ion trap* (LIT) and Orbitrap (LTQ-Orbitrap). The method is similar to PRM in acquiring full fragment ion spectra, but the targeted precursor ions are isolated in the LIT instead of in a quadrupole. The method works best for non-complex samples, as the ion accumulation in LIT can result in poor performance due to repulsive forces (Law and Lim, 2013).

To overcome the limitation of reproducibility and poor dynamic range of shotgun proteomics, and the relatively low throughput of targeted proteomics, many alternative precursor ion selection methods have been developed. In these *data independent acquisition* (DIA) approaches, the instrument fragments *all* precursor ions within a predetermined *m/z* window, instead of fragmenting only the most abundant ions across the complete precursor mass range as in DDA. Once the fragment ion spectra of the specific MS1 isolation window have been collected, the instrument proceeds to collect data from subsequent *m/z* windows until the complete precursor mass range is covered. At this point a new cycle through the *m/z* range can start, and be repeated across the HPLC chromatogram. There are several variants of DIA methods, which differentiate mainly on the basis of i) the instrument used, ii) the cycle time to measure the complete precursor *m/z* range, and iii) the width of the precursor isolation window (Shi et al., 2016). For example, in *precursor acquisition independent from ion count* (PAcIFIC) (Panchaud et al., 2009) the precursor isolation window is only 2.5 *m/z*, while in *sequential windowed acquisition of all theoretical fragment ion mass spectra* (SWATH) (Gillet et al., 2012) the window is 25 *m/z*. The wider isolation window in SWATH decreases the number of sample injections, but results in more complex fragment ion spectra as the link to the precursor ions is lost. This complicates the

subsequent data-analysis, which requires advanced tools and informatics resources, such as Spectronaut™ software (Biognosys)(Bruderer et al., 2015). The data-analysis is essentially based on information from existing spectral libraries, which are used for peptide identification. Thus, by using spectral libraries and targeted data-analysis, DIA combines the advantages of both DDA and SRM methods. Despite the recent advances, the DIA data-analysis still remains challenging. In addition, the sensitivity, specificity, and reproducibility of these methods do not reach the same levels as in SRM (Shi et al., 2016).

1.3.3. Targeted proteomics: Selected Reaction Monitoring

In order to contribute to the scope of comparable omics data in systems biology, the data generated should be reproducible, accurate and entail comprehensive information on as many proteins as possible, irrespective of their concentration in the sample. The unique capabilities of triple quadrupole (QQQ) instruments to select only the predetermined ions for MS-analysis, allow precise measurements of also the lowest abundant peptides in SRM.

Although SRM allows sensitive detection and provides reproducible results (Picotti et al., 2009; Abbatiello et al., 2015), the method development requires significant effort as the targeted precursor-to-fragment ion transitions need to be optimized for these assays. The SRM assay design is generally carried out *in silico* using either Skyline (MacLean et al., 2010), OpenMS (Rost et al., 2016), or MaxQuant (Cox and Mann, 2008) software platforms. For each targeted protein, prior MS information is required, and only those peptides that are known to consistently give good MS signals and uniquely represent the protein of interest are selected for the assay. Usually three to five of these *proteotypic peptides* (PTPs) are selected for each protein to ensure minimal variation and reliability in result interpretation. Typically, PTPs with +2 or +3 charge states, length from six to 25 amino acids, without ragged ends (*i. e.* without consecutive arginines and lysines), missed cleavage sites, and without methionines are preferred. Further, sites prone to glycosylation (N/E-X-N-X-S/T) (Kowarik et al., 2006) are avoided, if not specifically targeted. For the selection of fragment ions, three to five singly charged y-ions with *m/z* values higher than that of the precursor ion are preferred. Altogether, the selection of the best transitions comprises an explicit and reliable SRM assay.

The SRM assays are designed based on data acquired from the shotgun or directed MS experiments that may be found from repositories such as PeptideAtlas (Deutsch et al., 2008). However, if the MS/MS data (referred to as spectral libraries) cannot be obtained for peptides which fulfill the PTP criteria, the best theoretical PTPs can be

synthetized after their evaluation by peptide prediction tools (Tang et al., 2006; Mallick et al., 2007; Fusaro et al., 2009) and then used for assay development (Picotti et al., 2010). The synthetic peptides can be utilized to increase the proteome coverage, especially with respect to the low abundance proteins, which are often missed in the DDA methods.

The validated SRM assays are usually the outcome of multiple iterative MS-runs with several optimization steps (Lange et al., 2008). The optimization includes at least i) good correlation between the peptide elution time (retention time; RT) and the predicted or empirical retention times (Krokhin, 2006; Escher et al., 2012), ii) at least three co-eluting transition peaks to rule out the interfering signals, and iii) the correlation of relative intensities of the SRM transition peaks with the corresponding MS/MS spectral library. Commonly, decoy peptides are used to assign confidence levels for the target peptides using an mProphet peak scoring model (Reiter et al., 2011).

In order to take advantage of the full potential of SRM, *i. e.* to use it for the quantitation of as many proteins as possible with high sensitivity and accuracy, three interdependent parameters need to be in balance; namely, dwell time, cycle time and the number of measured transitions. Dwell time is the time that QQQ-MS spends in measuring a single predefined precursor-to-fragment ion transition. During a defined cycle time, the instrument cycles through a set of transitions, and records a signal from them. To measure the transitions with high sensitivity and accuracy in a single MS-run, the dwell time needs to be long enough (10 - 100 ms) and cycle time as short as possible (1,5 - 3 s) to obtain sufficient data points for each SRM-peak representing the transitions (Lange et al., 2008). This restricts the number of reliably measured concurrent transitions, unless the transitions are measured only at around a defined, expected elution time window of the corresponding peptide, instead of across the whole MS run. Thus, by multiplexing the SRM run by predefined data-acquisition time windows for each transition, the number of measurable transitions across the MS run can be increased without compromising the sensitivity (dwell time) and accuracy (cycle time).

The acquired SRM data are most commonly processed in Skyline software, where the peak areas of all of the peptide-specific transitions are integrated. The subsequent statistical analysis includes, for example, normalization and quantification. If known concentrations of heavy isotope-labeled internal standards are spiked into the sample, absolute quantification can be used to determine the exact protein concentration. However, a label-free approach is also possible, which relies on relative quantification between the tested sample and the control.

As setting up optimized SRM assays require significant effort, and as often there are common research interests focused on the same proteins in different projects and laboratories, open access to the established parameters facilitates the progress of research. There are several publicly available data repositories, such as the PeptideAtlas SRM Experiment Library (PASSEL)(Farrah et al., 2012) and Panorama Public (Sharma et al., 2014), where all of the validated SRM-parameters can be deposited and experimental files visualized.

2. AIMS OF THE STUDY

One of the founding aims of this Thesis work was to expand the scope of validated analytical techniques for the cyanobacterial model species *Synechocystis* sp. PCC 6803 by establishing a targeted proteomics method, *selected reaction monitoring* (SRM). The objectives of the method development were to (i) allow sensitive and accurate measurement of protein expression level changes at high throughput, (ii) provide a comprehensive overview of number of cellular functions and metabolic interactions at the protein level, and (iii) form a foundation for subsequent studies with expanded target libraries. The primary biological focus was on iron metabolism and Fe-S cluster biogenesis, with the objective of identifying associated protein level changes under iron deprivation, in response to deletion of genes for the transcriptional regulators *sufR* and *isaR1*, and in response to IsaR1 overexpression.

The primary research questions were:

1. To what extent the SRM method developed specifically for *Synechocystis* would improve the accuracy and depth in protein quantitation?

2. What kind of effects the induced iron-sulfur cluster biogenesis in the *sufR* deletion strain has on *Synechocystis* proteome under iron sufficient and depleted conditions?

3. How and to what extent the iron starvation inducible small RNA, IsaR1, affects the acclimation of *Synechocystis* to iron depletion?

3. METHODOLOGY

3.1. Cyanobacterial strains and growth conditions

The *Synechocystis* sp. PCC 6803 control (WT, WT+pVZ) and mutant (Δ*sufR*, Δ*isaR1*, *isaR1OE*, Δ*isaR1*+*isaR1OE*) strains were cultivated under photoautotrophic conditions under controlled, 1% (vol/vol) (Publication I, II) or atmospheric (Publication IV) CO_2, at +30°C, under a light intensity of 50 µmol photons m^{-2} s^{-1}. The cells were grown in BG-11 medium (Rippka et al., 1979), buffered with 10-20 mM TES-KOH (pH 8.0) in Erlenmeyer culture flasks shaking at 120 rpm.

Iron starvation was initiated by washing the precultures three times with iron-depleted BG-11 medium (that lacks $FeNH_4$-citrate), followed by inoculation into Fe-free BG-11 to obtain a starting $OD_{750\ nm}$ of 0,1 (Publication I, II). These cells were harvested at OD_{750nm}=1,0 from both iron sufficient and deprived conditions. Additional cultures were harvested after 12 days under iron deprivation. For the time-course analysis of the Δ*isaR1* mutant, iron starvation was triggered at the mid-logaritmic growth phase by addition of the iron-chelator desferrioxamine B (DFB, Sigma-Aldrich) to a final concentration of 100 µM. For the IsaR1OE and control strains, copper-free BG11 medium was used and induction of *isaR1* overexpression was achieved by the addition of 2 µM $CuSO_4$.

The deletion constructs Δ*sufR* and Δ*isaR1* were obtained by insertion of chloramphenicol resistance (Cm^R) and kanamycin resistance (Km^R) cassettes by homologous recombination to disrupt the *sufR* and *isaR1* genes, respectively (Publication II, IV). The IsaR1OE overexpression strain was obtained by inserting the *Synechocystis isaR1* gene between the copper inducible P_{petE} promoter and *oop* terminator in plasmid pVZ322. The plasmid was used in both WT and Δ*isaR1* background to make the control and complementation strains (Publication IV).

3.2. Measurement of *in vivo* absorbance spectra

In vivo absorption spectra were measured with an Infinite 200 PRO multiplate reader (Tecan) from 400 to 750 nm to evaluate the pigment composition under iron sufficient and deprived conditions in all characterized strains.

3.3. Protein extraction and immunodetection

Proteins were extracted as whole cell lysates in 0,1 M NH_4HCO_3, 8 M urea, 0,1% (w/v) Rapigest SF (Waters Corporation, Milford, MA) and 0,2 mM PMSF. The cells were

disrupted with glass beads, and the protein concentration was determined from the soluble fraction with the Bradford assay (Bradford, 1976). For immunoblots, protein samples were separated by 12% SDS-PAGE and transferred to PVDF membranes (Immobilon-P; Millipore). PsaB, PetA, PetF and PsbA antibodies were used for the immunodetection of the respective proteins on these membranes.

3.4. SRM-analysis

3.4.1. Design of the assay

SRM assays were designed in the open source software Skyline (MacLean et al., 2010). The amino acid sequences of *Synechocystis* sp. PCC 6803 from Cyanobase (Kaneko et al., 1996) were used as a background proteome, and *in silico* digested to find the potential PTPs and fragment ions to target in SRM. The 106 target proteins with precursor and fragment ions were filtered so that they fulfilled the criteria of quantifiable transitions (Publication I). The PTPs had to be unique for the protein and have either doubly or triply charged precursor ions, with six to 25 amino acids. The peptides with ragged ends and missed cleavages were excluded similarly as the peptides with methionines and sites prone to glycosylation. In the fragment ion selection, y-ions with *m/z* -ratios higher than the precursor were preferred.

3.4.2. Sample preparation

The extracted proteins were reduced with 5 mM dithiothreitol (DTT; Sigma) and alkylated with 10 mM iodoacetamide (IAA; Sigma), followed by overnight precipitation with acetone:ethanol (1:1) at -20°C. The protein pellets were solubilized in a buffer containing 50 mM NH_4HCO_3 and 5% (v/v) acetonitrile (ACN), to which trypsin (Sequence grade modified, Promega, Madison, WI, USA) was added twice at a 1:100 (w/w) trypsin to protein ratio followed by overnight incubation at +37°C. The peptides were desalted by solid phase extraction cartridge (3M Empore™ C18-SD), and the dried and purified samples were reconstituted in an aqueous solution containing 2% ACN and 0,1% formic acid.

3.4.3. LC-MS/MS analysis

The digested peptides (250 ng/ 5 µl) were separated and identified on a nanoflow HPLC system (EasyNanoLC 1000, Thermo Fisher Scientific) coupled to Orbitrap Velos Pro (Thermo Scientific) or Q Exactive (Thermo Scientific) mass spectrometer equipped with nano-ESI source. The peptides were loaded onto a trapping column and separated on an analytical column, where a 110 min gradient was used by increasing the solvent B percentage relative to solvent A (B = ACN:water, 95:5 (v/v), A = water:ACN, 98:2 (v/v))

with a 300 nl/ min flow rate from 5% to 20% in 70 minutes and 20% to 40% in 30 minutes.

LC-MS/MS settings were adjusted separately for the Orbitrap Velos Pro and Q Exactive mass spectrometers, which were used in data-dependent acquisition (DDA) mode. The ten or fifteen most intensive ions from the scan range of 300-2000 *m/z* with charges of +2 and +3 were selected for HCD or CID fragmentation. Further information about the LC-MS/MS settings on both mass spectrometers can be found from Publication I.

The LC-MS/MS spectra were searched against the *Synechocystis* protein database obtained from Cyanobase, using an in-house Mascot (v.2.4) search engine with search parameters described in Publication I. The data were analyzed with Proteome Discoverer (v.1.4) Software (Thermo Scientific) and the Percolator algorithm (v 2.04) was used to validate the peptide identifications with an FDR threshold of < 0,05.

3.4.4. LC-QQQ analysis

Peptides were loaded as 150 ng/ 5 µl injections onto the nanoflow HPLC system described earlier and separated by using a 60 min gradient at a flow rate of 300 nl/min (5-20% B in 35 min; 20–35% B during the following 15 min). The peptides were ionized by nano-electrospray and analyzed in a triple quadrupole mass spectrometer (TSQ Vantage, Thermo Scientific). The mass spectrometer operated in SRM mode as described in detail in Publication I. In all experiments the selected transitions were measured with a 2.5 s cycle time and >20 ms dwell time. Where applicable, the peptides were randomly distributed to different transition lists and the samples were randomly ordered to avoid bias in the experimental setup.

In the SRM -method development, up to five transitions for each 2 to 5 peptide precursors were targeted, to single out the best transitions to be used. The MS2 spectra from the DDA analyses from both iron sufficient and deprived conditions were used as a reference to compare the relative fragment intensities within the co-eluting transitions analyzed by SRM. The SSRCalc 3.0 –predictor (Krokhin, 2006), which is based on retention times and hydrophilicities of carbonic anhydrase peptides, was used initially to roughly evaluate the retention times (RT) of the targeted peptides. For those peptides that could not be found on the basis of SSRCalc predictions, unscheduled SRM runs were performed where all the transitions were monitored throughout the LC-gradient. The precision of RT estimation was improved further by the use of iRT standard peptides (Biognosys AG) together with endogenous and synthetic peptides, allowing an indexed retention time to be defined for each targeted peptide (Escher et

al., 2012). Both SSRCalc and iRT –based retention time predictors required initial calibration runs prior to their use in estimating retention times for target peptides.

3.4.5. Data-analysis

The SRM transitions were evaluated with mProphet peak scoring model (Reiter et al., 2011) implemented in Skyline. The algorithm compared the selected target transitions to generated reverse sequence decoy signals, and allowed training of the mProphet scoring model, which was used to improve peptide peak picking in Skyline.

The statistical analysis and protein quantification was performed with an R-based software package MSstats (v.2.6.0.) (Chang et al., 2012). The statistical analysis included recognition of the applied experimental design, *i. e.* group comparison experiment in Publication I, II and III, and a time-course experiment in Publication IV. Three biological replicates in each experiment determined the scope of conclusions from the data to be "restricted". The normalization method was based on global standard peptides used in all applied studies. In Publication I and II (and III) the normalization was based on peptides of the RNA polymerase omega subunit (*ssl2982*), while in the Publication IV, the peptides of the drug sensory protein A (DspA; *sll0698*) were used. The significant protein abundance changes were detected by applying linear mixed-effects models.

3.5. Determination of photosystem stoichiometry

The room temperature electron paramagnetic resonance (EPR) spectroscopy was performed with intact *Synechocystis* cells to record the relative quantities of PSII and PSI as described below. The Chl *a* concentration was determined after 90% methanol extraction by multiplying the absorbance at 665 nm with extinction coefficient of 78,74 $l\ g^{-1}\ cm^{-1}$ (Meeks and Castenholz, 1971), after which the concentration was adjusted to 4 mg/ml in all tested samples. The samples were illuminated with saturating light (5000 µmol photons $m^{-2}\ s^{-1}$), after which the samples were dark-adapted to obtain a stable tyrosine $D^{\bullet}$ radical for quantitation of PSII. The fully oxidized P700 of PSI was obtained by chemical oxidation in darkness, using 100 mM of the PSI electron acceptor $K_3[Fe(CN)_6]$. The relative quantification of $P700^+$ was performed by dividing the spin numbers of $P700^+$ with that of tyrosine $D^{\bullet}$ (Publication II).

3.6. Reverse transcriptase quantitative PCR

The RNA for reverse transcriptase quantitative PCR (RT-qPCR) analysis was extracted from *Synechocystis* cells by a phenol:chloroform method as described in paper II (adapted from (Tyystjärvi et al., 2001)). The RNA was precipitated and treated with

DNase (TURBO DNA-free kit Ambion), whereafter complementary DNA was synthetized from 1 µg of pure RNA (iScript™ cDNA synthesis kit, Biorad). The samples for RT-qPCR were labeled by iQ SYBR Green Supermix (BioRad). The qPCR was performed on an iCycler IQ Thermal Cycler (v. 4.006) and the data were analyzed with iQ™5 Optical System Software (v. 2.0) (BioRad). For the measurements, the optimal annealing temperature and amplification efficiency was determined for every amplicon, and the relative change in gene expression was determined by the Pfaffl method (Pfaffl, 2001), where *rimM* (*slr0808*) was used as a normalization gene (Mustila et al., 2016).

3.7. Microarray analysis

The RNA for microarray analysis was isolated by phenol:chlorophorm:isoamyl alcohol (25:24:1) extraction as described in Publication IV and in (Pinto et al., 2009). For the hybridization on custom microarray chips [Agilent; described in (Hernández-Prieto et al., 2012)], 1,65 µg of the labelled RNA was used. Data-analysis with Limma software (Ritchie et al., 2015), included correction for background fluorescence by the Normexp –method, as well as quantile normalization.

3.8. Computational prediction analysis for sRNA targets

Twenty cyanobacterial genomes containing homologs for IsaR1 were analyzed by the IntaRNA (Interacting RNA) tool (v. 2.0.2) (Busch et al., 2008; Wright et al., 2014), which was used to predict interaction sites between IsaR1 homologs and mRNAs in distinct genomes. The CopraRNA (Comparative prediction algorithm for small RNA targets) (v. 2.0.3.2) (Wright et al., 2013; Wright et al., 2014) was thereafter applied to predict the IsaR1 targets among all the 20 cyanobacterial species. The targets were further processed by functional enrichment analysis to distinguish the most affected functional categories. The IntaRNA predictions for the *Synechocystis* genome were additionally compared against the microarray results (Publication IV).

3.9. 77 K fluorescence and photosynthetic electron transfer measurements

The 77 K chlorophyll fluorescence emission spectra of intact *Synechocystis* cells were measured using a USB4000-FL-450 spectrofluorometer (Ocean Optics) with 440 nm excitation. The samples were adjusted to 7,5 µg/ml Chl *a* concentration and snap-frozen in liquid nitrogen.

PSI and PSII activities were measured with a pulse amplitude modulated fluorometer Dual-PAM-100 (Walz), from intact cells adjusted to a Chl *a* concentration of 15 µg/ml. The complete oxidation of P700 (P_m) was obtained by applying saturating pulses (5000

µmol photons m^{-2} s^{-1}, 300 ms), after far-red light illumination (720 nm, 75 W/m^{-2}). The effective yield, Y(I), as well as the non-photochemical quantum yield, Y(NA), of PSI was determined by application of saturating pulses (giving rise to parameter $P_{m'}$) on a background of actinic light illumination (giving rise to parameter P). The $P_{m'}$ and P parameters were used for calculating Y(I) from $(P_{m'}-P)/P_m$, and Y(NA) from $(P_m-P_{m'})/P_m$. The maximum yield of PSII, Y(II), was calculated as $(F_m-F_0)/F_m$, where F_0 is the minimum fluorescence recorded from dark-adapted samples upon turning on the measuring light, and F_m is the maximum fluorescence measured in the presence of 20 µM DCMU.

3.10. Fluorescence measurements of translational gene repression by IsaR1

To test the regulation of 22 mRNAs by IsaR1, a fluorescence based 5'UTR-sGFP (sGFP; superfolder green fluorescent protein) fusion system (Corcoran et al., 2012) was applied in *E. coli* (Publication IV). The fluorescence was measured directly from single colonies by means of an Accuri C6 flow cytometer (BD Biosciences). The colonies were inoculated into 2 ml LB medium, cultivated at 30°C for 12 h, and treated with 4% paraformaldehyde/1×PBS (pH 7,4). The cells were then washed with 1xPBS, and analyzed by flow cytometry. For each clone, 50 000 fluorescence events were collected, and six independent biological replicates were used. To calculate the *regulated specific fluorescence* of the 5'UTR–sGFP fusion for each target mRNA in the presence of IsaR1, the background fluorescence from the combination of IsaR1 and a negative control plasmid pXG-0 (Urban and Vogel, 2007) was subtracted from the obtained fluorescence. The *unregulated specific fluorescence* from the 5'UTR-sGFP fusion construct in the presence of negative control plasmid pJV300 (Sittka et al., 2007) was subtracted by the background fluorescence from the combined pJV300 and pXG-0 signals. Finally, the unregulated specific fluorescence was divided by the regulated specific fluorescence to obtain a fold change for the regulatory effect of IsaR1 on the specific mRNA.

3.11. Bioluminescence-based promoter induction analysis

To test the dynamic response of IsaR1 transcription activation in the course of iron deprivation, bioluminescence based promoter assays were performed (Klahn et al., 2014). The upstream sequences of both *isaR1* and *isiA* were fused to *luxAB* genes in plasmid pILA (Kunert et al., 2000) and introduced into *Synechocystis* expressing *luxCDE* genes. A plasmid lacking the promoter region served as a negative control.

3.12. Electrophoretic mobility shift assay

For the promoter gel shift experiments, an *isaR1* promoter fragment was amplified from the *Synechocystis* genome and cloned into the pT7Blue T-vector (Novagen). The free DNA (here the *isaR1* promoter in pT7Blue) and protein bound DNA (here FurA bound to the *isaR1* promoter) were separated on the basis of their different mobility on native polyacrylamide gel. Digoxigenin (DIG)-labeling-based gel mobility shift assay was used for detecting the protein bound DNA fragments. The assay was performed according to the protocol for the Roche's DIG gel shift reagent kit (2nd generation), and additionally, to avoid precipitation of the DIG-labeled probe, Zeba Desalt Spin Columns (Thermo Scientific) were used for buffer exchange.

His-tagged FurA was constructed in *E. coli*. The *furA* (*sll0567*) coding region was first amplified and cloned into the pT7Blue T-vector (Novagen), and then subcloned into the expression vector pET28a (Novagen). The obtained N-terminal 6xHis-tag expression construct was subsequently introduced into *E.coli* Origami2 (DE3) competent cells (Novagen), and induced by addition of 100 µM IPTG, after which the 6xHis-FurA protein was purified by means of cobalt -based immobilized metal affinity-chromatography (IMAC).

4. OVERVIEW OF THE RESULTS

4.1. Development of SRM assays for *Synechocystis* sp. PCC 6803

4.1.1. Selection of 106 target proteins

The first step in the SRM method development for *Synechocystis* was to select 106 proteins of interest as targets (Publication I, Table 1). As the focus of the Thesis was to study the metabolic effects of varying iron concentrations and associated regulatory systems, special emphasis was placed on proteins related to iron metabolism in terms of transport, Fe-S cluster biogenesis and use of iron as a cofactor. In addition, to obtain a more comprehensive overview of the changes within the cell, key proteins involved in photosynthesis, other anabolic reactions/auxiliary metabolism, and catabolic/amphibolic pathways were also selected for SRM assay development.

4.1.2. Protein identification by Data Dependent Acquisition (DDA)

For designing the SRM assays, the targeted proteins were first identified by shotgun LC-MS/MS analysis. Iterative shotgun runs for the samples collected from iron sufficient and iron deprived conditions resulted in identification of a total of 1710 proteins, with 15 031 unique peptides. Altogether 60 of the target proteins were identified in the DDA-based shotgun runs with more than two *proteotypic peptides* (PTPs) with good fragmentation spectra, and this information was subsequently used for the SRM assay design in Skyline and validation by QQQ-MS. For the remaining target proteins, which were not identified with sufficient number of PTPs, synthetic peptides were used. The peptides which fulfilled the criteria for PTPs in Skyline, and were the best ranked in the peptide detectability prediction tools, were chosen for synthesis. A total of 85 PTPs were synthetized (Publication I, Supplemental Table S-2), enabling reliable detection of 46 target proteins, which were not detected in the shotgun analysis due to their low relative abundance in the sample. As a consequence, the synthetic peptides enabled the design of SRM method for the low-abundance proteins (listed in Publication I; Table S-1), increasing the number of quantifiable proteins to 106.

4.1.3. SRM assay parameters

The definite SRM assays comprised several validated parameters which have been described in detail in Section 1.3.3. Establishment of the SRM assays for the 106 targeted proteins in *Synechocystis* included i) selection of the most optimal precursor-to-fragment ion transitions for two to three most abundant PTPs based on their precursor signal intensities. In this process, up to five fragment ions were chosen for each PTP, and ultimately the three most intense co-eluting fragment ions were

used in the quantification. The requirements for reliable SRM assays also included ii) good correlation between the relative fragment ion intensities in the SRM transition peaks and spectral library, and iii) a correlation between the target peptide retention times and predicted (SSRCalc) or empirical (iRT) retention time estimation. To maximize the throughput in the final experiment, indexed retention time (iRT) - standard peptides were used as references to obtain iRT values for each target peptide. As a result, after the initial alignment run with standard iRT peptides, the exact retention times and multiplexed assays with narrow retention time windows could be obtained in the following runs. Eventually, the 106 target proteins were randomly divided into three transition lists (Publication I, Supplemental Table S-2), allowing dwell times over 20 ms for each transition at any given time during the LC-gradient, and cycle times of 2,5 s with 5 min retention time windows for each peptide. The determined SRM parameters allowed sensitive assays at relatively high throughput for the selected target proteins in *Synechocystis*. These parameters are presented as a processed Skyline document published in Panorama Public (https://panoramaweb.org/labkey/ Vuorijoki_et_al_2015.url).

4.1.4. Application of SRM analysis to study iron deprivation

In the first case-study (Publication I), the established SRM assays were used for analysis of the iron-sufficient and iron-deprived *Synechocystis* batch cultivations harvested at OD_{750nm}=1,0, and after 12 days under iron deprivation. The first sampling point represented cultures in which the effects of iron limitation could already be observed in spectrophotometric analysis, and was based on optical density to avoid variation resulting from possible growth rate differences. The 12-d samples corresponded more drastic conditions, under which phenotypic effects were clearly visible. Out of the 106 target proteins, 96 proteins were quantified with an overall coefficient of variation (CV) of 10% for all these peptides (Publication I, Supplemental Table S-4). The remaining 10 undetected proteins that could not be quantified were ones that in some cases were not expressed at all under the tested conditions. These included, for example, the Flv2 and Flv4 proteins as well as CmpA, which are known to have negligible or markedly decreased expression levels under high carbon conditions (Omata et al., 1999; Zhang et al., 2009).

Of the quantified 96 proteins, 87 and 92 showed adjusted p-values <0,01 under short-term (OD_{750nm}=1,0) and long-term (12 days) iron deficiency, respectively. Significant expression level changes (*i. e.* fold changes >1,5; Log_2 fold change >0,585), as determined by MSstats analysis, were recorded for 57 proteins in short-term and 71 proteins in long-term treatment. The SRM analysis for the short-term iron-deprived samples (Publication I, Table 1) revealed systematic and significant decrease of the protein complexes in photosynthetic electron transfer chain, including the proteins

associated with phycobilisomes, PSII, the Cyt b_6f complex and PSI. The decrease in the iron-rich photosynthetic complexes was accompanied by a decrease in the SdhB and NDH-1 proteins NdhB and NdhI, which take part in respiration and donate electrons to the PQ pool and subsequently to the Cyt b_6f complex (Cooley and Vermaas, 2001). In parallel, the expression of terminal respiratory oxidases, which alleviate the reduction of the PQ pool upon insufficient capacity of Cyt b_6f (Vermaas et al., 1994; Berry et al., 2002), increased, although their upregulation under short-term iron deprivation was below the significance threshold (Log_2FC >0,585). Along with decreased photosynthetic capacity under iron deprivation, there was also a decrease in the expression of several soluble electron carrier proteins with iron or iron-sulfur clusters, which are involved in the photosynthetic electron transfer reactions. These proteins included several ferredoxins (Fdx2, Fdx4, Fdx5 and Fed7) and the flavodiiron proteins Flv1 and Flv3. On the contrary, the chlorophyll-binding iron-stress-induced protein A (IsiA), the ferredoxin -substituting electron carrier flavodoxin (IsiB), the phycobilisome core - associated photoprotective orange carotenoid protein (OCP), IdiA, which protects the acceptor side of PSII and binds the non-haem ferric iron between the Q_A and Q_B sites, as well as carbon-fixation-related proteins (CcmM, CupA, and RbcL) were all upregulated. In addition, the targeted thioredoxins which, for example, affect the activity of RuBisCo (Lindahl and Florencio, 2003), as well as enzymes in the pentose phosphate pathway, were induced by iron deprivation. The upregulation of phosphoenolpyruvate carboxylase and isocitrate dehydrogenase (ICD), which are responsible for the formation of the central TCA cycle intermediates oxaloacetate and *α*-ketoglutarate, respectively, was also observed. However, pyruvate:flavodoxin oxidoreductase as well as other Fe-S cluster containing proteins in the TCA and glycolate cycles were decreased. Other significantly downregulated iron or Fe-S cluster containing proteins were superoxide dismutase and the diaphorase subunits of bidirectional hydrogenase. In contrast to the downregulated Fe-S cluster-containing proteins, the transcriptional repressor of the Fe-S cluster biogenesis, SufR, was distinctly upregulated. This was accompanied by increased levels of cysteine desulfurase IscS1 (Slr0387) and cystine lyase (CefD), which are involved in mobilization of sulfur into the Fe−S clusters (Behshad et al., 2004). The ferric uptake regulatory protein FurA, which is the global repressor of several iron acquisition proteins under iron sufficient conditions, was significantly downregulated, and this was accompanied by the induction of the proteins associated with iron transport (Fut-proteins, FhuA, FeoB) and mobilization (MrgA).

The long-term iron deprivation induced extensive changes in the overall protein expression profile (Publication I, Table 1), characterized by enhanced impacts on the levels of many proteins as compared to the short-term treatment. As an example, the

expression level of the RNA polymerase sigma factors, SigB and SigC, increased already in response to a short-term iron deprivation, but the increase was even more pronounced under extended iron deprivation. In contrast, the level of the primary sigma factor, SigA, was markedly reduced. Besides the diaphorase subunits of the bidirectional hydrogenase, which were negatively affected already under short-term treatment, the prolonged iron stress resulted in significant downregulation also of the hydrogenase subunit HoxH. Upregulation of the SufD and SufS proteins involved in Fe-S cluster biogenesis was accompanied by elevated expression of SufR under long-term iron deprivation. Further interesting observations included an increase in expression of Flv1 under long-term iron deprivation, contrary to the opposite effect under short-term treatment. Also Flv3 exhibited similar but less significant expression changes. In general, the expression of thioredoxins, and proteins with regulatory functions (LexA, NtcA, and GlgP) was further increased in the long-term treatment.

4.2. Characterization of SufR in *Synechocystis* sp. PCC 6803

4.2.1. Inactivation of SufR and resulting phenotype

The *sufR* gene (*sll0088*), encoding the *suf* operon repressor protein SufR in *Synechocystis*, was inactivated to evaluate associated factors and metabolic interactions in regards to Fe-S cluster biogenesis. The deletion was achieved by targeted insertion of a chloramphenicol resistance (Cm^R) cassette in the middle of *sufR,* separating the N-terminal DNA-binding motif from the C-terminal domain involved in [4Fe-4S] cluster binding (Wang et al., 2004; Shen et al., 2007). The Δ*sufR* mutant strain did not differ from WT *Synechocystis* in terms of growth under either iron sufficient or depleted conditions, but the culture absorbance spectra revealed an increase in the amount of carotenoids, and reduced phycobilisome and Chl *a* content in the mutant under all tested conditions. These differences became more pronounced during the long-term (12-day) iron depletion in batch culture, and resulted in a clear brownish phenotype as judged by visual inspection (Publication II, Fig. 4 C).

4.2.2. SRM analysis of the Δ*sufR* mutant

The developed SRM assays were applied to study the detailed protein-level effects resulting from the deletion of *sufR* in *Synechocystis*. The Δ*sufR* mutant and WT were both analyzed under iron sufficient and deprived conditions after short-term cultivation (at OD_{750nm}=1,0) and extended incubation (12 days). Altogether 94 proteins, including ones with very low expression levels and small expression fold changes, were quantified with low p-values in the designed assays. To differentiate the effects of *sufR* deletion from iron deprivation, all the tested conditions and strains were first

compared against the WT strain under iron sufficient conditions, after which the mutant was compared against WT in each separate condition. The SRM experiment details, including the transition list and raw files can be found in PASSEL (Farrah et al., 2012) with a dataset identifier PASS00765, and the SRM results can be accessed in Panorama Public (Sharma et al., 2014) as a complete Skyline document (https://panoramaweb.org/labkey/SufR).

4.2.3. Induction of Fe-S cluster biogenesis results in suppression of Fe-S proteins under iron sufficient conditions

The *suf* operon proteins, SufB, SufC, SufD and SufS, in addition to SufA were all highly induced in the Δ*sufR* mutant under iron sufficient conditions, demonstrating for the first time at protein level that SufR acts as a repressor of the *suf* operon in *Synechocystis*. This effect coincided with a decrease in the amount of several Fe-S cluster proteins and in this respect resembled the effects observed under iron deprivation. The most downregulated Fe-S proteins included pyruvate:flavodoxin oxidoreductase NifJ, succinate dehydrogenase Fe-S protein SdhB, diaphorase subunit HoxF and hydrogenase subunit HoxH of the bidirectional hydrogenase. Other expression trends analogous to those induced by iron deprivation were the downregulation of Flv1 and Flv3, and of phycobilisome proteins.

Contrary to the effects induced by iron insufficiency, the proteins involved in carbon fixation, iron transport, and fatty acid metabolism were downregulated in the Δ*sufR* mutant. The decrease in the carbon-fixation-associated proteins was accompanied by an elevated expression of the glycolate oxidase iron-sulfur subunit, GlcF, involved in the photorespiratory pathway (Publication II).

4.2.4. Long-term iron deprivation induces the expression of Fe-S proteins in the Δ*sufR* mutant

The short-term iron deprivation resulted in only modest changes in the Δ*sufR* mutant in comparison to the WT, with the most distinct changes observed in the induction of GlcF and *suf* operon proteins. Under long-term iron deprivation the overall protein expression profile was altered more extensively, but the Suf protein expression remained only moderately induced in the mutant. The clearest effects under the long-term treatment were the decrease of PSII-associated proteins, an increase in the expression of Fe-S proteins, and differential expression of ferrous and ferric iron transport systems. The proteins of PSII, phycobilisomes and the iron-rich Cyt b_6f complex were all downregulated, while the PSI proteins were repressed to a lower extent in the Δ*sufR* mutant than in the WT (Publication II, Table 3). Despite of the differences observed in the expression of PSII and PSI proteins, the relative ratio of

functional PSI and PSII reaction centers was not affected on the basis of electron paramagnetic resonance (EPR) analysis. The EPR profiles of oxidized P700 and TyrD$^{\bullet}$ representing PSI and PSII, respectively, were similar in both the Δ*sufR* mutant and the WT under long-term iron-deprived conditions.

In addition to the alleviated repression of PSI subunits in the mutant in comparison to the WT under extended iron deprivation, other Fe-S proteins such as the diaphorase subunits of the bidirectional hydrogenase and the NdhI subunit of the NADH dehydrogenase showed less repression in the Δ*sufR* strain. The ferrous iron transport and binding proteins were downregulated together with the alternative respiratory terminal oxidase (CtaDII), suggesting a decrease in the reductive iron uptake capacity in the Δ*sufR* mutant (Kranzler et al., 2014). At the same time the ferric-iron-specific Fut system was increased in comparison to WT.

4.2.5. Transcript analysis verifies *sufB* and *nifJ* as targets for SufR regulation

Seven representatives from the set of most affected proteins in Δ*sufR* mutant under differing iron concentrations were selected as targets for transcript-level analysis to see if the same expression trends would also be reflected in the amount of the respective mRNAs, thus indicating a direct transcriptional regulation by SufR (Publication II). A quantitative reverse transcriptase PCR (RT-qPCR) analysis was applied to study the genes encoding the proteins, which exhibited similar expression trends under all the tested conditions *i. e.* Fed4 (*slr0150*) and SufB (*slr0074*), or iron-dependent expression (upregulation in iron sufficiency and downregulation in iron deficiency) in the Δ*sufR* mutant *i. e.* Fed2 (*sll1382*). The Fe-S cluster proteins NifJ (*sll0741*) and SdhB (*sll0823*) were also selected as targets for the transcript analysis because they were clearly downregulated at the protein level under iron sufficient conditions. In addition, the genes for SufR (*sll0088*) and SyNifU (*ssl2667*) were included in the analysis. SyNifU had not been included in the SRM analysis due to lack of quantifiable PTPs, but the gene was selected as a relevant target for RT-qPCR since it has been suggested to participate in Fe-S cluster assembly (Nishio and Nakai, 2000).

The relative transcript-level changes in *fed2*, *fed4*, *sdhB*, and *synifU* were negligible across all tested conditions in the Δ*sufR* mutant, suggesting that the expression changes observed in SRM may not have been direct consequences of SufR inactivation, and rather associated with regulation specifically at the translational level. The expression of the *nifJ* and *sufB* genes, on the other hand, was in agreement with the expression level changes observed at the protein level, implying that these two genes could be direct targets for SufR-mediated transcriptional regulation.

4.3. The function of regulatory sRNA IsaR1 under iron deprivation

4.3.1. IsaR1 expression is regulated by FurA, and induced by iron deprivation

The regulatory sRNA IsaR1 (Iron-stress activated RNA 1) is a 68 nt long non-coding RNA, which earlier has been referred to as NC-181 (Hernández-Prieto et al., 2012), and found to be the sixth most highly-induced transcriptional unit in *Synechocystis* under iron deprivation (Kopf et al., 2014). IsaR1 has homologs across the cyanobacterial phylum, and the conserved sequences tend to form a stem-loop secondary structures followed by a poly-uracil tail, which is characteristic for Rho-independent terminators. The alignment of *isaR1* promoter regions of 31 cyanobacterial homologs revealed a potential binding site for the global transcriptional regulator FurA (Publication IV), similar to that on the promoter region of the chlorophyll-binding, iron-stress-inducible protein, IsiA (Kunert et al., 2003). To evaluate the *in vivo* promoter activity, bioluminescence-detection -based promoter fusion assays were carried out to compare the promoter activation of both *isaR1* and *isiA* in the course of iron deprivation. Iron deprivation was shown to trigger *isaR1* expression, following similar dynamics as the induction of *isiA*, indicating a released repression by FurA. The binding of FurA to the *isaR1* promoter region was further tested with electrophoretic mobility shift assays (EMSA), which gives an indication of direct interaction between the protein and DNA. The observed gel shifts caused by FurA binding were in agreement with the suggested role of FurA as a transcriptional repressor of *isaR1*.

4.3.2. Characterization of IsaR1 mutants reveal a link to the photosynthetic apparatus

To characterize the effects of IsaR1 in detail, *isaR1* deletion and overexpression strains were generated. The deletion strain was obtained by disrupting the *isaR1* gene with a kanamycin resistance cassette, and the overexpression of *isaR1* (IsaR1OE) was generated by introducing *isaR1* into plasmid pVZ under the control of the copper-inducible PetE promoter. A complementation strain was built the same way as the overexpression strain, but in the deletion background. The absorption spectra of the *isaR1* deletion strain from both iron-sufficient and iron-deprived conditions showed a more extensive decrease in pigmentation than the WT or the complementation strain (Publication IV, Fig. 1 A-C). Biophysical measurements were conducted to evaluate the effects of IsaR1 overexpression on the photosynthetic machinery in a time course experiment under iron sufficient conditions (Publication IV, Fig. 1 D-H). A clear increase in the PSII/PSI ratio was observed in 77 K Chl *a* fluorescence-emission spectra in comparison to the control strain harboring the empty plasmid (WT_pVZ_P_{petE}) after four days of copper induction. In agreement with this result, there was a drastic decrease in the amount of oxidizable P700 (P_m) of PSI as well as a decreased expression of the PsaB protein. Furthermore, a decreased photochemical quantum yield, Y(I), and

an increased acceptor side limitation, Y(NA), of PSI was recorded. The significant reduction in PSI capacity was accompanied by only a moderate decrease in the maximum quantum yield of PSII (F_v/F_m), suggesting that the photosynthetic electron flow was mainly affected downstream of PSII.

IsaR1 was further characterized at the transcript level in a time course experiment, where the effect of the *isaR1* deletion was studied in the presence and absence of iron. Despite the low expression level of *isaR1* under iron-sufficient conditions, the deletion caused notable changes in the balance between carbon and nitrogen metabolism; the genes involved in carbon uptake were downregulated, whilst nitrogen assimilation genes were upregulated. In addition to these transcriptomic changes, the *in vivo* absorption spectra revealed decreased Chl *a* and phycobilisome contents in the Δ*isaR1* mutant in comparison to the WT under iron sufficiency. Under iron deficiency, the depigmentation of the Δ*isaR1* mutant became more pronounced and this phenotypic effect could also be seen at the transcript level, as the expression of several phycobilisome-encoding genes along with PSII, PSI, and carbon-fixation-associated genes were decreased. On the contrary, several genes encoding iron-containing proteins, such as superoxide dismutase (SodB), aconitate hydrogenase (AcnB) and ferredoxin 1 (Fed1), in addition to the Suf proteins of the Fe-S cluster biogenesis machinery, were upregulated.

4.3.3. Prediction tools and microarray data address targets for IsaR1 regulation

To predict the interaction between IsaR1 homologs and the target mRNAs across 20 distinct cyanobacterial strains, the separate IntaRNA predictions from different species were computed with CopraRNA software to find the best scoring targets for IsaR1 regulation. Those targets, which were in the top-100 list predicted by IntaRNA or CopraRNA, and had a $\log_2$FC > ±0,5 in the microarray analysis of the IsaR1 overexpression strain at 6 h, were considered as possible IsaR1 targets (Table 1). In addition, the genes which showed differential expression between mutant and control after 6 hours of induction with a $\log_2$FC > ±0,9 (adjusted *p*-value <0,05) (Table 1; column A), and those which were likewise affected upon copper induction [(IsaR1OE 6h – IsaR1OE 0h) – (WT+pVZ 6h – WT+pVZ 0h)], were selected as potential targets (Table 1; column B). Those genes which were differentially (Log_2FC ≥ ±0.8) expressed at the beginning of the experiment (at 0 h) were excluded (Table 1; column C). Of the qualified targets, 19 transcripts were induced and 41 repressed upon IsaR1 induction. The genes associated with carbon uptake comprised the major functional group among the upregulated targets, while a set of mRNAs and 5' UTRs of genes closely associated with photosynthesis, in addition to the genes encoding iron-containing proteins were amongst the repressed targets. The photosynthesis-associated targets included the transcripts for the PSI associated Fed1, as well as for Cyt *f*, Cyt b_6 and subunit IV of the Cyt b_6f complex.

Transcription of the genes encoding iron-binding superoxide dismutase and SufC, which is part of the SufBCDS complex involved in Fe-S cluster biogenesis, were repressed. Interestingly, *sufZ* which is transcribed at the 5' UTR of *sufB* was among the most highly-induced IsaR1 targets, while the *sufB* transcription was repressed, although to a lesser extent than that of *sufC*.

Table 1. Forty-one repressed and 19 induced IsaR1 targets fulfilling the selection criteria described in the text. Column A; IsaR1OE - WT_pVZ (6h), Column B; (IsaR1OE_6h-IsaR1OE_0h) - (WT_pVZ_6h-WT_pVZ_0h), Column C; IsaR1OE - WT_pVZ (0h). IsaR1OE refers to the IsaR1 overexpression strain with induction by Cu.

Nr. of targets	Protein names	Gene names	A	B	C	adj.*p*-value	Rank CopraRNA	Rank IntaRNA
1	Ferredoxin 1	*petF, ssl0020*	-2,51	-2,25	-0,25	3,46E-15	2	8
2	Cytochrome b6	*petB, slr0342*	-1,52	-1,54	0,02	2,13E-14		21
3	PatA subfamily	*slr1594*	-1,48	-1,17	-0,31	5,13E-08		
4	Negative aliphatic amidase regulator	*urtA, slr0447*	-1,45	-1,82	0,36	2,83E-11		
5	Cyanoglobin (Hemoglobin)	*glbN, slr2097*	-1,44	-1,21	-0,23	5,75E-14		
6	Superoxide dismutase[Fe]	*sodB, slr1516*	-1,39	-1,07	-0,33	4,12E-12	4	71
7	Ssr2848 protein	*ssr2848*	-1,38	-0,82	-0,56	7,78E-08		
8	Slr1667 protein	*cccS, slr1667*	-1,21	-1,40	0,19	9,99E-06		
9	SufC, probable ATP-dependent transporter	*ycf16, slr0075, sufC*	-1,20	-1,33	0,12	7,59E-08	70	
10	Cytochrome b6-f complex subunit 4	*petD, slr0343*	-1,09	-1,18	0,09	4,58E-12	7	
11	NA	*ncr0380,SyR14, CsiR1*	-1,08	-0,50	-0,58	6,52E-12		
12	Apocytochrome f	*petA, sll1317*	-1,01	-1,07	0,05	5,87E-10	84	
13	NA	*ycf64, slr1846*	-1,00	-0,91	-0,09	2,49E-08		
14	Slr0708 protein	*slr0708*	-0,97	-1,22	0,25	1,01E-09		
15	Aconitate hydratase 2	*slr0665*	-0,95	-1,01	0,06	7,44E-11	15	
16	Sll0536 protein	*sll0536*	-0,94	-1,30	0,36	9,74E-11		
17	Ssl2384 protein	*ssl2384*	-0,93	-1,73	0,79	1,37E-12		
18	Slr1677 protein	*slr1677*	-0,92	-0,62	-0,30	1,56E-11		
19	Slr1593 protein	*slr1593*	-0,91	-1,15	0,24	6,82E-09		
20	SufD	*slr0076, sufD*	-0,91	-1,05	0,13	2,68E-07		
21	Uncharacterized protein sll0944	*sll0944*	-0,91	-1,59	0,68	8,47E-10		
22	Slr1676 protein	*slr1676*	-0,91	-0,60	-0,31	1,47E-10	5	52
23	Dihydroxy-aciddehydratase (DAD)	*ilvD, slr0452*	-0,88	-1,04	0,17	2,17E-08	43	100
24	Cytochrome c-550	*psbV, sll0258*	-0,80	-1,03	0,22	1,49E-10	24	
25	Mg-chelatase subunit	*chlH, slr1055*	-0,78	-0,75	-0,04	7,00E-08		61
26	Cyanophycin synthetase	*cphA, slr2002*	-0,77	-0,97	0,20	3,06E-11		
27	Cytochrome b-559 subunit alpha	*psbE, ssr3451*	-0,74	-0,40	-0,34	2,50E-05		63
28	Sll0733 protein	*sll0733*	-0,73	-1,15	0,42	2,02E-07		
29	Glutamine-binding periplasmic protein	*bgtB, sll1270*	-0,71	-1,04	0,34	1,82E-12		
30	Sll0327 protein	*sll0327*	-0,69	-1,33	0,64	1,06E-11		
31	Glutamyl-tRNA reductase	*hemA, slr1808*	-0,68	-0,77	0,09	1,45E-13	10	25
32	Heterodisulfide reductase subunit B	*hdrB, slr0201*	-0,68	-0,37	-0,31	7,53E-09		48
33	Molybdopterin biosynthesis protein	*moeA, slr0900*	-0,61	-1,31	0,70	8,59E-06		
34	Slr1201 protein	*slr1201*	-0,58	-1,23	0,64	1,08E-09	37	
35	Sll0783 protein	*sll0783*	-0,55	-1,14	0,60	1,28E-06		
36	SufB	*ycf24, slr0074, sufB*	-0,54	-0,75	0,21	7,80E-05	3	17
37	Putative ammonium transporter sll1017	*amt2, sll1017*	-0,54	-1,09	0,56	2,86E-05		
38	PatA subfamily	*sll1291*	-0,50	-0,56	0,06	5,81E-09		87
39	Photosystem II reaction center protein J	*psbJ, smr0008*	-0,45	-0,51	0,06	1,81E-05	30	
40	Nitratereductase	*narB, sll1454*	-0,45	-1,01	0,56	6,55E-06		
41	Molybdenum cofactor biosynthesis protein A	*moaA, slr0901*	-0,42	-0,98	0,56	4,84E-06		
1	Orange carotenoid-binding protein	*slr1963, ocp*	0,42	0,93	-0,50	4,73E-03		
2	HTH-type transcriptional activator cmpR	*cmpR, sll0030*	0,48	1,24	-0,75	2,31E-10		
3	NA	*ncRNA_983563:983626*	0,52	1,06	-0,54	1,16E-10		
4	Slr1544 protein	*slr1544*	0,55	1,00	-0,45	2,66E-11		
5	Ssr1562 protein	*ssr1562*	0,64	1,15	-0,50	1,50E-13		
6	Heat shock protein	*htpG, sll0430*	0,65	0,95	-0,30	2,88E-03		
7	Uncharacterized isomerase slr1019	*slr1019*	0,68	1,23	-0,55	3,37E-11		
8	Cytochrome b subunit of nitric oxide reductase	*norB, sll0450*	0,70	-0,09	0,78	1,16E-09		32
9	Ssl1911 protein	*gifA, ssl1911*	0,92	1,01	-0,09	2,65E-15		
10	Ssr1038 protein	*ssr1038*	0,93	1,19	-0,26	3,52E-09		
11	Glyceraldehyde-3-phosphate dehydrogenase 1	*gap1, slr0884*	1,01	1,22	-0,21	1,63E-08		
12	Rubisco operon transcriptional regulator	*ndhR, sll1594*	1,13	1,47	-0,34	3,39E-05		
13	Slr2006 protein	*slr2006*	1,34	1,40	-0,06	4,68E-04		
14	Slr1512 protein	*sbtA, slr1512*	1,44	1,50	-0,06	3,45E-07		
15	NA	*ndhF3, sll1732*	1,58	1,80	-0,21	4,12E-07		
16	Slr0616 protein	*slr0616*	1,59	2,13	-0,54	1,09E-07		
17	NA	*ndhD5, slr2007*	1,59	1,75	-0,15	5,45E-07		
18	5'UTR of SufB	*sufZ*	1,97	1,76	0,21	1,54E-09		
19	Bicarbonate-binding protein cmpA	*cmpA, slr0040*	2,08	2,79	-0,71	3,70E-11		

4.3.4. Effects of IsaR1 on protein levels and the photosynthetic apparatus

The selected set of potential IsaR1 targets were analyzed at the protein level by SRM and immunoblot analyses, as well as by heterologous, superfolder GFP (sGFP) reporter system. *Fed1* and *sufB* were the highest ranking targets in the CopraRNA prediction, followed by SodB, AcnB and Cyt *c*-553, in addition to the components of the Cyt b_6f complex and tetrapyrrole biosynthesis enzymes. All of these targets were repressed in the IsaR1 overexpression strain after 6 h of copper induction, as indicated by microarray and sGFP analysis (Publication IV; Data S2 and Fig. S4 and S5). Out of the eight IsaR1 target proteins selected for SRM, five (SufB, SufC, SufD, AcnB and PsbE) showed similar expression trends in the IsaR1 overexpression strain as observed on transcript level. This was further supported by the analysis of the deletion strain, which gave an opposite expression pattern (Table 2). The function of IsaR1 as a repressor was also verified by immunoblot analysis of the overexpression strain targeting Fed1 and PsaB, which was in agreement with microarray experiments of Δ*isaR1* mutant under iron deprivation (Publication IV; Data S1). Furthermore, a number of genes *(sufB, sodB, chlN, petJ, petF, psaA, acnB, psbE, ilvD and hemA)* were shown to be direct targets of IsaR1 -mediated repression, by fusing the target gene 5' UTRs to sGFP, followed by fluorescence analysis in the presence of IsaR1 in *E. coli*. In addition, the opposite role of IsaR1 as an activator of gene expression was verified both on protein and transcript level for bicarbonate binding protein, CmpA (Tables 1 and 2).

Interestingly, despite the observed repressive effect of IsaR1 on *suf* operon transcription based on microarray data, the transcriptional start site (TSS) 119 nt upstream of the *sufB* start codon was found to be the tenth most highly-induced during iron deprivation (Kopf et al., 2014). As indicated by Northern blot analysis in the current study (Publication IV; Fig. 6B), this TSS was found to be transcribed only in the presence of IsaR1 and turned out to be an sRNA, annotated as *sufZ*. In parallel, the *sufBCDS* transcript and the corresponding protein levels were downregulated in IsaR1OE, while they were highly induced under iron deprivation in the Δ*isaR1* mutant. These analyses revealed yet another level of regulation associated with the SUF system, as the transcriptional repressor of the *suf* operon, SufR, was strongly upregulated in IsaR1OE, and downregulated in the deletion mutant (Table 2). In summary, the expression of IsaR1 coincided with induced transcription of *sufR* and *sufZ*, while the binding of IsaR1 to the seed region at the 5'UTR of *sufB* led to repression of the *suf* operon.

Table 2. Quantified proteins in SRM assays for IsaR1 overexpression (IsaR1OE) and deletion (Δ*isaR1*) strains after 96 hours of induction and iron depletion, respectively. The green to red gradient represents increase in the expression levels at Log2 scale. Particular emphasis was placed on the putative IsaR1 targets identified based on microarray and prediction tools (bold text, Table1). The expression fold change -values with asterisk are measured with adjusted p-value >0,05.

Protein	Gene names	Log_2FC_IsaR1OE_96h	Log_2FC_Δ*isaR1*_96h
Sll0219	*flv2*	-4,31	0,35
Slr0074	***ycf24, sufB***	**-1,34**	**1,85**
Slr1516	***sodB***	**-1,27**	**-1,12**
Slr0665	***acnB***	**-1,19**	**0,28**
Slr0075	***ycf16, sufC***	**-1,15**	**2,08**
Slr0077	*sufS, nifS*	-1,07	1,64
Slr0148	*fdx*	-0,95	-0,37
Sll0306	*rpoD, sigB, sigB2*	-0,93	-0,56
Sll1316	*petC, petC1*	-0,87	-0,18
Slr0737	*psaD*	-0,85	-0,19
Sll1221	*hoxF*	-0,82	-0,20
Slr0076	***sufD, sufB***	**-0,79**	**1,93**
Slr0150	*petF, fdx, fdx IV*	-0,79	-0,38
Slr1329	*atpD, atpB*	-0,66	-0,22
Sll1626	*lexA*	-0,57	-0,63
Slr1643	*petH*	-0,57	-0,30
Slr1835	*psaB, psaA*	-0,44	-0,01*
Slr2094	*fbpI, glpX*	-0,35	-0,69
Sll0427	*psbO*	-0,31	-0,16
Sll0849	*psbD1, psbD, psbD-1, psbDI*	-0,31	0,22
Sll0662	*fed7*	-0,27*	-0,71
Slr2067	*apcA*	-0,27	-0,36
Ssr3451	***psbE***	**-0,26**	**0,44**
Sll0223	*ndhB*	-0,23*	-0,50
Sll0208	*ado*	-0,17*	-0,87
Sll0698	*hik33, chk33, ycf26, dspA, nblS*	-0,12*	0,12
Slr0335	*apcE*	-0,12*	-0,63
Ssl2982	*ycf61*	0,03*	0,03*
Sll0329	*gnd*	0,03*	-0,72
Sll0567	*fur, furA*	0,06*	-0,91
Slr0009	*rbcL*	0,07*	-0,74
Ssl0563	*psaC, psaC2*	0,14*	-0,13*
Sll1226	*hoxH*	0,15	-0,29
Slr1417	*ycf57, iscA, sufA, iscA1*	0,20	-0,44
Sll1578	*cpcA*	0,26	-0,62
Sll1454	***narB***	**0,30**	**-0,55**
Sll0520	*ndhI*	0,41*	-0,59
Slr1239	*pntA*	0,43	-0,78
Sll0248	*isiB, flaA*	0,45	-0,88
Slr0040	***cmpA***	**0,99**	**0,07***
Sll0088	*sufR*	1,05	-0,96

5. DISCUSSION

5.1. The use of SRM to study iron-deprived cyanobacteria

The access to comprehensive and accurate proteomics datasets on metabolic interactions and regulatory mechanisms is increasingly important for the progress of cyanobacterial research. This is particularly relevant for harnessing the biosynthetic potential of cyanobacteria for future biotechnological applications in a current day bioeconomy. The downfall in acquiring high-quality datasets by most proteomics methods relates to the lack of sensitivity, reproducibility, or throughput. Shotgun proteomics has long been the most widely used method as it allows the identification of even thousands of proteins in a single MS run (Washburn et al., 2001). But despite its superior efficiency, it still lacks the ability to detect low abundance proteins, and due to the nature of the data dependent acquisition, it suffers from poor run-to-run reproducibility. In this Thesis, a targeted proteomics method, *selected reaction monitoring* (SRM), was designed for *Synechocystis* in order to monitor the expression level changes of also physiologically relevant low abundance proteins -both consistently and at relatively high throughput. The work demonstrated quantification of a set of previously undetected proteins from unfractionated cell lysates without compromising data quality nor consuming excess time on sample processing.

SRM-assays were designed for a set of proteins with a central importance in iron metabolism, photosynthesis or closely related functions. The separate case studies focusing on i) iron deprivation (Publication I, II, IV), ii) Fe-S cluster metabolism (Publication II), and iii) photosynthesis (Publication IV), were explored by SRM to gain in-depth protein level information about the complex metabolic interconnections. This Thesis work provided important new information about the regulatory networks associated with iron and iron-sulfur cluster metabolism as well as photosynthesis, in addition to verifying and expanding several earlier observations in iron-deprived *Synechocystis* cells. In brief, the work demonstrated the importance of the tightly regulated iron-sulfur cluster biogenesis by transcriptional regulator SufR and sRNA IsaR1 under varying iron concentrations, and the role of post-transcriptional regulation by IsaR1 in the acclimation of *Synechocystis* to iron deprivation.

5.2. Evaluation of the established SRM protocol for *Synechocystis*

5.2.1. Fulfillment of the assay criteria for SRM

The careful selection and validation of the targeted three transitions for the two to three proteotypic peptides for each protein were a prerequisite for the successful SRM

assays described in this Thesis. While the selected parameters gave SRM the potential to reach excellent analytical depth and accuracy, the strict requirements also limited the number of quantifiable SRM targets. Thus, several low molecular mass proteins of potential interest, which were not represented by enough quantifiable PTPs, had to be excluded from the developed SRM assays (Publication I).

To exclude interfering false signals that commonly arise from the sample matrix in the low-resolution triple quadrupole MS-instruments (QQQ-MS), the co-eluting transitions with Gaussian peak shape, and good correlation between the SRM-traces and the reference spectra from shotgun analyses increased the confidence for measuring correct transitions. To further rule out any interfering signals in the established SRM assays, the selected transitions were evaluated by an mProphet peak scoring model (Reiter et al., 2011), which distinguished the selected target transitions from decoy signals, resulting in a false discovery rate (q-value) <0,05 for each correct SRM-peak.

In addition to the assay development and signal processing in Skyline software, an essential part of the SRM workflow was the protein significance analysis with the MSstats software (Chang et al., 2012). This statistical analysis supported unbiased quantification of the proteins, including the recognition of the applied experimental design, the extent of the conclusions, the data quality assessment and normalization.

5.2.2. Technical and biological comparison of SRM and DDA

Sensitive and reliable SRM assays were developed and validated for 106 proteins with central roles in responses to iron deprivation and related cellular processes in *Synechocystis*. The method was first applied to test the effects of iron deprivation and to compare the performance of SRM against the discovery proteomics (DDA) carried out by Wegener et al. under similar conditions (Wegener et al., 2010).

The higher sensitivity of the SRM method was demonstrated by the finding that two thirds of the quantified target proteins (64/96) remained undetected in the DDA approach (Publication I). The use of synthetic peptides facilitated the SRM assay development for the quantification of those PTP's which could not be detected due to the technical limitations of the DDA, and thus considerably increased the dynamic coverage of the SRM method.

The SRM and shotgun-based analysis (Wegener et al., 2010) of iron-deprived *Synechocystis* cells resulted in different expression patterns for seven of the 32 proteins quantified in both studies. In addition, the microarray data from three earlier studies on iron deprivation experiments (Singh et al., 2003; Shcolnick et al., 2009; Hernández-Prieto et al., 2012), revealed several divergently expressed genes in comparison to the

protein level changes recorded by SRM (Publication I; Supporting Table S-10). These opposite trends in regulation may reflect differences in culture conditions, sampling times and sample processing, but also altered translational efficiency. Complex regulatory systems involving sRNAs appear to be rather common in *Synechocystis* (Georg et al., 2009), and may account for a translational repression of a given transcript and consequent reduction of the corresponding protein-level signal. Alternatively, mRNA instability, high translational efficiency, increased protein stability, and/or possibly a slow turnover and dilution of the proteins during deferred cell division could explain the higher relative protein levels in comparison to the transcripts. A high protein to transcript ratio was apparent, for example, for the proteins related to carbon fixation (CcmM, CupA, RbcL). A similar discrepancy on transcript and protein abundance levels was observed earlier for *ccmK* and *rbcL* upon the shift from high to low-carbon conditions (Eisenhut et al., 2007).

5.2.3. Metabolic interconnections revealed by SRM under iron deprivation

The results obtained from SRM were in agreement with several known cellular responses to iron deprivation (Hernández-Prieto et al., 2012; Fraser et al., 2013), which served as an additional validation for the developed assays. The observed iron-starvation-triggered changes were seen as reorganization of the photosynthetic apparatus in response to a decreased capacity to perform photosynthesis. The enzyme-level reorganization was specifically characterized by changes which serve to protect the photosynthetic apparatus upon over-reduction of the electron transfer chain (Fig. 3).

The observed decrease of PSII proteins and associated phycobiliproteins was accompanied by an accumulation of OCP, which is known to function in the dissipation of excess energy arriving to PSII (Wilson et al., 2006; Wilson et al., 2007). Similar level of downregulation as with PSII was recorded for the proteins associated with the Cyt b_6f complex, and even greater decrease in relative abundance was seen with PSI associated iron-rich proteins. This highlights the importance of decreasing the electron flow to PSI in response to the lowered capacity of the complex to participate in electron transfer reactions, which would otherwise lead to over-reduction of the photosynthetic electron transfer chain. SRM analysis provided important direct information on how *Synechocystis* cells tackled this problem by inducing non-photochemical quenching (NPQ) by increased expression of OCP, concurrently with elevated expression of electron sinks such as respiratory terminal oxidases (Ermakova et al., 2016). On the other hand, the expression of the Fe-S cluster -containing respiratory complexes NDH-1 and SDH, which feed electrons into the PQ pool (Cooley and Vermaas, 2001), were greatly decreased (Publication I, Table 1). Interestingly, the change from short-term to long-term iron deprivation led to upregulation of the flavodiiron proteins Flv1 and Flv3,

which have been shown to function as electron sinks providing protection for PSI (Allahverdiyeva et al., 2011; Allahverdiyeva et al., 2013). This may be an indication of acclimation to a new redox balance, which is reached upon extended iron deprivation.

Cell growth in the stationary phase in the absence of iron also involves physiological changes which do not reflect the direct effects of iron deprivation itself. These general stress responses include, for example, the observed induction of group 2 RNA polymerase sigma factors (Sig). SigB and SigC, in particular, have shown be important for gene expression at the stationary growth phase and to induce expression of NtcA-dependent genes, such as the PII transcription factor (GlnB) (Asayama et al., 2004; Imamura et al., 2006), which binds *α*-ketoglutarate and consequently induces nitrate uptake (Lee et al., 2000). In accordance with the effects of SigB and SigC on the nitrogen metabolism, an increased expression of proteins with key regulatory functions in nitrogen (NtcA) and carbon (LexA) metabolism (Alfonso et al., 2001; Domain et al., 2004), was observed under extended iron deprivation by SRM. In cyanobacteria, these two metabolic pathways are interdependent; the nitrate uptake requires sufficient cellular CO_2 fixation (Flores et al., 1983), and is also activated by *α*-ketoglutarate (Lee et al., 2000). The global nitrogen regulator NtcA activates the expression of ICD (Muro-Pastor et al., 1996), which catalyzes the conversion of isocitrate to *α*-ketoglutarate, while LexA activates bicarbonate transport and respiratory genes, but also reduces the conversion of pyruvate to phosphoenolpyruvate via phosphoenolpyruvate synthase (PEPS) (Domain et al., 2004), promoting the flux towards TCA-cycle. LexA also represses the glycolytic EMP-pathway via downregulation of phosphofructokinase (Domain et al., 2004), thus inducing the flux through oxidative pentose phosphate pathway for increased production of NADPH. Taken together, the upregulation of NtcA, LexA, ICD, SigB and SigC under iron deprivation with the observed increase in enzymes related to CO_2 fixation (Publication I), implied that nitrogen assimilation would be enhanced at the stationary growth phase under extended iron deprivation. The upregulation of nitrogen assimilation has been associated with iron deprivation also earlier, but at transcript level (Hernández-Prieto et al., 2012). It is conceivable that the signal which activates the nitrogen metabolism and to which SigB and SigC respond to, is the decreased growth rate, which is encountered in the absence of iron. In parallel to ICD, another iron-independent enzyme associated with the TCA-cycle, phosphoenylpyruvate carboxylase, was upregulated, which suggests further increase in the carbon flux towards the biosynthesis of glutamate, aspartate and the derived amino acids. In addition, the pronounced upregulation of the pentose phosphate pathway (PPP) enzymes, despite the elevated levels of phosphofructokinase, suggested diversion of the metabolic flux towards pathways which compensate for the reduced NADPH/NADH ratio when photosynthetic activity is compromised. Altogether,

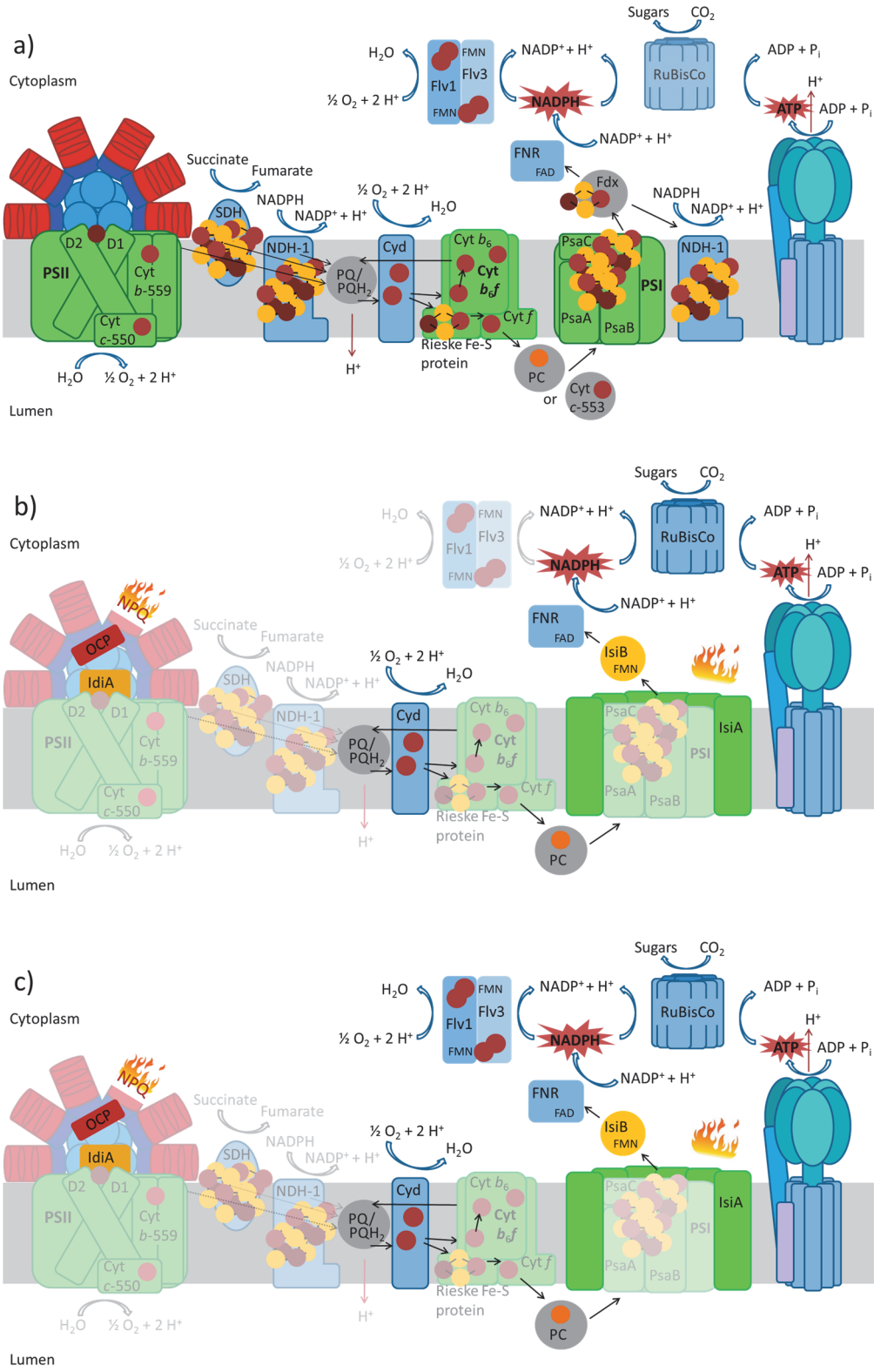
a)
Cytoplasm
Lumen
Sugars
CO2
RuBisCo
ADP + Pi
ATP
H+
NADP+ + H+
NADPH
H2O
½ O2 + 2 H+
FMN
Flv3
Flv1
FNR
FAD
Fdx
Succinate
Fumarate
SDH
NDH-1
PQ/
PQH2
Cyd
Cyt b6
Cyt b6f
Cyt f
Rieske Fe-S
protein
PC
or
Cyt
c-553
PsaC
PsaA
PsaB
PSI
PSII
D2
D1
Cyt
b-559
Cyt
c-550
b)
NPQ
OCP
IdiA
IsiB
IsiA
c)

these processes contribute to providing biosynthetic building blocks and energy to the cell which may act to compensate for the downregulation of autotrophic metabolism.

The acclimation to iron deficiency also included elevated expression of iron-deficiency-induced protein A (IdiA), which protects the acceptor side of PSII (Exss-Sonne et al., 2000). IdiA (also named as FutA1) functions also as part of the Fut system, which is required for iron transport and is highly-induced together with other iron transport and mobilization proteins under iron starvation. The induction of IdiA expression has been shown to be followed by an accumulation of the iron-starvation-induced, chlorophyll binding antenna protein CP43' (IsiA) as well as flavodoxin (IsiB) (Yousef et al., 2003) – the elevated levels of these proteins were also observed in SRM. IsiA is known to form protective rings around the monomeric or trimeric PSI under iron starvation (Bibby et al., 2001; Yeremenko et al., 2004), but it also serves as a dissipator of excess energy as a self-aggregated multimeric complex (Ihalainen et al., 2005). IsiB, on the other hand, replaces Fdx as the main electron transfer protein when sufficient iron is not available for Fdx to function properly (Laudenbach et al., 1988). Many of the above mentioned iron-deficiency-induced proteins are known to be repressed by the global transcriptional regulator FurA, which is degraded upon iron deprivation by the FtsH1/ FtsH3 protease complex (Krynická et al., 2014). The decreased level of FurA under iron deprivation was confirmed also in the SRM-analysis.

Figure 3. Simplified representation of acclimation of the photosynthetic apparatus to iron deprivation in *Synechocystis*, based on the expression changes observed in SRM. Photosynthetic electron transfer components in the thylakoid membrane of WT cells **a)** under iron-sufficiency, **b)** under short-term iron deprivation (OD_{750nm}=1,0), and **c)** in long-term iron deprivation (12 d). Protein downregulation as compared to iron sufficient conditions is represented in dim colours and upregulation or steady expression levels in bright colours. Iron atoms are marked with red, sulfur atoms with yellow and copper with orange dots. In the course of iron deprivation the photosynthetic apparatus is reorganized so that the main structural components PSII, the Cyt b_6f complex and PSI are downregulated, together with the associated phycobiliproteins and Fe-S cluster containing respiratory NDH-1 and SDH complexes. While the proteins, which feed electrons into the electron transfer chain are downregulated, the proteins which serve to protect the photosynthetic complexes, are upregulated. These include OCP and IdiA associated with the protection of PSII, respiratory terminal oxidases, such as Cyd (putative cytochrome *bd*-type quinol oxidase) which alleviates the reduction of PQ-pool upon limited Cyt b_6f functionality, and IsiA, which forms single and double rings around trimeric and monomeric PSI complexes, respectively. The iron or Fe-S cluster containing proteins Fdx and Cyt *c*-553, are replaced upon iron deprivation with IsiB and PC, respectively. The electrons are passed on from PSI to Fdx or IsiB, and further to Ferredoxin-NADP($^+$) oxidoreductase (FNR), which generates NADPH that is mainly used by RuBisCo in CO_2 fixation, and Flv1/3 heterodimer in oxygen photoreduction. Upon iron deprivation, the elevated expression levels of RuBisCo large subunit is initially accompanied by decreased expression of Flv1/3 (b), but upon long-term iron deprivation, the expression levels are elevated (c).

The iron deprivation also led to a decrease in several iron-sulfur cluster as well as other iron-containing proteins in different functional categories. These included several enzymes of the TCA-cycle (excluding ICD and phosphoenylpyruvate carboxylase), as well as the subunits of the bidirectional hydrogenase. The subtle increase in Fe-S cluster biogenesis enzymes (SufBCDS) was accompanied by substantially higher induction of SufR, the transcriptional regulator of *suf* operon genes. This difference suggests that besides the SufR –mediated regulation, there is an additional regulatory level for the *suf* operon which does not affect SufR expression. In addition, there was a clearly higher induction of the CefD cystine lyase and IscS1 cysteine desulfurase enzymes, in comparison to SufS cysteine desulfurase. While SufS requires SufE to enable the persulfide cleavage and sulfur mobilization for the target proteins (Loiseau et al., 2003), CefD and IscS1 can mobilize sulfur independently and thus more readily (Behshad et al., 2004).

5.3. The Fe-S cluster biogenesis in *Synechocystis* is controlled by an iron-dependent mixed regulatory circuit

The SUF system has been suggested to function mainly under oxidative and iron stress on the basis of studies carried out in the marine cyanobacterium *Synechococcus* sp. PCC 7002 and in the enterobacterium *E. coli* (Outten et al., 2004; Wang et al., 2004). SUF comprise the main Fe-S cluster biogenesis machinery in cyanobacteria, while ISC, which has a housekeeping role in *E. coli*, is only partially represented in cyanobacterial genomes and thus considered to have a less important role in Fe-S cluster biogenesis.

The primary goal of the Fe-S cluster biogenesis machinery is to supply adequate levels of Fe-S clusters for the target apoproteins, while the system reacts to sufficient Fe-S cluster levels by repressing cluster biogenesis via a feedback loop – typically by an Fe-S cluster -binding transcription factor. The balance between the demand and supply of Fe-S clusters is further affected by the availability of iron and the expression levels of the corresponding iron-dependent proteins; it would be physiologically most cost-effective to allocate the iron to the most essential Fe-S cluster proteins, while avoiding wasteful excess production of the clusters. Thus, while the *suf* genes responsible for Fe-S cluster biogenesis are essential in *Synechocystis* (Balasubramanian et al., 2006), they need to be controlled across a wide range of iron concentrations to avoid futile (Publication II), or on the other hand non-sufficient (Zang et al., 2017), Fe-S cluster biogenesis.

In this Thesis, the tight regulation of the *suf* operon genes was demonstrated under varying iron concentrations (Fig. 4). An sRNA IsaR1 and the transcriptional regulator SufR were found to be responsible for this control under different iron concentrations,

forming a *mixed regulatory circuit* for *suf* operon expression. In the presence of sufficient iron and Fe-S clusters, SufR was shown to be the main repressor of the *suf* operon (Publication II), while under iron deprivation repression occurred via IsaR1 (Publication IV). An indication of the strictly balanced Fe-S cluster biogenesis

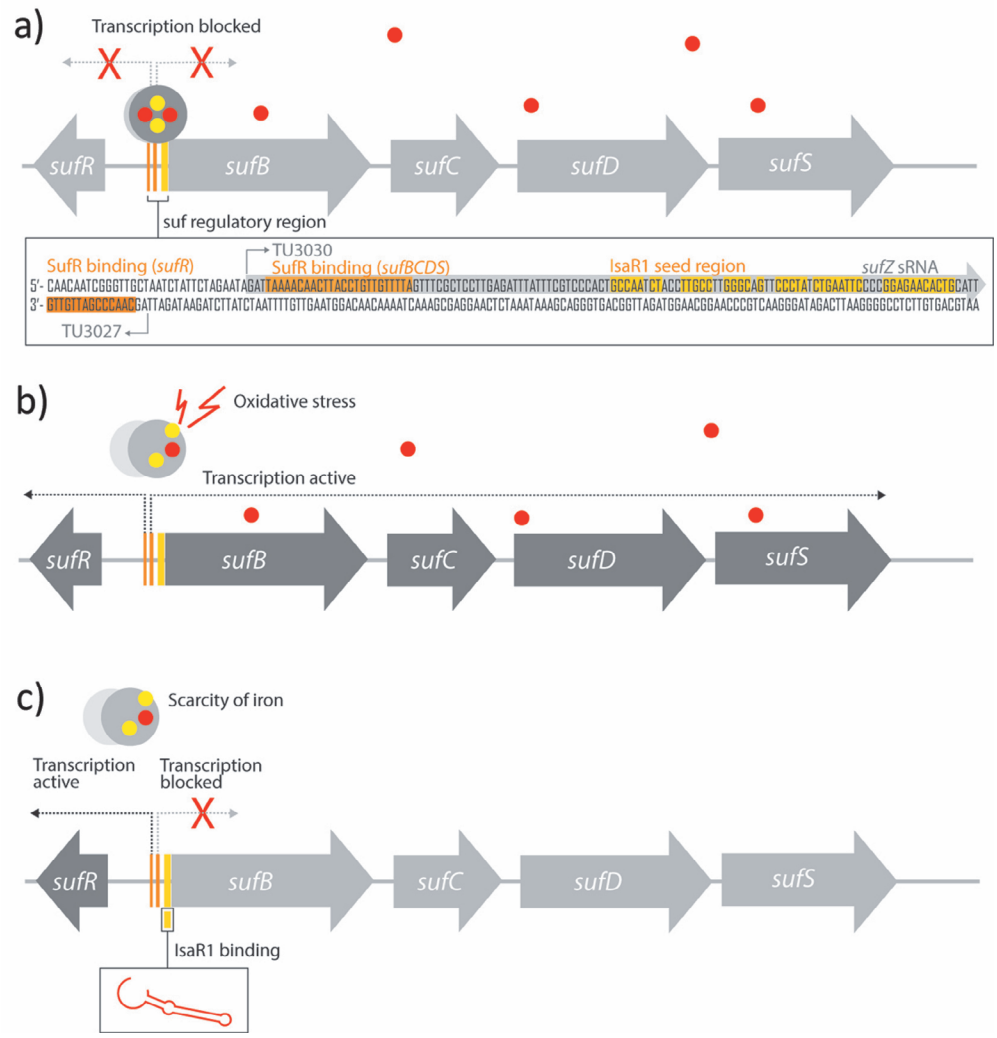

Figure 4. **The regulatory regions of *sufBCDS* and *sufR*, with conditions for repression and induction.** Under iron sufficient conditions, when there is no need for biogenesis of additional Fe-S clusters, (a) the holo-SufR harboring intact [4Fe-4S] clusters binds to the adjacent promoters of the *sufR* and *suf* operon, and represses the transcription of *sufR* and *sufBCDS*. Under oxidative stress conditions, (b) the SufR Fe-S cluster becomes damaged and apo-SufR detaches from the promoter sites, inducing the transcription of both *sufR* and *suf* operon. Under iron deprived conditions, (c) the apo-SufR is detached from the promoters, causing elevated transcription of *sufR*, while the *suf* operon remains repressed, due to the binding of IsaR1 to its seed region (marked in yellow) upstream of SufB. The expressed genes are colored with dark grey, while repressed genes are colored with light grey. The SufR protein is represented by dark or light grey dots, depending on the presence of its Fe-S cluster, illustrated as red (Fe) and yellow (S) dots.

under varying iron concentrations was a slight increase in *suf* operon expression in both WT and the *sufR* deletion strain both under short- and long-term iron deprivation (Publication I and II). This shows that in the complete absence of SufR, and in the presence of apo-SufR (which does not bind to the promoter), the *suf* operon can still be induced despite the presence of IsaR1. In this way the need for essential Fe-S cluster biogenesis under iron deprivation can be fulfilled.

Although the two applied methods to induce iron deprivation differed quite substantially, the overall resulting trends could be clearly seen in both treatments. The major differences between the two treatments were the extent and controllability of the iron deficiency. The treatment where iron is excluded from the growth medium (Publication I and II) requires repeated washing, but is rather efficient. In the other method, iron deficiency is triggered by chelation with desferrioxamine (DFB) at mid-logarithmic growth phase (Publication IV), inducing less severe but still sufficient effects, without impacting the cell growth (Shcolnick et al., 2009). Alternatively, iron could be removed from the growth media with 2,2'-dipyridyl, which chelates iron even more effectively than the two abovementioned treatments (Cheng and He, 2014).

A similar regulatory model for Fe-S cluster biogenesis has been observed also in *E. coli,* underlining the importance of this type of control system especially under iron deprivation. The *iscRSUA* operon as well as the A-type Fe-S cluster carrier protein ErpA, both central components of the Fe-S cluster biogenesis in *E. coli* (Desnoyers et al., 2009; Mandin et al., 2016), are regulated by the transcriptional regulator IscR and sRNA RyhB, resembling the *suf* operon regulation by SufR and IsaR1 in *Synechocystis*. Curiously, *A. thaliana sufB* homolog (*AtNAP1*) has also been shown to become downregulated upon iron deprivation (Xu et al., 2005), suggesting that a possible iron deprivation –induced post-transcriptional repression occurs also in plants –at the same time as the iron dependent ATPase activity of AtNAP1 is decreased (Xu et al., 2005).

5.4. Complex regulatory region of the *suf* operon modulates Fe-S cluster biogenesis, while SufR additionally controls Fe-S protein expression

Supported by the proteomic analysis carried out in this Thesis, SufR has been characterized as a transcriptional repressor of the *suf* operon and also as an autoregulator controlling its own expression (Shen et al., 2007). Binding of SufR to its promoter regions depends on the presence and redox state of the Fe-S cluster. Apo-SufR and SufR with reduced $[4Fe\text{-}4S]^{1+}$ clusters do not bind to the DNA, unlike the holo-SufR with oxidized $[4Fe\text{-}4S]^{2+}$ cluster (Shen et al., 2007). There are two adjacent SufR binding sites on opposite strands in the intergenic region of *sufR* and *sufB*; a low affinity region with short palindromic sequences for regulation of *sufR*, and a high affinity

region with long palindromic sequences for regulation of the *suf* operon (Fig. 4a, orange highlights). The SufR binding sites coincide with the overlapping transcriptional start sites (TSS) of the *sufR* and *suf* operon, arranged in opposite orientations (Kopf et al., 2014). The TSS for the *suf* operon (transcription unit TU3030) also gives rise to an sRNA, SufZ, in addition to the *sufBCDS* transcript (Fig. 4a, top strand). It appears that expression of IsaR1 under iron deprivation, and its binding to the *sufZ* transcript region 7 nt upstream of the *sufB* start codon, results in repression of the *suf* operon, while the *sufZ* transcript remains induced, as does *sufR*, possibly due to derepression by apo-SufR on the promoter region. Overall, alleviated repression of the *suf* operon due to detachment of apo-SufR from the promoter under iron deprivation has a small but noticeable effect on the *suf* operon induction (Publication I and II).

Expression of the *suf* operon, induced either by *sufR* deletion or natively by iron-deficient growth conditions, is expected to result in enhanced biogenesis of Fe-S clusters. If the process is not in balance with the expression of proteins which natively bind the clusters, as in the Δ*sufR* strain in the presence of iron, uncontrolled biogenesis leads to the excess of free Fe-S clusters. Accumulation of Fe-S clusters is, in turn, linked with increased intracellular oxidative stress, and may explain the observed depigmentation of the mutant strain under iron sufficiency (Publication II). Under prolonged iron-deprived conditions the continued induction of the *suf* operon in Δ*sufR* mutant resulted eventually in an opposite imbalance; an excess of proteins that bind Fe-S clusters, and insufficient supply of Fe-S clusters. Because of the lack of iron needed for Fe-S cluster biogenesis, these Fe-S proteins (*e. g.* PSI subunits, hydrogenase subunits, and TCA cycle components) accumulate primarily as inactive cluster-free apo-proteins, emphasizing the fact that the expression level changes observed in SRM do not always directly represent the corresponding catalytic activities.

The downregulation of NifJ (PFOR, P52965 in UniProtKB) is understandable under iron deprivation, as it harbors as many as three [4Fe-4S] clusters (based on UniProtKB). This makes NifJ one of the highest iron consumers in *Synechocystis*, and highly sensitive toward low-iron conditions. NifJ is a central protein in carbon metabolism as it catalyzes the conversion of pyruvate into acetyl CoA (Schmitz et al., 2001), thus affecting downstream processes, such as the biosynthesis of fatty acids, terpenoids and amino acids, as well as the TCA-cycle. All these pathways contain several Fe-S cluster proteins, highlighting the importance of controlling this key metabolic enzyme under iron deprivation. In line with this, the NifJ as well as other Fe-S cluster proteins were downregulated in *sufR* deletion mutant based on SRM analysis, resembling similar but less pronounced effect than observed under iron deprivation in WT cells. Interestingly, it appears that the cluster-bound SufR is needed to maintain NifJ expression levels

under iron sufficient conditions, as opposed to *sufR* and *suf* operon regulation for which the holo-form acts as a repressor.

5.5. sRNA IsaR1 is a major regulator under iron deprivation

Iron starvation is known to induce several dramatic changes in cyanobacteria, including the downregulation of the structural components of the photosynthetic apparatus, increased expression of photoprotective and iron scavenging proteins, and replacement of iron-containing proteins with iron-independent counterparts [(Fraser et al., 2013); Publication I]. Although these events are well known, the regulatory factors associated with the dynamic responses and acclimation have remained less comprehensively identified. While the global transcriptional regulator FurA affects the expression of several iron-stress -responsive genes (Gonzalez et al., 2014), the repression of many iron-containing proteins associated with photosynthetic electron transport, as revealed in this Thesis, is mediated by an sRNA IsaR1 (Publication IV).

The IsaR1 regulon was found to comprise mRNAs that encode components associated with electron transfer, pigment biosynthesis, and Fe-S cluster biogenesis, as well as iron and iron-sulfur cluster containing proteins. Thus, IsaR1 affects the photosynthetic apparatus both directly by affecting structural genes of photosynthetic electron transport chain, and indirectly via tetrapyrrole pigment and Fe-S cluster biogenesis. By repressing the overall number of proteins which utilize Fe cofactors, IsaR1 allocates the available iron to the most essential proteins, and directs the cell towards an energy-conserving mode under iron deprivation.

In addition to the repression of genes encoding the proteins of Cyt b_6f complex and Cyt *c*-553, the photosynthetic performance was significantly affected by repression of Fed1, the primary ferredoxin in *Synechocystis*. Fed1 mediates electron flow from PSI to FNR, which reduces $NADP^+$ to NADPH, the end-product of photosynthetic light reactions. The increased PSI acceptor-side limitation in the IsaR1 overexpression strain could therefore be explained by a decreased amount of Fed1. The negative effects of IsaR1 on the expression of PSI core proteins (PsaA/B and PsaD), as seen in SRM (Table 2), immunoblot and sGFP analyses, further resulted in a decrease in the total amount of photooxidizable P700. This is in line with the characteristic decrease of iron-rich PSI complexes upon iron starvation (Fraser et al., 2013), which seems to be influenced by IsaR1-mediated repression. The downregulated proteins, which have a clear connection to the functionality of the photosynthetic apparatus, were the Fe-S biogenesis proteins (SufB, SufC, SufD and SufS), Fe and Fe-S cluster binding superoxide dismutase (SodB) and aconitate hydratase (AcnB), respectively (Table 2), and the genes encoding proteins associated with tetrapyrrole biogenesis, HemA and ChlN. By

repressing the tetrapyrrole biogenesis, IsaR1 affects the synthesis of haem as well as phycobilin and Chl *a* pigments –all central components of the photosynthetic apparatus. The observed depigmentation under iron sufficient and iron-deprived conditions in the IsaR1 deletion mutant was thus a result of excessively produced free pigments resulting from the released repression of pigment biosynthesis and the insufficient amount of the chlorophyll-binding proteins (Yin and Bauer, 2013). Thus, the increased pigment synthesis apparently leads to especially deleterious effects under iron starvation when the photosynthetic complexes are downregulated. This again highlights the need for fine-tuned control over the expression of biogenesis proteins to avoid imbalances in the associated pathways, which could lead to harmful effects.

6. CONCLUDING REMARKS

In my Thesis work, a targeted proteomics method, *selected reaction monitoring* (SRM), was developed for detailed analysis of the *Synechocystis* sp. PCC 6803 proteome. SRM was applied to study the effects of iron deprivation and to investigate the regulatory roles of SufR and sRNA IsaR1 under varying iron concentrations. The SRM method demonstrated its efficacy by enabling the quantification of several previously undetected, low-abundance proteins from unfractionated samples, thereby increasing the dynamic range of high-throughput protein quantification. The method further allowed an evaluation of the impacts of SufR and IsaR1 on iron-sulfur cluster metabolism. These two regulators were shown to control the expression of Fe-S cluster biogenesis proteins under conditions of opposing, sufficient and insufficient, iron concentrations. Such regulation is highly important for the maintenance of physiological balance between the use and demand of scarce resources. In addition to controlling the expression of the *suf* operon, SufR was shown to act as an autoregulator of its own transcription, as well as an activator of NifJ, which is a central Fe-S protein in carbon metabolism. The sRNA IsaR was found to be a key regulator under iron deprivation, affecting the expression of multiple proteins involved either directly or indirectly in the function of the photosynthetic apparatus.

ACKNOWLEDGEMENTS

This Thesis work was carried out at the Molecular Plant Biology Unit, University of Turku, Finland, under the supervision of Academician, Prof. Eva-Mari Aro and Dr. Pauli Kallio.

The research at the Molecular Plant Biology unit is highly appreciated worldwide -owing to Eva-Mari's 40-year long lifework in photosynthesis research. I am extremely grateful and privileged that I've had the opportunity to work with her. Her curiosity and enthusiasm towards understanding photosynthesis is truly inspiring. Thank you Eva-Mari for your support and belief in me.

My other supervisor, Pauli, came to work in our group during somewhat desperate times. The work Pauli put into getting our act together, solving the past and present problems, and helping us to focus on the relevant issues, has been invaluable to so many. The respect and dedication Pauli has towards the integrity of science really is admirable. Thanks Pauli for being such a good supervisor and a friend!

Dorota – I am so happy I had you with me to go through the tough times and challenges in our SRM-project. Thanks for your help, support and friendship!

In addition to my supervisors, I want to thank all those who contributed to the research presented in this Thesis, especially Arjun Tiwari, Gergana Kostova, Tuomas Huokko, Janne Isojärvi, Yagut Allahverdiyeva-Rinne and Wolfgang Hess. I would also like to thank the Proteomics facility in Turku Centre for Biotechnology, particularly Arttu Heinonen and Petri Kouvonen, for helping me with the MS-instruments.

I am thankful for Dr. Janneke Balk for agreeing to be my learned Opponent. I am also grateful for the Reviewers of this Thesis, Prof. Karin Stensjö and Prof. Toivo Kallas, for the constructive criticism and comments, and Prof. Eevi Rintamäki for guiding me through the last steps of my PhD degree.

This graduation is totally worth a happy dance with my dear friend Martina! Thanks for the support during the PhD studies, and for the positive energy and attitude you shared with me during the Thesis writing. I also want to thank my other coworkers and allies for the nice working atmosphere throughout these years. I am also deeply grateful to my loyal dear friends outside the Molecular Plant Biology unit.

Most importantly, I want to thank my dear family for all the love, support, faith, trust and good times. Mum, Dad, Lotta, Laura, Iida, Eve, Venla, Silja, Tilda et al. you are my rock.

REFERENCES

Abbatiello SE, Schilling B, Mani DR, Zimmerman LJ, Hall SC, MacLean B, Albertolle M, Allen S, Burgess M, Cusack MP, Gosh M, Hedrick V, Held JM, Inerowicz HD, Jackson A, Keshishian H, Kinsinger CR, Lyssand J, Makowski L, Mesri M, Rodriguez H, Rudnick P, Sadowski P, Sedransk N, Shaddox K, Skates SJ, Kuhn E, Smith D, Whiteaker JR, Whitwell C, Zhang S, Borchers CH, Fisher SJ, Gibson BW, Liebler DC, MacCoss MJ, Neubert TA, Paulovich AG, Regnier FE, Tempst P, Carr SA (2015) Large-Scale Interlaboratory Study to Develop, Analytically Validate and Apply Highly Multiplexed, Quantitative Peptide Assays to Measure Cancer-Relevant Proteins in Plasma. Mol Cell Proteomics **14:** 2357-2374

Aebersold R, Mann M (2003) Mass spectrometry-based proteomics. Nature **422:** 198-207

Agrò AF, Cannella C, Graziani MT, Cavallini D (1971) A possible role for rhodanese: The formation of 'labile' sulfur from thiosulfate. FEBS Letters **16:** 172-174

Alfonso M, Perewoska I, Kirilovsky D (2001) Redox control of ntcA gene expression in Synechocystis sp. PCC 6803. Nitrogen availability and electron transport regulate the levels of the NtcA protein. Plant Physiol **125:** 969-981

Allahverdiyeva Y, Ermakova M, Eisenhut M, Zhang P, Richaud P, Hagemann M, Cournac L, Aro E-M (2011) Interplay between Flavodiiron Proteins and Photorespiration in Synechocystis sp. PCC 6803. Journal of Biological Chemistry **286:** 24007-24014

Allahverdiyeva Y, Mustila H, Ermakova M, Bersanini L, Richaud P, Ajlani G, Battchikova N, Cournac L, Aro EM (2013) Flavodiiron proteins Flv1 and Flv3 enable cyanobacterial growth and photosynthesis under fluctuating light. Proc Natl Acad Sci U S A **110:** 4111-4116

Anderson L, Hunter CL (2006) Quantitative mass spectrometric multiple reaction monitoring assays for major plasma proteins. Mol Cell Proteomics **5:** 573-588

Anderson SL, McIntosh L (1991) Light-activated heterotrophic growth of the cyanobacterium Synechocystis sp. strain PCC 6803: a blue-light-requiring process. J Bacteriol **173:** 2761-2767

Angelini S, Gerez C, Ollagnier-de Choudens S, Sanakis Y, Fontecave M, Barras F, Py B (2008) NfuA, a new factor required for maturing Fe/S proteins in Escherichia coli under oxidative stress and iron starvation conditions. J Biol Chem **283:** 14084-14091

Angermayr SA, Gorchs Rovira A, Hellingwerf KJ (2015) Metabolic engineering of cyanobacteria for the synthesis of commodity products. Trends Biotechnol **33:** 352-361

Asayama M, Imamura S, Yoshihara S, Miyazaki A, Yoshida N, Sazuka T, Kaneko T, Ohara O, Tabata S, Osanai T, Tanaka K, Takahashi H, Shirai M (2004) SigC, the group 2 sigma factor of RNA polymerase, contributes to the late-stage gene expression and nitrogen promoter recognition in the cyanobacterium Synechocystis sp. strain PCC 6803. Biosci Biotechnol Biochem **68:** 477-487

Ayala-Castro C, Saini A, Outten FW (2008) Fe-S cluster assembly pathways in bacteria. Microbiol Mol Biol Rev **72:** 110-125

Badger MR, Price GD (2003) CO2 concentrating mechanisms in cyanobacteria: molecular components, their diversity and evolution. J Exp Bot **54:** 609-622

Badger MR, Price GD, Long BM, Woodger FJ (2006) The environmental plasticity and ecological genomics of the cyanobacterial CO2 concentrating mechanism. J Exp Bot **57:** 249-265

Balasubramanian R, Shen G, Bryant DA, Golbeck JH (2006) Regulatory roles for IscA and SufA in iron homeostasis and redox stress responses in the cyanobacterium Synechococcus sp. strain PCC 7002. J Bacteriol **188:** 3182-3191

Barten R, Lill H (1995) DNA-uptake in the naturally competent cyanobacterium, *Synechocystis sp.* PCC 6803. FEMS Microbiology Letters **129:** 83–87

Bassham JA, Benson AA, Calvin M (1950) The path of carbon in photosynthesis. J Biol Chem **185:** 781-787

Behshad E, Parkin SE, Bollinger JM, Jr. (2004) Mechanism of cysteine desulfurase Slr0387 from Synechocystis sp. PCC 6803: kinetic analysis of cleavage of the persulfide intermediate by chemical reductants. Biochemistry **43:** 12220-12226

Beinert H, Kiley PJ (1999) Fe-S proteins in sensing and regulatory functions. Curr Opin Chem Biol **3:** 152-157

Bekker A, Holland HD, Wang PL, Rumble D, Stein HJ, Hannah JL, Coetzee LL, Beukes NJ (2004) Dating the rise of atmospheric oxygen. Nature **427:** 117-120

Berkovitch F, Nicolet Y, Wan JT, Jarrett JT, Drennan CL (2004) Crystal structure of biotin synthase, an S-adenosylmethionine-dependent radical enzyme. Science **303:** 76-79

Berla BM, Saha R, Maranas CD, Pakrasi HB (2015) Cyanobacterial Alkanes Modulate Photosynthetic Cyclic Electron Flow to Assist Growth under Cold Stress. Sci Rep **5:** 14894

Berry S, Schneider D, Vermaas WF, Rogner M (2002) Electron transport routes in whole cells of Synechocystis sp. strain PCC 6803: the role of the cytochrome bd-type oxidase. Biochemistry **41:** 3422-3429

Bersanini L, Battchikova N, Jokel M, Rehman A, Vass I, Allahverdiyeva Y, Aro EM (2014) Flavodiiron protein Flv2/Flv4-related photoprotective mechanism dissipates excitation pressure of PSII in cooperation with phycobilisomes in Cyanobacteria. Plant Physiol **164:** 805-818

Bibby TS, Nield J, Barber J (2001) Iron deficiency induces the formation of an antenna ring around trimeric photosystem I in cyanobacteria. Nature **412:** 743-745

Birrell JA, Laurich C, Reijerse EJ, Ogata H, Lubitz W (2016) Importance of Hydrogen Bonding in Fine Tuning the

[2Fe-2S] Cluster Redox Potential of HydC from Thermotoga maritima. Biochemistry **55:** 4344-4355

Boekema EJ, Hifney A, Yakushevska AE, Piotrowski M, Keegstra W, Berry S, Michel KP, Pistorius EK, Kruip J (2001) A giant chlorophyll-protein complex induced by iron deficiency in cyanobacteria. Nature **412:** 745-748

Bottin H, Lagoutte B (1992) Ferredoxin and flavodoxin from the cyanobacterium Synechocystis sp PCC 6803. Biochim Biophys Acta **1101:** 48-56

Boyd PW, Jickells T, Law CS, Blain S, Boyle EA, Buesseler KO, Coale KH, Cullen JJ, de Baar HJW, Follows M, Harvey M, Lancelot C, Levasseur M, Owens NPJ, Pollard R, Rivkin RB, Sarmiento J, Schoemann V, Smetacek V, Takeda S, Tsuda A, Turner S, Watson AJ (2007) Mesoscale Iron Enrichment Experiments 1993-2005: Synthesis and Future Directions. Science **315:** 612

Bradford MM (1976) A rapid and sensitive method for the quantitation of microgram quantities of protein utilizing the principle of protein-dye binding. Analytical Biochemistry **72:** 248-254

Brettel K (1997) Electron transfer and arrangement of the redox cofactors in photosystem I. Biochimica et Biophysica Acta (BBA) - Bioenergetics **1318:** 322-373

Brosch M, Yu L, Hubbard T, Choudhary J (2009) Accurate and sensitive peptide identification with Mascot Percolator. J Proteome Res **8:** 3176-3181

Bruderer R, Bernhardt OM, Gandhi T, Miladinovic SM, Cheng LY, Messner S, Ehrenberger T, Zanotelli V, Butscheid Y, Escher C, Vitek O, Rinner O, Reiter L (2015) Extending the limits of quantitative proteome profiling with data-independent acquisition and application to acetaminophen-treated three-dimensional liver microtissues. Mol Cell Proteomics **14:** 1400-1410

Busch A, Richter AS, Backofen R (2008) IntaRNA: efficient prediction of bacterial sRNA targets incorporating target site accessibility and seed regions. Bioinformatics **24:** 2849-2856

Byrne RH, Kester DR (1976) Solubility of hydrous ferric oxide and iron speciation in seawater. Marine Chemistry **4:** 255-274

Canfield DE, Rosing MT, Bjerrum C (2006) Early anaerobic metabolisms. Philosophical Transactions of the Royal Society of London B: Biological Sciences **361:** 1819-1836

Cerletti P (1986) Seeking a better job for an under-employed enzyme: rhodanese. Trends in Biochemical Sciences **11:** 369-372

Chahal HK, Dai Y, Saini A, Ayala-Castro C, Outten FW (2009) The SufBCD Fe-S scaffold complex interacts with SufA for Fe-S cluster transfer. Biochemistry **48:** 10644-10653

Chandramouli K, Unciuleac MC, Naik S, Dean DR, Huynh BH, Johnson MK (2007) Formation and properties of [4Fe-4S] clusters on the IscU scaffold protein. Biochemistry **46:** 6804-6811

Chang CY, Picotti P, Hüttenhain R, Heinzelmann-Schwarz V, Jovanovic M, Aebersold R, Vitek O (2012) Protein significance analysis in selected reaction monitoring (SRM) measurements. Mol Cell Proteomics **11:** M111.014662

Cheng D, He Q (2014) PfsR Is a Key Regulator of Iron Homeostasis in Synechocystis PCC 6803. PLoS ONE **9:** e101743

Chong PK, Gan CS, Pham TK, Wright PC (2006) Isobaric tags for relative and absolute quantitation (iTRAQ) reproducibility: Implication of multiple injections. J Proteome Res **5:** 1232-1240

Chukhutsina V, Bersanini L, Aro EM, van Amerongen H (2015) Cyanobacterial flv4-2 Operon-Encoded Proteins Optimize Light Harvesting and Charge Separation in Photosystem II. Mol Plant **8:** 747-761

Cooley JW, Vermaas WF (2001) Succinate dehydrogenase and other respiratory pathways in thylakoid membranes of Synechocystis sp. strain PCC 6803: capacity comparisons and physiological function. J Bacteriol **183:** 4251-4258

Corcoran CP, Podkaminski D, Papenfort K, Urban JH, Hinton JC, Vogel J (2012) Superfolder GFP reporters validate diverse new mRNA targets of the classic porin regulator, MicF RNA. Mol Microbiol **84:** 428-445

Cox J, Mann M (2008) MaxQuant enables high peptide identification rates, individualized p.p.b.-range mass accuracies and proteome-wide protein quantification. Nat Biotechnol **26:** 1367-1372

Crack JC, Green J, Thomson AJ, Le Brun NE (2014) Iron-sulfur clusters as biological sensors: the chemistry of reactions with molecular oxygen and nitric oxide. Acc Chem Res **47:** 3196-3205

Cramer WA, Soriano GM, Ponomarev M, Huang D, Zhang H, Martinez SE, Smith JL (1996) SOME NEW STRUCTURAL ASPECTS AND OLD CONTROVERSIES CONCERNING THE CYTOCHROME b6f COMPLEX OF OXYGENIC PHOTOSYNTHESIS. Annual Review of Plant Physiology and Plant Molecular Biology **47:** 477-508

de Baar HJW, de Jong JTM, Bakker DCE, Loscher BM, Veth C, Bathmann U, Smetacek V (1995) Importance of iron for plankton blooms and carbon dioxide drawdown in the Southern Ocean. Nature **373:** 412-415

de Lorenzo V, Wee S, Herrero M, Neilands JB (1987) Operator sequences of the aerobactin operon of plasmid ColV-K30 binding the ferric uptake regulation (fur) repressor. J Bacteriol **169:** 2624-2630

Desnoyers G, Morissette A, Prevost K, Masse E (2009) Small RNA-induced differential degradation of the polycistronic mRNA iscRSUA. Embo j **28:** 1551-1561

Deutsch EW, Lam H, Aebersold R (2008) PeptideAtlas: a resource for target selection for emerging targeted proteomics workflows. EMBO Rep **9:** 429-434

Ding H, Hidalgo E, Demple B (1996) The redox state of the [2Fe-2S] clusters in SoxR protein regulates its activity as a transcription factor. J Biol Chem **271:** 33173-33175

Dixon R, Kahn D (2004) Genetic regulation of biological nitrogen fixation. Nat Rev Micro **2:** 621-631

Domain F, Houot L, Chauvat F, Cassier-Chauvat C (2004) Function and regulation of the cyanobacterial genes

lexA, recA and ruvB: LexA is critical to the survival of cells facing inorganic carbon starvation. Mol Microbiol **53:** 65-80

Domon B, Aebersold R (2010) Options and considerations when selecting a quantitative proteomics strategy. Nat Biotechnol **28:** 710-721

Dugdale RC (1967) NUTRIENT LIMITATION IN THE SEA: DYNAMICS, IDENTIFICATION, AND SIGNIFICANCE. Limnology and Oceanography **12:** 685-695

Edgar RC (2004) MUSCLE: multiple sequence alignment with high accuracy and high throughput. Nucleic Acids Res **32:** 1792-1797

Eisenhut M, Aguirre von Wobeser E, Jonas L, Schubert H, Ibelings BW, Bauwe H, Matthijs HC, Hagemann M (2007) Long-term response toward inorganic carbon limitation in wild type and glycolate turnover mutants of the cyanobacterium Synechocystis sp. strain PCC 6803. Plant Physiol **144:** 1946-1959

Emptage MH, Kent TA, Kennedy MC, Beinert H, Munck E (1983) Mossbauer and EPR studies of activated aconitase: development of a localized valence state at a subsite of the [4Fe-4S] cluster on binding of citrate. Proc Natl Acad Sci U S A **80:** 4674-4678

Ermakova M, Huokko T, Richaud P, Bersanini L, Howe CJ, Lea-Smith DJ, Peltier G, Allahverdiyeva Y (2016) Distinguishing the Roles of Thylakoid Respiratory Terminal Oxidases in the Cyanobacterium Synechocystis sp. PCC 6803. Plant Physiol **171:** 1307-1319

Escher C, Reiter L, MacLean B, Ossola R, Herzog F, Chilton J, MacCoss MJ, Rinner O (2012) Using iRT, a normalized retention time for more targeted measurement of peptides. Proteomics **12:** 1111-1121

Escolar L, Perez-Martin J, de Lorenzo V (1999) Opening the iron box: transcriptional metalloregulation by the Fur protein. J Bacteriol **181:** 6223-6229

Exss-Sonne P, Tölle J, Bader KP, Pistorius EK, Michel KP (2000) The IdiA protein of Synechococcus sp. PCC 7942 functions in protecting the acceptor side of Photosystem II under oxidative stress. Photosynth Res **63:** 145-157

Falkowski PG (1997) Evolution of the nitrogen cycle and its influence on the biological sequestration of CO2 in the ocean. Nature **387:** 272-275

Falkowski PG (2002) The ocean's invisible forest - Marine phytoplankton play a critical role in regulating the earth's climate. Could they also be used to combat global warming. Scientific American **287:** 54-61

Farrah T, Deutsch EW, Kreisberg R, Sun Z, Campbell DS, Mendoza L, Kusebauch U, Brusniak MY, Hüttenhain R, Schiess R, Selevsek N, Aebersold R, Moritz RL (2012) PASSEL: the PeptideAtlas SRMexperiment library. Proteomics **12:** 1170-1175

Fay P (1965) Heterotrophy and Nitrogen Fixation in Chlorogloea fritschii. Microbiology **39:** 11-20

Fenn JB, Mann M, Meng CK, Wong SF, Whitehouse CM (1989) Electrospray ionization for mass spectrometry of large biomolecules. Science **246:** 64-71

Field CB, Behrenfeld MJ, Randerson JT, Falkowski P (1998) Primary production of the biosphere: integrating terrestrial and oceanic components. Science **281:** 237-240

Finn RD, Mistry J, Tate J, Coggill P, Heger A, Pollington JE, Gavin OL, Gunasekaran P, Ceric G, Forslund K, Holm L, Sonnhammer EL, Eddy SR, Bateman A (2010) The Pfam protein families database. Nucleic Acids Res **38:** D211-222

Finney LA, O'Halloran TV (2003) Transition metal speciation in the cell: insights from the chemistry of metal ion receptors. Science **300:** 931-936

Fleischhacker AS, Stubna A, Hsueh KL, Guo Y, Teter SJ, Rose JC, Brunold TC, Markley JL, Munck E, Kiley PJ (2012) Characterization of the [2Fe-2S] cluster of Escherichia coli transcription factor IscR. Biochemistry **51:** 4453-4462

Flint DH, Tuminello JF, Emptage MH (1993) The inactivation of Fe-S cluster containing hydro-lyases by superoxide. J Biol Chem **268:** 22369-22376

Flores E, Romero JM, Guerrero MG, Losada M (1983) Regulatory interaction of photosynthetic nitrate utilization and carbon dioxide fixation in the cyanobacterium Anacystis nidulans. Biochimica et Biophysica Acta (BBA) - Bioenergetics **725:** 529-532

Fraser JM, Tulk SE, Jeans JA, Campbell DA, Bibby TS, Cockshutt AM (2013) Photophysiological and photosynthetic complex changes during iron starvation in Synechocystis sp. PCC 6803 and Synechococcus elongatus PCC 7942. PLoS One **8:** e59861

Frazzon J, Dean DR (2001) Feedback regulation of iron-sulfur cluster biosynthesis. Proceedings of the National Academy of Sciences **98:** 14751-14753

Fromme P, Grotjohann I (2006) Structural analysis of cyanobacterial photosystem I. *In* JH Golbeck, ed, Photosystem I: The Light-Driven Plastocyanin: Ferredoxin Oxidoreductase. Advances in Photosynthesis and Respiration, Vol 24. Springer, Dordrecht, Netherlands, pp 47-69

Fujii M, Dang TC, Rose AL, Omura T, Waite TD (2011) Effect of light on iron uptake by the freshwater cyanobacterium Microcystis aeruginosa. Environ Sci Technol **45:** 1391-1398

Fusaro VA, Mani DR, Mesirov JP, Carr SA (2009) Prediction of high-responding peptides for targeted protein assays by mass spectrometry. Nat Biotechnol **27:** 190-198

Gan CS, Reardon KF, Wright PC (2005) Comparison of protein and peptide prefractionation methods for the shotgun proteomic analysis of Synechocystis sp. PCC 6803. Proteomics **5:** 2468-2478

Geiß U, Vinnemeier J, Kunert A, Lindner I, Gemmer B, Lorenz M, Hagemann M, Schoor A (2001) Detection of the isiA Gene across Cyanobacterial Strains: Potential for Probing Iron Deficiency. Applied and Environmental Microbiology **67:** 5247-5253

Georg J, Voss B, Scholz I, Mitschke J, Wilde A, Hess WR (2009) Evidence for a major role of antisense RNAs in cyanobacterial gene regulation. Mol Syst Biol **5:** 305

Giel JL, Rodionov D, Liu M, Blattner FR, Kiley PJ (2006) IscR-dependent gene expression links iron-sulphur cluster assembly to the control of O2-regulated

genes in Escherichia coli. Mol Microbiol **60:** 1058-1075

Gillet LC, Navarro P, Tate S, Rost H, Selevsek N, Reiter L, Bonner R, Aebersold R (2012) Targeted data extraction of the MS/MS spectra generated by data-independent acquisition: a new concept for consistent and accurate proteome analysis. Mol Cell Proteomics **11:** O111.016717

Golbeck JH (1999) A comparative analysis of the spin state distribution of in vitro and in vivo mutants of PsaC. A biochemical argument for the sequence of electron transfer in Photosystem I as FX → FA → FB → ferredoxin/flavodoxin. Photosynthesis Research **61:** 107-144

Golecki JR (1988) Analysis of structure and development of bacterial membranes/outer, cytoplasmic, and intracytoplasmic membranes. *In* Methods in Microbiology, Vol 20, pp 61–77

Gonzalez A, Angarica VE, Sancho J, Fillat MF (2014) The FurA regulon in Anabaena sp. PCC 7120: in silico prediction and experimental validation of novel target genes. Nucleic Acids Res **42:** 4833-4846

Gruner I, Fradrich C, Bottger LH, Trautwein AX, Jahn D, Hartig E (2011) Aspartate 141 is the fourth ligand of the oxygen-sensing [4Fe-4S]2+ cluster of Bacillus subtilis transcriptional regulator Fnr. J Biol Chem **286:** 2017-2021

Gudmundsson S, Nogales J (2015) Cyanobacteria as photosynthetic biocatalysts: a systems biology perspective. Mol Biosyst **11:** 60-70

Guo J, Nguyen AY, Dai Z, Su D, Gaffrey MJ, Moore RJ, Jacobs JM, Monroe ME, Smith RD, Koppenaal DW, Pakrasi HB, Qian WJ (2014) Proteome-wide light/dark modulation of thiol oxidation in cyanobacteria revealed by quantitative site-specific redox proteomics. Mol Cell Proteomics **13:** 3270-3285

Gurbiel RJ, Batie CJ, Sivaraja M, True AE, Fee JA, Hoffman BM, Ballou DP (1989) Electron-nuclear double resonance spectroscopy of 15N-enriched phthalate dioxygenase from Pseudomonas cepacia proves that two histidines are coordinated to the [2Fe-2S] Rieske-type clusters. Biochemistry **28:** 4861-4871

Hantke K (1981) Regulation of ferric iron transport in Escherichia coli K12: isolation of a constitutive mutant. Mol Gen Genet **182:** 288-292

Hedges SB, Blair JE, Venturi ML, Shoe JL (2004) A molecular timescale of eukaryote evolution and the rise of complex multicellular life. BMC Evol Biol **4:** 2

Hernandez JA, Bes MT, Fillat MF, Neira JL, Peleato ML (2002) Biochemical analysis of the recombinant Fur (ferric uptake regulator) protein from Anabaena PCC 7119: factors affecting its oligomerization state. Biochem J **366:** 315-322

Hernández-Prieto MA, Schön V, Georg J, Barreira L, Varela J, Hess WR, Futschik ME (2012) Iron deprivation in Synechocystis: inference of pathways, non-coding RNAs, and regulatory elements from comprehensive expression profiling. G3 (Bethesda) **2:** 1475-1495

Hoiczyk E, Hansel A (2000) Cyanobacterial cell walls: news from an unusual prokaryotic envelope. J Bacteriol **182:** 1191-1199

Holland HD (2002) Volcanic gases, black smokers, and the great oxidation event. Geochimica et Cosmochimica Acta **66:** 3811-3826

Holton B, Wu X, Tsapin AI, Kramer DM, Malkin R, Kallas T (1996) Reconstitution of the 2Fe-2S center and g = 1.89 electron paramagnetic resonance signal into overproduced Nostoc sp. PCC 7906 Rieske protein. Biochemistry **35:** 15485-15493

Hopkinson BM, Morel FMM (2009) The role of siderophores in iron acquisition by photosynthetic marine microorganisms. BioMetals **22:** 659-669

Hu Y, Ribbe MW (2011) Biosynthesis of Nitrogenase FeMoco. Coord Chem Rev **255:** 1218-1224

Huang S, Chen L, Te R, Qiao J, Wang J, Zhang W (2013) Complementary iTRAQ proteomics and RNA-seq transcriptomics reveal multiple levels of regulation in response to nitrogen starvation in Synechocystis sp. PCC 6803. Mol Biosyst **9:** 2565-2574

Hutber GN, Hutson KG, Rogers LJ (1977) Effect of iron deficiency on levels of two ferredoxins and flavodoxin in a cyanobacterium. *In* FEMS Microbiology Letters, Vol 1, pp 193-196

Ibelings BW, Maberly SC (1998) Photoinhibition and the availability of inorganic carbon restrict photosynthesis by surface blooms of cyanobacteria. Limnology and Oceanography **43:** 408-419

Ideker T, Thorsson V, Ranish JA, Christmas R, Buhler J, Eng JK, Bumgarner R, Goodlett DR, Aebersold R, Hood L (2001) Integrated genomic and proteomic analyses of a systematically perturbed metabolic network. Science **292:** 929-934

Ihalainen JA, D'Haene S, Yeremenko N, van Roon H, Arteni AA, Boekema EJ, van Grondelle R, Matthijs HC, Dekker JP (2005) Aggregates of the chlorophyll-binding protein IsiA (CP43') dissipate energy in cyanobacteria. Biochemistry **44:** 10846-10853

Imamura S, Tanaka K, Shirai M, Asayama M (2006) Growth phase-dependent activation of nitrogen-related genes by a control network of group 1 and group 2 sigma factors in a cyanobacterium. J Biol Chem **281:** 2668-2675

Imlay JA (2006) Iron-sulphur clusters and the problem with oxygen. Mol Microbiol **59:** 1073-1082

Ivanov AG, Krol M, Sveshnikov D, Selstam E, Sandström S, Koochek M, Park Y-I, Vasil'ev S, Bruce D, Öquist G, Huner NPA (2006) Iron Deficiency in Cyanobacteria Causes Monomerization of Photosystem I Trimers and Reduces the Capacity for State Transitions and the Effective Absorption Cross Section of Photosystem I in Vivo. Plant Physiology **141:** 1436-1445

Jaffe JD, Keshishian H, Chang B, Addona TA, Gillette MA, Carr SA (2008) Accurate Inclusion Mass Screening: A Bridge from Unbiased Discovery to Targeted Assay Development for Biomarker Verification. Molecular & Cellular Proteomics : MCP **7:** 1952-1962

Jiang H-B, Lou W-J, Ke W-T, Song W-Y, Price NM, Qiu B-S (2015) New insights into iron acquisition by

cyanobacteria: an essential role for ExbB-ExbD complex in inorganic iron uptake. ISME J **9:** 297-309

Jiang HB, Lou WJ, Du HY, Price NM, Qiu BS (2012) Sll1263, a unique cation diffusion facilitator protein that promotes iron uptake in the cyanobacterium Synechocystis sp. Strain PCC 6803. Plant Cell Physiol **53:** 1404-1417

Johnson KS, Gordon RM, Coale KH (1997) What controls dissolved iron concentrations in the world ocean? Marine Chemistry **57:** 137-161

Jones DT, Taylor WR, Thornton JM (1992) The rapid generation of mutation data matrices from protein sequences. Comput Appl Biosci **8:** 275-282

Jürgens UJ, Weckesser J (1985) Carotenoid-containing outer membrane of Synechocystis sp. strain PCC6714. Journal of Bacteriology **164:** 384-389

Kamiya N, Shen JR (2003) Crystal structure of oxygen-evolving photosystem II from Thermosynechococcus vulcanus at 3.7-A resolution. Proc Natl Acad Sci U S A **100:** 98-103

Kaneko T, Sato S, Kotani H, Tanaka A, Asamizu E, Nakamura Y, Miyajima N, Hirosawa M, Sugiura M, Sasamoto S, Kimura T, Hosouchi T, Matsuno A, Muraki A, Nakazaki N, Naruo K, Okumura S, Shimpo S, Takeuchi C, Wada T, Watanabe A, Yamada M, Yasuda M, Tabata S (1996) Sequence analysis of the genome of the unicellular cyanobacterium Synechocystis sp. strain PCC6803. II. Sequence determination of the entire genome and assignment of potential protein-coding regions. DNA Res **3:** 109-136

Karas M, Hillenkamp F (1988) Laser desorption ionization of proteins with molecular masses exceeding 10,000 daltons. Anal Chem **60:** 2299-2301

Katoh H, Hagino N, Grossman AR, Ogawa T (2001) Genes essential to iron transport in the cyanobacterium Synechocystis sp. strain PCC 6803. J Bacteriol **183:** 2779-2784

Keren N, Aurora R, Pakrasi HB (2004) Critical Roles of Bacterioferritins in Iron Storage and Proliferation of Cyanobacteria. Plant Physiology **135:** 1666-1673

Kessler D (2004) Slr0077 of Synechocystis has cysteine desulfurase as well as cystine lyase activity. Biochem Biophys Res Commun **320:** 571-577

Kitaoka S, Wada K, Hasegawa Y, Minami Y, Fukuyama K, Takahashi Y (2006) Crystal structure of Escherichia coli SufC, an ABC-type ATPase component of the SUF iron-sulfur cluster assembly machinery. FEBS Lett **580:** 137-143

Klahn S, Baumgartner D, Pfreundt U, Voigt K, Schon V, Steglich C, Hess WR (2014) Alkane Biosynthesis Genes in Cyanobacteria and Their Transcriptional Organization. Front Bioeng Biotechnol **2:** 24

Klemer AR, Hendzel LL, Findlay DL, Hedin RA, Mageau MT, Konopka A (1995) CARBON AVAILABILITY AND THE PATTERN OF CYANOBACTERIAL DOMINANCE IN ENRICHED LOW-CARBON LAKES. Journal of Phycology **31:** 735–744

Kolling DJ, Brunzelle JS, Lhee S, Crofts AR, Nair SK (2007) Atomic resolution structures of rieske iron-sulfur protein: role of hydrogen bonds in tuning the redox potential of iron-sulfur clusters. Structure **15:** 29-38

Kopf M, Klähn S, Scholz I, Matthiessen JKF, Hess WR, Voß B (2014) Comparative Analysis of the Primary Transcriptome of Synechocystis sp. PCC 6803. DNA Research **21:** 527-539

Kowarik M, Young NM, Numao S, Schulz BL, Hug I, Callewaert N, Mills DC, Watson DC, Hernandez M, Kelly JF, Wacker M, Aebi M (2006) Definition of the bacterial N-glycosylation site consensus sequence. Embo j **25:** 1957-1966

Kranzler C, Lis H, Finkel OM, Schmetterer G, Shaked Y, Keren N (2014) Coordinated transporter activity shapes high-affinity iron acquisition in cyanobacteria. ISME J **8:** 409-417

Kranzler C, Lis H, Shaked Y, Keren N (2011) The role of reduction in iron uptake processes in a unicellular, planktonic cyanobacterium. Environ Microbiol **13:** 2990-2999

Krokhin OV (2006) Sequence-specific retention calculator. Algorithm for peptide retention prediction in ion-pair RP-HPLC: application to 300- and 100-A pore size C18 sorbents. Anal Chem **78:** 7785-7795

Krynická V, Tichý M, Krafl J, Yu J, Kaňa R, Boehm M, Nixon PJ, Komenda J (2014) Two essential FtsH proteases control the level of the Fur repressor during iron deficiency in the cyanobacterium Synechocystis sp. PCC 6803. Mol Microbiol **94:** 609-624

Kumar S, Stecher G, Tamura K (2016) MEGA7: Molecular Evolutionary Genetics Analysis Version 7.0 for Bigger Datasets. Molecular Biology and Evolution **33:** 1870-1874

Kunert A, Hagemann M, Erdmann N (2000) Construction of promoter probe vectors for Synechocystis sp. PCC 6803 using the light-emitting reporter systems Gfp and LuxAB. J Microbiol Methods **41:** 185-194

Kunert A, Vinnemeier J, Erdmann N, Hagemann M (2003) Repression by Fur is not the main mechanism controlling the iron-inducible isiAB operon in the cyanobacterium Synechocystis sp. PCC 6803. FEMS Microbiol Lett **227:** 255-262

Kurisu G, Zhang H, Smith JL, Cramer WA (2003) Structure of the cytochrome b6f complex of oxygenic photosynthesis: tuning the cavity. Science **302:** 1009-1014

Käll L, Canterbury JD, Weston J, Noble WS, MacCoss MJ (2007) Semi-supervised learning for peptide identification from shotgun proteomics datasets. Nat Methods **4:** 923-925

Käll L, Vitek O (2011) Computational mass spectrometry-based proteomics. PLoS Comput Biol **7:** e1002277

Kämäräinen J, Huokko T, Kreula S, Jones PR, Aro EM, Kallio P (2016) Pyridine nucleotide transhydrogenase PntAB is essential for optimal growth and photosynthetic integrity under low-light mixotrophic conditions in Synechocystis sp. PCC 6803. New Phytol

Lange V, Picotti P, Domon B, Aebersold R (2008) Selected reaction monitoring for quantitative proteomics: a tutorial. Mol Syst Biol **4:** 222

Latifi A, Jeanjean R, Lemeille S, Havaux M, Zhang CC (2005) Iron starvation leads to oxidative stress in Anabaena sp. strain PCC 7120. J Bacteriol **187:** 6596-6598

Laudenbach DE, Ehrhardt D, Green L, Grossman A (1991) Isolation and characterization of a sulfur-regulated gene encoding a periplasmically localized protein with sequence similarity to rhodanese. J Bacteriol **173:** 2751-2760

Laudenbach DE, Herbert SK, McDowell C, Fork DC, Grossman AR, Straus NA (1990) Cytochrome c-553 is not required for photosynthetic activity in the cyanobacterium Synechococcus. Plant Cell **2:** 913-924

Laudenbach DE, Reith ME, Straus NA (1988) Isolation, sequence analysis, and transcriptional studies of the flavodoxin gene from Anacystis nidulans R2. J Bacteriol **170:** 258-265

Laudenbach DE, Straus NA (1988) Characterization of a cyanobacterial iron stress-induced gene similar to psbC. J Bacteriol **170:** 5018-5026

Law KP, Lim YP (2013) Recent advances in mass spectrometry: data independent analysis and hyper reaction monitoring. Expert Rev Proteomics **10:** 551-566

Lax JE, Arteni AA, Boekema EJ, Pistorius EK, Michel KP, Rogner M (2007) Structural response of Photosystem 2 to iron deficiency: characterization of a new photosystem 2-IdiA complex from the cyanobacterium Thermosynechococcus elongatus BP-1. Biochim Biophys Acta **1767:** 528-534

Lee H-M, Flores E, Forchhammer K, Herrero A, Tandeau de Marsac N (2000) Phosphorylation of the signal transducer PII protein and an additional effector are required for the PII-mediated regulation of nitrate and nitrite uptake in the cyanobacterium Synechococcus sp. PCC 7942. European Journal of Biochemistry **267:** 591-600

Lee JH, Yeo WS, Roe JH (2004) Induction of the sufA operon encoding Fe-S assembly proteins by superoxide generators and hydrogen peroxide: involvement of OxyR, IHF and an unidentified oxidant-responsive factor. Mol Microbiol **51:** 1745-1755

Lill R, Mühlenhoff U (2005) Iron–sulfur-protein biogenesis in eukaryotes. Trends in Biochemical Sciences **30:** 133-141

Lindahl M, Florencio FJ (2003) Thioredoxin-linked processes in cyanobacteria are as numerous as in chloroplasts, but targets are different. Proceedings of the National Academy of Sciences of the United States of America **100:** 16107-16112

Liu H, Sadygov RG, Yates JR (2004) A model for random sampling and estimation of relative protein abundance in shotgun proteomics. Anal Chem **76:** 4193-4201

Loiseau L, Gerez C, Bekker M, Ollagnier-de Choudens S, Py B, Sanakis Y, Teixeira de Mattos J, Fontecave M, Barras F (2007) ErpA, an iron sulfur (Fe S) protein of the A-type essential for respiratory metabolism in Escherichia coli. Proc Natl Acad Sci U S A **104:** 13626-13631

Loiseau L, Ollagnier-de-Choudens S, Nachin L, Fontecave M, Barras F (2003) Biogenesis of Fe-S cluster by the bacterial Suf system: SufS and SufE form a new type of cysteine desulfurase. J Biol Chem **278:** 38352-38359

Lovenberg W, Sobel BE (1965) Rubredoxin: a new electron transfer protein from Clostridium pasteurianum. Proc Natl Acad Sci U S A **54:** 193-199

MacCoss MJ, Wu CC, Yates JR (2002) Probability-Based Validation of Protein Identifications Using a Modified SEQUEST Algorithm. Analytical Chemistry **74:** 5593-5599

MacLean B, Tomazela DM, Shulman N, Chambers M, Finney GL, Frewen B, Kern R, Tabb DL, Liebler DC, MacCoss MJ (2010) Skyline: an open source document editor for creating and analyzing targeted proteomics experiments. Bioinformatics **26:** 966-968

Mallick P, Schirle M, Chen SS, Flory MR, Lee H, Martin D, Ranish J, Raught B, Schmitt R, Werner T, Kuster B, Aebersold R (2007) Computational prediction of proteotypic peptides for quantitative proteomics. Nat Biotechnol **25:** 125-131

Mandin P, Chareyre S, Barras F (2016) A Regulatory Circuit Composed of a Transcription Factor, IscR, and a Regulatory RNA, RyhB, Controls Fe-S Cluster Delivery. mBio **7**

Marquez FJ, Sasaki K, Kakizono T, Nishio N, Nagai S (1993) Growth characteristics of Spirulina platensis in mixotrophic and heterotrophic conditions. Journal of Fermentation and Bioengineering **76:** 408-410

Martin JH, Fitzwater SE (1988) Iron deficiency limits phytoplankton growth in the north-east Pacific subarctic. Nature **331:** 341-343

Martin JH, Gordon M, Fitzwater SE (1991) The case for iron. Limnology and Oceanography **36:** 1793-1802

Marx V (2013) Targeted proteomics. Nat Meth **10:** 19-22

Massé E, Gottesman S (2002) A small RNA regulates the expression of genes involved in iron metabolism in Escherichia coli. Proceedings of the National Academy of Sciences **99:** 4620-4625

Mawji E, Gledhill M, Milton JA, Tarran GA, Ussher S, Thompson A, Wolff GA, Worsfold PJ, Achterberg EP (2008) Hydroxamate siderophores: occurrence and importance in the Atlantic Ocean. Environ Sci Technol **42:** 8675-8680

McDermott AE, Yachandra VK, Guiles RD, Sauer K, Klein MP, Parrett KG, Golbeck JH (1989) EXAFS structural study of FX, the low-potential Fe-S center in photosystem I. Biochemistry **28:** 8056-8059

Meeks JC, Castenholz RW (1971) Growth and photosynthesis in an extreme thermophile, Synechococcus lividus (Cyanophyta). Arch Mikrobiol **78:** 25-41

Michalski A, Cox J, Mann M (2011) More than 100,000 Detectable Peptide Species Elute in Single Shotgun Proteomics Runs but the Majority is Inaccessible to

Data-Dependent LC–MS/MS. Journal of Proteome Research **10:** 1785-1793

Michel KP, Pistorius EK (2004) Adaptation of the photosynthetic electron transport chain in cyanobacteria to iron deficiency: The function of IdiA and IsiA. Physiol Plant **120:** 36-50

Mitschke J, Georg J, Scholz I, Sharma CM, Dienst D, Bantscheff J, Voss B, Steglich C, Wilde A, Vogel J, Hess WR (2011) An experimentally anchored map of transcriptional start sites in the model cyanobacterium Synechocystis sp. PCC6803. Proc Natl Acad Sci U S A **108:** 2124-2129

Moore RE, Young MK, Lee TD (2002) Qscore: an algorithm for evaluating SEQUEST database search results. J Am Soc Mass Spectrom **13:** 378-386

Morel FMM, Price NM (2003) The Biogeochemical Cycles of Trace Metals in the Oceans. Science **300:** 944-947

Mullineaux CW (2014) Co-existence of photosynthetic and respiratory activities in cyanobacterial thylakoid membranes. Biochimica et Biophysica Acta (BBA) - Bioenergetics **1837:** 503-511

Muro-Pastor MI, Reyes JC, Florencio FJ (1996) The NADP+-isocitrate dehydrogenase gene (icd) is nitrogen regulated in cyanobacteria. J Bacteriol **178:** 4070-4076

Murphy TP, Lean DRS, Nalewajko C (1976) BLUE-GREEN-ALGAE - THEIR EXCRETION OF IRON-SELECTIVE CHELATORS ENABLES THEM TO DOMINATE OTHER ALGAE. Science **192:** 900-902

Mustila H, Paananen P, Battchikova N, Santana-Sánchez A, Muth-Pawlak D, Hagemann M, Aro EM, Allahverdiyeva Y (2016) The Flavodiiron Protein Flv3 Functions as a Homo-Oligomer During Stress Acclimation and is Distinct from the Flv1/Flv3 Hetero-Oligomer Specific to the O2 Photoreduction Pathway. Plant Cell Physiol **57:** 1468-1483

Nachin L, Loiseau L, Expert D, Barras F (2003) SufC: an unorthodox cytoplasmic ABC/ATPase required for [Fe-S] biogenesis under oxidative stress. EMBO J **22:** 427-437

Nesbit AD, Giel JL, Rose JC, Kiley PJ (2009) Sequence-specific binding to a subset of IscR-regulated promoters does not require IscR Fe-S cluster ligation. J Mol Biol **387:** 28-41

Nishio K, Nakai M (2000) Transfer of iron-sulfur cluster from NifU to apoferredoxin. J Biol Chem **275:** 22615-22618

North RL, Guildford SJ, Smith REH, Havens SM, Twiss MR (2007) Evidence for phosphorus, nitrogen, and iron colimitation of phytoplankton communities in Lake Erie. Limnology and Oceanography **52**

Novichkov PS, Kazakov AE, Ravcheev DA, Leyn SA, Kovaleva GY, Sutormin RA, Kazanov MD, Riehl W, Arkin AP, Dubchak I, Rodionov DA (2013) RegPrecise 3.0--a resource for genome-scale exploration of transcriptional regulation in bacteria. BMC Genomics **14:** 745

Ollagnier-de-Choudens S, Lascoux D, Loiseau L, Barras F, Forest E, Fontecave M (2003) Mechanistic studies of the SufS-SufE cysteine desulfurase: evidence for sulfur transfer from SufS to SufE. FEBS Lett **555:** 263-267

Olsen JV, de Godoy LMF, Li G, Macek B, Mortensen P, Pesch R, Makarov A, Lange O, Horning S, Mann M (2005) Parts per Million Mass Accuracy on an Orbitrap Mass Spectrometer via Lock Mass Injection into a C-trap. Molecular & Cellular Proteomics **4:** 2010-2021

Omata T, Price GD, Badger MR, Okamura M, Gohta S, Ogawa T (1999) Identification of an ATP-binding cassette transporter involved in bicarbonate uptake in the cyanobacterium Synechococcus sp. strain PCC 7942. Proceedings of the National Academy of Sciences of the United States of America **96:** 13571-13576

Outten FW, Djaman O, Storz G (2004) A suf operon requirement for Fe-S cluster assembly during iron starvation in Escherichia coli. Mol Microbiol **52:** 861-872

Outten FW, Theil EC (2009) Iron-based redox switches in biology. Antioxid Redox Signal **11:** 1029-1046

Outten FW, Wood MJ, Munoz FM, Storz G (2003) The SufE protein and the SufBCD complex enhance SufS cysteine desulfurase activity as part of a sulfur transfer pathway for Fe-S cluster assembly in Escherichia coli. J Biol Chem **278:** 45713-45719

Panchaud A, Scherl A, Shaffer SA, von Haller PD, Kulasekara HD, Miller SI, Goodlett DR (2009) Precursor Acquisition Independent From Ion Count: How to Dive Deeper into the Proteomics Ocean. Analytical Chemistry **81:** 6481-6488

Pandhal J, Snijders APL, Wright PC, Biggs CA (2008) A cross-species quantitative proteomic study of salt adaptation in a halotolerant environmental isolate using 15N metabolic labelling. Proteomics **8:** 2266-2284

Patzer SI, Hantke K (1999) SufS Is a NifS-Like Protein, and SufD Is Necessary for Stability of the [2Fe-2S] FhuF Protein in Escherichia coli. Journal of Bacteriology **181:** 3307-3309

Pecqueur L, D'Autreaux B, Dupuy J, Nicolet Y, Jacquamet L, Brutscher B, Michaud-Soret I, Bersch B (2006) Structural changes of Escherichia coli ferric uptake regulator during metal-dependent dimerization and activation explored by NMR and X-ray crystallography. J Biol Chem **281:** 21286-21295

Perkins DN, Pappin DJ, Creasy DM, Cottrell JS (1999) Probability-based protein identification by searching sequence databases using mass spectrometry data. Electrophoresis **20:** 3551-3567

Peschek GA, Molitor V, Trnka M, Wastyn M, Erber W (1988) Characterization of cytochrome-c oxidase in isolated and purified plasma and thylakoid membranes from cyanobacteria. *In* Methods in Enzymology, Vol 167. Academic Press, pp 437-449

Petering D, Fee JA, Palmer G (1971) The oxygen sensitivity of spinach ferredoxin and other iron-sulfur proteins. The formation of protein-bound sulfur-zero. J Biol Chem **246:** 643-653

Peterson AC, Russell JD, Bailey DJ, Westphall MS, Coon JJ (2012) Parallel reaction monitoring for high

resolution and high mass accuracy quantitative, targeted proteomics. Mol Cell Proteomics **11:** 1475-1488

Pfaffl MW (2001) A new mathematical model for relative quantification in real-time RT-PCR. Nucleic Acids Res **29:** e45

Picotti P, Bodenmiller B, Mueller LN, Domon B, Aebersold R (2009) Full dynamic range proteome analysis of S. cerevisiae by targeted proteomics. Cell **138:** 795-806

Picotti P, Rinner O, Stallmach R, Dautel F, Farrah T, Domon B, Wenschuh H, Aebersold R (2010) High-throughput generation of selected reaction-monitoring assays for proteins and proteomes. Nat Methods **7:** 43-46

Pinto FL, Thapper A, Sontheim W, Lindblad P (2009) Analysis of current and alternative phenol based RNA extraction methodologies for cyanobacteria. BMC Molecular Biology **10:** 79

Py B, Gerez C, Angelini S, Planel R, Vinella D, Loiseau L, Talla E, Brochier-Armanet C, Garcia Serres R, Latour JM, Ollagnier-de Choudens S, Fontecave M, Barras F (2012) Molecular organization, biochemical function, cellular role and evolution of NfuA, an atypical Fe-S carrier. Mol Microbiol **86:** 155-171

Rantamaki S, Meriluoto J, Spoof L, Puputti EM, Tyystjarvi T, Tyystjarvi E (2016) Oxygen produced by cyanobacteria in simulated Archaean conditions partly oxidizes ferrous iron but mostly escapes-conclusions about early evolution. Photosynth Res **130:** 103-111

Raven JA (1988) The iron and molybdenum use efficiencies of plant growth with different energy, carbon and nitrogen sources. New Phytologist **109:** 279–287

Redfield AC (1958) The Biological Control of Chemical Factors in the Environment. American Scientist **46:** 205-221

Reiter L, Rinner O, Picotti P, Hüttenhain R, Beck M, Brusniak MY, Hengartner MO, Aebersold R (2011) mProphet: automated data processing and statistical validation for large-scale SRM experiments. Nat Methods **8:** 430-435

Resch CM, Gibson J (1983) Isolation of the carotenoid-containing cell wall of three unicellular cyanobacteria. J Bacteriol **155:** 345-350

Rippka R (1972) Photoheterotrophy and chemoheterotrophy among unicellular blue-green algae. Archiv für Mikrobiologie **87:** 93-98

Rippka R, Deruelles J, Waterbury JB, Herdman M, Stanier RY (1979) Generic Assignments, Strain Histories and Properties of Pure Cultures of Cyanobacteria. Microbiology **111:** 1-61

Rippka R, Waterbury JB, Stanier RY (1981) Isolation and Purification of Cyanobacteria: Some General Principles. *In* MP Starr, H Stolp, HG Trüper, A Balows, HG Schlegel, eds, The Prokaryotes: A Handbook on Habitats, Isolation, and Identification of Bacteria. Springer Berlin Heidelberg, Berlin, Heidelberg, pp 212-220

Ritchie ME, Phipson B, Wu D, Hu Y, Law CW, Shi W, Smyth GK (2015) limma powers differential expression analyses for RNA-sequencing and microarray studies. Nucleic Acids Res **43:** e47

Roepstorff P, Fohlman J (1984) Proposal for a common nomenclature for sequence ions in mass spectra of peptides. Biomed Mass Spectrom **11:** 601

Rost HL, Sachsenberg T, Aiche S, Bielow C, Weisser H, Aicheler F, Andreotti S, Ehrlich H-C, Gutenbrunner P, Kenar E, Liang X, Nahnsen S, Nilse L, Pfeuffer J, Rosenberger G, Rurik M, Schmitt U, Veit J, Walzer M, Wojnar D, Wolski WE, Schilling O, Choudhary JS, Malmstrom L, Aebersold R, Reinert K, Kohlbacher O (2016) OpenMS: a flexible open-source software platform for mass spectrometry data analysis. Nat Meth **13:** 741-748

Rouault TA, Tong W-H (2005) Iron-sulphur cluster biogenesis and mitochondrial iron homeostasis. Nat Rev Mol Cell Biol **6:** 345-351

Ryther JH, Dunstan WM (1971) Nitrogen, Phosphorus, and Eutrophication in the Coastal Marine Environment. Science **171:** 1008-1013

Sandmann G, Boger P (1980) Physiological factors determining formation of plastocyanin and plastidic cytochrome c-553 in Scenedesmus. Planta **147:** 330-334

Scherl A, Shaffer SA, Taylor GK, Kulasekara HD, Miller SI, Goodlett DR (2008) Genome-specific gas-phase fractionation strategy for improved shotgun proteomic profiling of proteotypic peptides. Anal Chem **80:** 1182-1191

Schirmer A, Rude MA, Li X, Popova E, del Cardayre SB (2010) Microbial biosynthesis of alkanes. Science **329:** 559-562

Schmidt A, Gehlenborg N, Bodenmiller B, Mueller LN, Campbell D, Mueller M, Aebersold R, Domon B (2008) An Integrated, Directed Mass Spectrometric Approach for In-depth Characterization of Complex Peptide Mixtures. Molecular & Cellular Proteomics **7:** 2138-2150

Schmitz O, Gurke J, Bothe H (2001) Molecular evidence for the aerobic expression of nifJ, encoding pyruvate:ferredoxin oxidoreductase, in cyanobacteria. FEMS Microbiol Lett **195:** 97-102

Schoemann V, de Baar HJW, de Jong JTM, Lancelot C (1998) Effects of phytoplankton blooms on the cycling of manganese and iron in coastal waters. Limnology and Oceanography **43:** 1427–1441

Schoffman H, Lis H, Shaked Y, Keren N (2016) Iron–Nutrient Interactions within Phytoplankton. Frontiers in Plant Science **7:** 1223

Schopf JW (1993) Microfossils of the Early Archean Apex Chert: New Evidence of the Antiquity of Life. Science **260:** 640-646

Schwartz CJ, Giel JL, Patschkowski T, Luther C, Ruzicka FJ, Beinert H, Kiley PJ (2001) IscR, an Fe-S cluster-containing transcription factor, represses expression of Escherichia coli genes encoding Fe-S cluster assembly proteins. Proc Natl Acad Sci U S A **98:** 14895-14900

Seidler A, Jaschkowitz K, Wollenberg M (2001) Incorporation of iron-sulphur clusters in membrane-bound proteins. Biochem Soc Trans **29:** 418-421

Sharma V, Eckels J, Taylor GK, Shulman NJ, Stergachis AB, Joyner SA, Yan P, Whiteaker JR, Halusa GN, Schilling B, Gibson BW, Colangelo CM, Paulovich AG, Carr SA, Jaffe JD, MacCoss MJ, MacLean B (2014) Panorama: a targeted proteomics knowledge base. J Proteome Res **13:** 4205-4210

Shcolnick S, Shaked Y, Keren N (2007) A role for mrgA, a DPS family protein, in the internal transport of Fe in the cyanobacterium Synechocystis sp. PCC6803. Biochimica et Biophysica Acta (BBA) - Bioenergetics **1767:** 814-819

Shcolnick S, Summerfield TC, Reytman L, Sherman LA, Keren N (2009) The mechanism of iron homeostasis in the unicellular cyanobacterium synechocystis sp. PCC 6803 and its relationship to oxidative stress. Plant Physiol **150:** 2045-2056

Shen G, Balasubramanian R, Wang T, Wu Y, Hoffart LM, Krebs C, Bryant DA, Golbeck JH (2007) SufR coordinates two [4Fe-4S]2+, 1+ clusters and functions as a transcriptional repressor of the sufBCDS operon and an autoregulator of sufR in cyanobacteria. J Biol Chem **282:** 31909-31919

Shi T, Song E, Nie S, Rodland KD, Liu T, Qian WJ, Smith RD (2016) Advances in targeted proteomics and applications to biomedical research. Proteomics **16:** 2160-2182

Shi T, Sun Y, Falkowski PG (2007) Effects of iron limitation on the expression of metabolic genes in the marine cyanobacterium Trichodesmium erythraeum IMS101. Environ Microbiol **9:** 2945-2956

Shomura Y, Yoon KS, Nishihara H, Higuchi Y (2011) Structural basis for a [4Fe-3S] cluster in the oxygen-tolerant membrane-bound [NiFe]-hydrogenase. Nature **479:** 253-256

Singh AK, McIntyre LM, Sherman LA (2003) Microarray analysis of the genome-wide response to iron deficiency and iron reconstitution in the cyanobacterium Synechocystis sp. PCC 6803. Plant Physiol **132:** 1825-1839

Sittka A, Pfeiffer V, Tedin K, Vogel J (2007) The RNA chaperone Hfq is essential for the virulence of Salmonella typhimurium. Mol Microbiol **63:** 193-217

Sleep NH, Bird DK (2008) Evolutionary ecology during the rise of dioxygen in the Earth's atmosphere. Philosophical Transactions of the Royal Society of London B: Biological Sciences **363:** 2651-2664

Sommer U (1989) Nutrient status and nutrient competition of phytoplankton in a shallow, hypertrophic lake. Limnology and Oceanography **34:** 1162-1173

Spät P, Maček B, Forchhammer K (2015) Phosphoproteome of the cyanobacterium Synechocystis sp. PCC 6803 and its dynamics during nitrogen starvation. Front Microbiol **6:** 248

Stroebel D, Choquet Y, Popot J-L, Picot D (2003) An atypical haem in the cytochrome b6f complex. Nature **426:** 413-418

Takahashi Y, Tokumoto U (2002) A Third Bacterial System for the Assembly of Iron-Sulfur Clusters with Homologs in Archaea and Plastids. Journal of Biological Chemistry **277:** 28380-28383

Tamura K, Battistuzzi FU, Billing-Ross P, Murillo O, Filipski A, Kumar S (2012) Estimating divergence times in large molecular phylogenies. Proc Natl Acad Sci U S A **109:** 19333-19338

Tang H, Arnold RJ, Alves P, Xun Z, Clemmer DE, Novotny MV, Reilly JP, Radivojac P (2006) A computational approach toward label-free protein quantification using predicted peptide detectability. Bioinformatics **22:** e481-488

Tirupati B, Vey JL, Drennan CL, Bollinger JM, Jr. (2004) Kinetic and structural characterization of Slr0077/SufS, the essential cysteine desulfurase from Synechocystis sp. PCC 6803. Biochemistry **43:** 12210-12219

Tolle J, Michel KP, Kruip J, Kahmann U, Preisfeld A, Pistorius EK (2002) Localization and function of the IdiA homologue Slr1295 in the cyanobacterium Synechocystis sp. strain PCC 6803. Microbiology **148:** 3293-3305

Twiss MR, Auclair JC, Charlton MN (2000) An investigation into iron-stimulated phytoplankton productivity in epipelagic Lake Erie during thermal stratification using trace metal clean techniques. Canadian Journal of Fisheries and Aquatic Sciences **57:** 86-95

Tyystjärvi T, Herranen M, Aro EM (2001) Regulation of translation elongation in cyanobacteria: membrane targeting of the ribosome nascent-chain complexes controls the synthesis of D1 protein. Mol Microbiol **40:** 476-484

Urban JH, Vogel J (2007) Translational control and target recognition by Escherichia coli small RNAs in vivo. Nucleic Acids Research **35:** 1018-1037

Varghese S, Tang Y, Imlay JA (2003) Contrasting sensitivities of Escherichia coli aconitases A and B to oxidation and iron depletion. J Bacteriol **185:** 221-230

Vermaas WF, Shen G, Styring S (1994) Electrons generated by photosystem II are utilized by an oxidase in the absence of photosystem I in the cyanobacterium Synechocystis sp. PCC 6803. FEBS Lett **337:** 103-108

Volbeda A, Amara P, Darnault C, Mouesca JM, Parkin A, Roessler MM, Armstrong FA, Fontecilla-Camps JC (2012) X-ray crystallographic and computational studies of the O2-tolerant [NiFe]-hydrogenase 1 from Escherichia coli. Proc Natl Acad Sci U S A **109:** 5305-5310

Vonshak A, Cheung SM, Chen F (2000) MIXOTROPHIC GROWTH MODIFIES THE RESPONSE OF *SPIRULINA (ARTHROSPIRA) PLATENSIS* (CYANOBACTERIA) CELLS TO LIGHT. Journal of Phycology **36:** 675–679

Wang T, Shen G, Balasubramanian R, McIntosh L, Bryant DA, Golbeck JH (2004) The sufR gene (sll0088 in Synechocystis sp. strain PCC 6803) functions as a repressor of the sufBCDS operon in iron-sulfur

cluster biogenesis in cyanobacteria. J Bacteriol **186:** 956-967

Washburn MP, Wolters D, Yates JR, 3rd (2001) Large-scale analysis of the yeast proteome by multidimensional protein identification technology. Nat Biotechnol **19:** 242-247

Webber AN, Lubitz W (2001) P700: the primary electron donor of photosystem I. Biochimica et Biophysica Acta (BBA) - Bioenergetics **1507:** 61-79

Wegener KM, Singh AK, Jacobs JM, Elvitigala T, Welsh EA, Keren N, Gritsenko MA, Ghosh BK, Camp DG, Smith RD, Pakrasi HB (2010) Global proteomics reveal an atypical strategy for carbon/nitrogen assimilation by a cyanobacterium under diverse environmental perturbations. Mol Cell Proteomics **9:** 2678-2689

Wilson A, Ajlani G, Verbavatz JM, Vass I, Kerfeld CA, Kirilovsky D (2006) A soluble carotenoid protein involved in phycobilisome-related energy dissipation in cyanobacteria. Plant Cell **18:** 992-1007

Wilson A, Boulay C, Wilde A, Kerfeld CA, Kirilovsky D (2007) Light-induced energy dissipation in iron-starved cyanobacteria: roles of OCP and IsiA proteins. Plant Cell **19:** 656-672

Wollenberg M, Berndt C, Bill E, Schwenn JD, Seidler A (2003) A dimer of the FeS cluster biosynthesis protein IscA from cyanobacteria binds a [2Fe2S] cluster between two protomers and transfers it to [2Fe2S] and [4Fe4S] apo proteins. Eur J Biochem **270:** 1662-1671

Wood PM (1978) Interchangeable copper and iron proteins in algal photosynthesis. Studies on plastocyanin and cytochrome c-552 in Chlamydomonas. Eur J Biochem **87:** 9-19

Wright PR, Georg J, Mann M, Sorescu DA, Richter AS, Lott S, Kleinkauf R, Hess WR, Backofen R (2014) CopraRNA and IntaRNA: predicting small RNA targets, networks and interaction domains. Nucleic Acids Res **42:** W119-123

Wright PR, Richter AS, Papenfort K, Mann M, Vogel J, Hess WR, Backofen R, Georg J (2013) Comparative genomics boosts target prediction for bacterial small RNAs. Proc Natl Acad Sci U S A **110:** E3487-3496

Wurtsbaugh WA, Horne AJ (1983) Iron in Eutrophic Clear Lake, California: Its Importance for Algal Nitrogen Fixation and Growth. Canadian Journal of Fisheries and Aquatic Sciences **40:** 1419-1429

Xu XM, Adams S, Chua N-H, Møller SG (2005) AtNAP1 Represents an Atypical SufB Protein in Arabidopsis Plastids. Journal of Biological Chemistry **280:** 6648-6654

Yachandra VK, Sauer K, Klein MP (1996) Manganese Cluster in Photosynthesis: Where Plants Oxidize Water to Dioxygen. Chem Rev **96:** 2927-2950

Yang X, Niu S, Ichiye T, Wang LS (2004) Direct measurement of the hydrogen-bonding effect on the intrinsic redox potentials of [4Fe-4S] cubane complexes. J Am Chem Soc **126:** 15790-15794

Yeo WS, Lee JH, Lee KC, Roe JH (2006) IscR acts as an activator in response to oxidative stress for the suf operon encoding Fe-S assembly proteins. Mol Microbiol **61:** 206-218

Yeremenko N, Kouril R, Ihalainen JA, D'Haene S, van Oosterwijk N, Andrizhiyevskaya EG, Keegstra W, Dekker HL, Hagemann M, Boekema EJ, Matthijs HC, Dekker JP (2004) Supramolecular organization and dual function of the IsiA chlorophyll-binding protein in cyanobacteria. Biochemistry **43:** 10308-10313

Yin L, Bauer CE (2013) Controlling the delicate balance of tetrapyrrole biosynthesis. Philosophical Transactions of the Royal Society B: Biological Sciences **368:** 20130416

Yousef N, Pistorius EK, Michel KP (2003) Comparative analysis of idiA and isiA transcription under iron starvation and oxidative stress in Synechococcus elongatus PCC 7942 wild-type and selected mutants. Arch Microbiol **180:** 471-483

Yu J, Shen G, Wang T, Bryant DA, Golbeck JH, McIntosh L (2003) Suppressor mutations in the study of photosystem I biogenesis: sll0088 is a previously unidentified gene involved in reaction center accumulation in Synechocystis sp. strain PCC 6803. J Bacteriol **185:** 3878-3887

Zang SS, Jiang HB, Song WY, Chen M, Qiu BS (2017) Characterization of the sulfur-formation (suf) genes in Synechocystis sp. PCC 6803 under photoautotrophic and heterotrophic growth conditions. Planta

Zhang B, Crack JC, Subramanian S, Green J, Thomson AJ, Le Brun NE, Johnson MK (2012) Reversible cycling between cysteine persulfide-ligated [2Fe-2S] and cysteine-ligated [4Fe-4S] clusters in the FNR regulatory protein. Proc Natl Acad Sci U S A **109:** 15734-15739

Zhang L, McSpadden B, Pakrasi HB, Whitmarsh J (1992) Copper-mediated regulation of cytochrome c553 and plastocyanin in the cyanobacterium Synechocystis 6803. J Biol Chem **267:** 19054-19059

Zhang P, Allahverdiyeva Y, Eisenhut M, Aro EM (2009) Flavodiiron proteins in oxygenic photosynthetic organisms: photoprotection of photosystem II by Flv2 and Flv4 in Synechocystis sp. PCC 6803. PLoS One **4:** e5331

Zhang P, Eisenhut M, Brandt AM, Carmel D, Silén HM, Vass I, Allahverdiyeva Y, Salminen TA, Aro EM (2012) Operon flv4-flv2 provides cyanobacterial photosystem II with flexibility of electron transfer. Plant Cell **24:** 1952-1971

Zheng L, Cash VL, Flint DH, Dean DR (1998) Assembly of iron-sulfur clusters. Identification of an iscSUA-hscBA-fdx gene cluster from Azotobacter vinelandii. J Biol Chem **273:** 13264-13272

Zheng L, White RH, Cash VL, Jack RF, Dean DR (1993) Cysteine desulfurase activity indicates a role for NIFS in metallocluster biosynthesis. Proc Natl Acad Sci U S A **90:** 2754-2758

Zouni A, Witt H-T, Kern J, Fromme P, Krauss N, Saenger W, Orth P (2001) Crystal structure of photosystem II from Synechococcus elongatus at 3.8 [angst] resolution. Nature **409:** 739-743

Annales Universitatis Turkuensis

Turun yliopisto
University of Turku

Painosalama Oy, Turku, Finland 2017

ISBN 978-951-29-6966-1 (PRINT)
ISBN 978-951-29-6967-8 (PDF)
ISSN 0082-7002 (PRINT) | ISSN 2343-3175 (PDF)